INTERFACES OF INDIUM TIN OXIDE AND ORGANIC SEMICONDUCTOR THIN FILM STUDIED BY OPTICAL SECOND HARMONIC GENERATION

SITI ZULAIKHA NGAH DEMON

Japan Advanced Institute of Science and Technology

Doctoral Dissertation

INTERFACES OF INDIUM TIN OXIDE AND ORGANIC SEMICONDUCTOR THIN FILM STUDIED BY OPTICAL SECOND HARMONIC GENERATION

SITI ZULAIKHA NGAH DEMON

Supervisor: Prof. Dr. Goro Mizutani

School of Materials Science
Japan Advanced Institute of Science and Technology (JAIST)
September 2014

Dissertation Abstract

The energetic structure at the interface that governs charge carrier dynamics in organic device has attracted abundance of interface related researches. Here, the scope of study is the interface between the indium tin oxide (ITO) and the organic semiconductor layer. The electronic properties at the interface of hole injection contact, the ITO with the organic semiconductor layer are the key factor to understand the injection barrier of the charge carriers during device operation. The nonlinear optical second harmonic generation (SHG) is employed as selective probe for surface and interface studies. The application of SHG has been demonstrated for wide range of organic and inorganic materials ever since the advancement of laser technology. Currently, the SHG investigation on organic semiconductor thin film is in favor of the contemporary interest in organic light emitting diodes and organic solar cells. The main idea of my research is to analyze the character of charge transfer dipole at the interface between the ITO and the organic semiconductor layer using the nonlinear effects of SHG. And, the second objective is to interpret the information of SHG phase obtained from the double layer structure.

In present study, the strength of the charge transfer complex at the interface of ITO is elucidated using the ionization energy of the organic semiconductor thin film. Sample of bare ITO substrate and organic thin film of m-MTDATA, 2-TNATA, CuPc, pentacene, α-6T and α-NPD are prepared for this purpose. In the first stage of experiment, the strength of electric field at the interface is analyzed from SHG intensity measurement of ITO and ITO/organic structures in the reflection geometry. The fundamental (1064 nm) and SHG (532 nm) lights are *p*-polarized. The Fresnel factor analysis is applied to treat the macroscopic local field effect (the *L* factors) at both fundamental and SHG light in the samples. In this first analysis, SHG interference from the interface has manifested in the result of ITO/2-TNATA, ITO/pentacene and ITO/α-6T structures. At this stage of experiment, I have recognized that the insufficiency of relying on the data of SHG intensity only, since the sign of SHG is also significant information. Thus, in order to process the SHG that emerged from the interface, the experiment of SHG phase has become an obligatory to this study.

Mainly featured as a sensitive probe for orientation of molecules, the SHG phase measurement is also known for many nonlinear effect applications. One of the prominent works in extracting SHG phase shift was demonstrated by K. Kemnitz and his co-workers in 1986 [4]. The technique is to use the phase difference given by the fundamental light at two SHG sources, the target sample and the reference. The same experiment is established in this study with α-quartz (0001) as the second source of SHG. The experimental steps and necessary groundwork to obtain the phase shift from the interface of ITO/organic have been properly addressed. The total phase shift of the ITO/organic samples is directly calculated using the phase of oscillation

pattern of bare ITO as reference. The next step of analyzing the phase, however, does not come in a straight forward fashion. I showed the method to apply the phase correction due to dielectric dispersion in organic thin films in order to extract the absolute phase of the charge transfer dipole. As a result, the SHG from the interface of ITO/CuPc and ITO/pentacene is presented using the solution of the complex plane. In another experiment, the phase of SHG from ITO/α-NPD indicated that the SHG from the interface is relatively weak when compared to the phase of bare interface of ITO.

The absolute phase from the interface, $\phi_{interface}$ has solved the ambiguity from the previous measurement of SHG intensity. For this particular experiment, the phase of SHG from the interface of ITO/organic semiconductor is found to yield not only from the effect of static dipole but also from the imaginary part of the susceptibility, χ. This finding is not in fine agreement with the static dipole model previously proposed by our group. Nevertheless this experiment is a direct observation of the phase thus, gives more accurate interpretation of the SHG at interface of organic semiconductor. The imaginary part of susceptibility implied that there may be electronic resonance in the origin of phase shift. The discussion is produced using the data of SHG spectroscopy and the spectra of absorption coefficient of organic molecules. But more importantly, I propose that the phase shift can be due to spatial fluctuation of dipole density at the interface of charge transfer.

The study of charge transfer at the interface of ITO/organic semiconductor is performed using the characteristics of SHG intensities and the SHG phases obtained from the ITO and the ITO/organic double layer structures. The nonlinear phase interferometry is demonstrated as the effective technique to avoid the misinterpretation of SHG measurement in general, other than being a potential probe of molecular orientation. Further application of this interferometry technique in the investigation of organic semiconductor system is currently being pursued by our group. My contribution to this field is by showing the extensive analysis of the phase shift from buried interface of ITO/organic thin film, this report is important for the study of SHG at the interface of organic device.

Keyword: second harmonic generation, interface, thin film, organic semiconductor, phase measurement

بِسْمِ اللَّهِ الرَّحْمَنِ الرَّحِيم

In the name of Allah S. W. T., I would like to express my acknowledgement to several individuals, family and friends whom has been consistently supporting me and giving me the strength during the years of study in Japan.

First of all, my utmost gratitude goes to Prof. Dr. Goro Mizutani, my supervisor for his dedicated guidance and support during my three years in JAIST. Being accepted in Mizutani lab has been one of greatest lifetime opportunity given to me and his patience in supervising me has led me to become what I am today. I would also like to extend my thanks to the former assistant professor of Mizutani Lab, Dr. Yoshihiro Miyauchi for his advice and support into producing this project. Both of them has been the my source of inspiration in all these years and I hold dear the knowledge they have taught me

The project will not be possible without the contribution from our collaborator from Murata Laboratory, I would like to give my gratitude to Prof. Dr. Murata, H. and Dr. Matsushima, T. for their co-operation in these years. Also, not forgetting my minor project advisor Assoc. Prof. Dr. Friedlein, R., for fascinating experience in his laboratory and in some way has motivated me into committing to this field of study.

I would also like extend my heartfelt thanks to my family and friends in Malaysia especially my mother for their emotional support and prayers. Also, I am very thankful for having such great friends during my stay in JAIST, them being thoroughly encouraging during the ups and downs of my research. People from Mizutani lab, I owe them many helpful advices and discussions in my research, we have shared many unforgettable moments and I wish our friendship will continue to flourish even after this.

For advices and some technical support, I owe to these people, Prof. T. Suzuki of National Defense Academy of Japan for useful advices to construct the SHG phase

measurement set-up, Assoc. Prof K. Ohdaira and T. Murakami of Center for Nano Materials and Technology, JAIST for the technical support in the ellipsometry measurement.

I would also like to acknowledge the financial support from Ministry of Education of Malaysia for the sponsorship under the Skim Latihan Akademik IPTA (SLAI) and National Defence University of Malaysia (UPNM) for my pursuit of doctoral degree.

Table of Contents

Chapter 1

Introduction

1.1 Introduction to interface of organic devices

Research into organic semiconductor and organic semiconductor devices has made a rapid progress in the recent years. The organic semiconductors with high mobility are beneficial to electronics device fabrication that featured lightness in weight and flexibility [1]. There is organic light emitting diode (OLED) that has attracted a great deal attention because it can be used in full-color flat-panel displays [2,3]. The organic solar cells become promising as the demand of renewable energies grows due to its simple fabrication on various substrates [4]. Due to this significant importance in the field of electronics application, numerous researches have been carried out to understand the carrier behavior in organic device. The number had sky rocketed after the breakthrough idea of double layer structure made by Tang et al in 1987 [5]. Even though the physics of organic devices are rather complex processes but the characterization techniques and methods have also evolved since then.

The structure at the interface is one of the most studied in organic device. For one, the interface structure has the control over the dynamics of the carriers when the device is in operation [6]. Hence, there is always a need to observe and improve the interface structure of

organic device. For instance, introduction of metal oxide and functional group to interface of organic semiconductor and electrode has been known to improve the charge injection current in the device [7,8,9]. Defect in organic devices can also be traced to the origin at the interface, the interface of α-NPD/Alq_3 is recently identified as the source of luminescence degradation in OLED [2,3].

Electrical measurement such as impedance spectroscopy, J-V measurements and displacement current measurement are common methods to characterize organic devices. However, the ultraviolet photoelectron spectroscopy, photoluminescence and electroluminescent measurement are to be employed in order to check the energetic structure of the interface [5]. Optical method is becoming favorable approach due to its transparency on buried thin film and vacuum environment are no longer required for some cases. Y. Nakano employed the deep level optical spectroscopy (DLOS) to characterize the deep levels electronic in the band gap of OLED. This technique enables the measurement of capacitance during monochromatic optical excitation [2]. The second order nonlinear effects also have the advantage for non-destructive probing of buried interface [10]. A series of electric field induced second harmonic generation (EFISHG) has been pioneered by Iwamoto's group to probe the electric field distribution in measurements on OLEDs and organic solar cells recently [4,5,11].

In this dissertation, the characterization of buried interface of the indium tin oxide (ITO) and organic semiconductor thin film by the optical second harmonic generation (SHG)

will be elaborated. The understanding of energy barrier at interface of ITO and organic semiconductor is beneficial in order to optimize the hole injection current at the ITO contact of organic device. Hence the ability to predict this property is a considerable interest to be studied upon. In this first chapter, a small introduction of the interface structure and the chronology of the second order nonlinear effects studies will be delivered.

1.1.1 The interface structure of organic semiconductor

The term organic semiconductor is used to describe organic materials that capable of transporting charge carriers [12]. The organic material, either conjugated oligomers or polymers may not be intrinsically charged, but the holes and electrons in the π orbitals are the potential charge carriers. The study of organic semiconductor went back as far as 1950s and their fundamental scientific importance includes application in photonics [12]. In organic device, the electrons and holes have to be injected through organic/electrode interfaces. The electron energetics between the metal electrode and organic molecules is determined by energy barrier between the Fermi level of the metal and the HOMO and LUMO levels across the organic material [10]. An efficient charge injection contact can be established by choosing the HOMO/LUMO energy that is closely matched with metal's work function. The study of dipole layer at the interface of metal/organic by Ishii et al summarized several origin of the dipole layer; 1. charge transfer 2. mirror force 3. push back effect (surface effect rearrangement) 4. chemical interaction 5. interface state and permanent dipole of the

adsorbates [10,13]. These factors imply the existence of interface dipole in the context of energy level alignment [14].

On the other hand, the interface dipole theory has been widely accepted in the case of traditional semiconductor to predict the band alignment of Schottky contact between the metal and semiconductor. According to the theory, interface dipole is formed due to charging of intrinsic interface states pushing the band alignment towards a zero net dipole charge [15]. The interface parameter S_b gives the variation of barrier as the function of metal work function, $\phi_{bh} \propto S_b \, x \, \phi_M$ [16]. In a paper by Braun et al [17], the study of energy level alignment at metal/organic and organic/organic interfaces has featured the interaction strength at the interface. Given by the complexity of the interface, they proposed a model to categorize the interface accordingly, varying from weak physisorption to strong chemisorption interactions. Extensive analysis has been applied by the X-ray photoemission spectroscopy (XPS) to observe the interface interactions such as, 1. ITO and copper phthalocyanine (CuPc)/ $CuPcF_4$ [18], 2. FePc on Au(110) [19], 3. ITO and self-assembled (SAM) monolayer [20], and 4. ITO and NPB [21].

The electronic property of the interface is closely related to the molecular orientation at the interface. Furthermore, the flexibility to control the molecular orientation has always been attractive in fabrication of organic device. The molecular orientation at the interface is dependent on the type of the molecule-substrate interfacial and intermolecular interaction [22]. It has been demonstrated that the CuPc molecules lie stable on the flat surface of graphite due

to interfacial dispersion force [22]. However, on a terminated SAM-Au(111) surface, the CuPc is found standing on the surface instead, due to minimization coupling between metal d-bands and conjugated π systems [22]. Other molecular orientation dependent studies were also shown for pentacene and α-6T [23,24,25].

Electron injection contact in organic device such as Al, Au and Ag are highly conductive and has low resistivity. As for ITO, the commonly used hole injection contact, its application is based on its transparent conducting properties, however, the lattice structure and electronic interaction within the compound is rather complex [13]. The morphology of ITO surface can be described as rough due to polycrystalline domains [26]. As a degenerate semiconductor, the surface of ITO is metallic because of the presence of metallic surface states [27]. Hence, electronic structure of ITO should be different from that of pure metal.

1.1.2 Charge transfer at ITO/MoO_3/α-NPD

In general, the mechanism of injection barrier at the interface dictates the performance, lifetime and stability of the device. The instability of hole transport layer of OLED has been pursued by several methods including introduction of CuPc as buffer layer between ITO and hole injection layer, and also by doping of the hole transport layer [3, 28]. The space-charge-limited-current or SCLC is the current induced by the formation of space charge dipole at the interface of electrode contact. As promoted by Matsushima et al and

others [8, 29], the SCLC was observed at the interface of ITO/MoO_3/α-NPD. The following example shows the energy level alignment and the interface study observed at this particular contact.

Thin film construction of an OLED is shown in Fig. 1.1. This construction is obtained from Murata Laboratory in School of Materials Science, Japan Advanced Institute of Science and Technology (JAIST). The three bottom layers consist of ITO, molybdenum trioxide (MoO_3) and the α-NPD. *N*,*N*'-diphenyl-*N*-*N*'-bis(1-naphthyl)-1,1'-byphenyl-4,4'-diamine (α-NPD) is hole transport layer with hole mobility of 10^{-4} cm^2 $V^{-1}s^{-1}$.

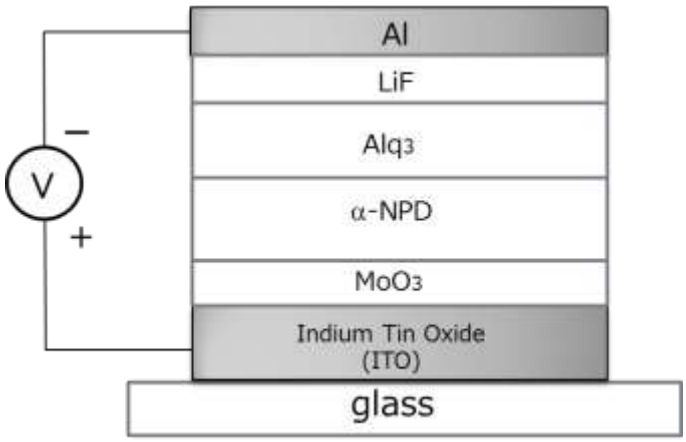

Figure 1.1 OLED construction.

In the highlight of the SCLC observation by Matsushima et al, doping of MoO_3 at 0.75 nm was suggested as maximum optimization at the contact [8]. The energy level relation

can be understood using the diagram in Fig. 1.2. The work function of ITO and MoO_3 are shown as -5.02 eV and -5.68 eV, respectively from the vacuum level. The HOMO energy levels of α-NPD layer is -5.40 eV and the LUMO is -2.35 eV from the vacuum level. At the contact of ITO/α-NPD only (Fig. 1.2 (A)), there is a hole injection barrier by the interface dipole due to much lower HOMO energy in α-NPD with respect to the work function of ITO. However as shown in Fig, 1.2 (B) and (C), the space charge layer has benefitted from the mechanism of electron transfer from the higher HOMO energy in α-NPD to MoO_3 in the construction of ITO/MoO_3/α-NPD. As a result, the electron-hole pairs that separated under the applied electric field will induce a negligible hole injection barrier at the contact.

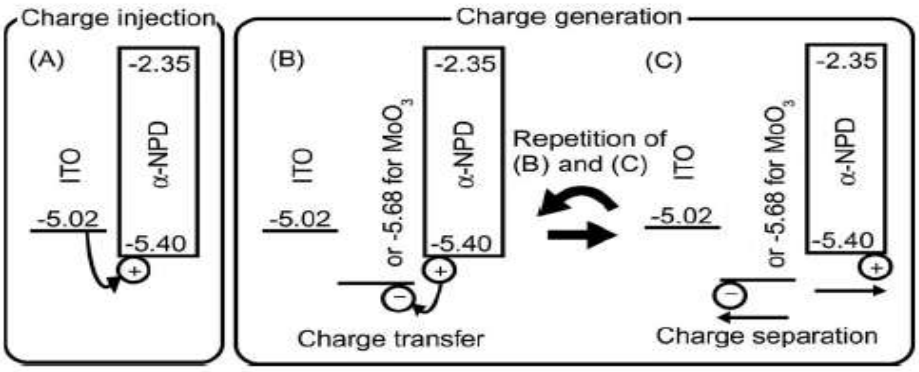

Figure 1.2 Energy level relations at the contact of (a) ITO/α-NPD and (b-c) ITO/MoO_3/α-NPD for comparison. The space charge layer was induced in the three layer configuration [8].

Also, the mechanism at the interface of ITO/MoO_3/α-NPD had been directly

observed by optical second harmonic observation (SHG) [30]. Result of SHG measurement and model of SHG polarization are shown in Fig. 1.3.

1.2 Background of surface second harmonic generation

Second harmonic generation (SHG) has developed into a powerful surface technique since the initial observation of SHG in quartz by Franken in 1961 [31]. SHG can originate from response of surface electric dipole, bulk magnetic quadrapole and bulk electric quadrapole in a material [32]. Hence, the sensitivity of SHG to the surface can be realized when only surface electric dipole from the first monolayer emits the SHG. This sensitivity on the level of a fractional monolayer can be achieved even in a electrochemical environment [31]. The SHG interface study had been demonstrated as early as 1965 in experiment of Brown, Park and Sleepers by measuring the SHG from the interface between two centrosymmetric media [31]. After a series of theoretical calculation by N. Bloembergen [31], the surface SHG technique is now a common optical probe for characterization of adsorption strength, surface coverage, molecular orientation, surface symmetry, interfacial electric field strength, reaction kinetics and surface diffusion [32]. In experimental point of view, the SHG has the advantage over other methods to probe adsorbed molecules and surface reactions since there is no restriction of ultra-high vacuum condition [33, 31]. Furthermore, the technique has the potential for surface-specific spectroscopy through the resonant SHG process [31].

As there are gaining interests in molecular solid, it was recognized that organic molecular solid like aniline, nitrobenzene and p-nitroanilline are also SHG active [34]. Kumagai et al had showed that SHG from copper phthalocyanine (CuPc) thin film due to the lack of inversion symmetry [35] and another organic semiconductor molecule, C_{60} also emits SHG due to oxidation at atmosphere [35]. As a potential diagnostic technique in the thin film processing, the application of SHG stems from the need to measure the intrinsic electric field in a semiconductor device. The SHG from DC electric field arises from space charge region at semiconductor surface. It is known as electric field induced SHG (EFISHG) that can also be a result of a fixed charge in the system and external DC bias electric field placed on the system [36]. In OLED, Yamada et al used the SHG technique to measure the dipole reorientation in polyurethane based OLED [37]. Interesting result was also shown by the work of Ito et al. In their experiment, the SHG had been emitted from the buildup dipole layer at the contact of Au and the electron transport layer of OLED, Alq_3 film [38]. As of recent, many work involving EFISHG to characterize carrier dynamics in organic devices were produced by Iwamoto group [1, 4, 5, 11]. It is noted that there is also an expanding interest in using sum frequency generation (SFG). In two separate papers, T. Miyamae had probed interface interaction of Al/Alq_3 and selectively probe buried organic layers of OLED under electric field with doubly resonant SFG [10, 39].

1.2.1 SHG at ITO/MoO3/α-NPD

Previously in our group, El-Basaty and his co-workers had conducted SHG measurement at the multilayer structure of ITO/MoO_3/α-NPD [30]. The measurement was motivated by the formation of space charge region established at the interface of hole injection contact in OLED [8].

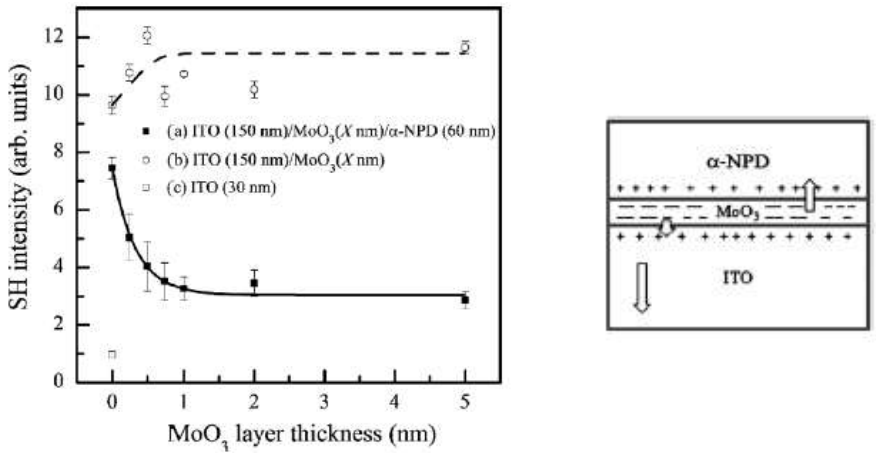

Figure 1.3 (left) SHG intensities at different doping of MoO_3 thicknesses and (right) the model of SHG polarization [30].

At the contact of MoO_3/α-NPD, the mechanism of charge transfer had been strongly observed by SHG intensity measurement. In Fig. 1.3 (left) as shown by the filled circles, there is decline of SHG intensity from 0 nm to 0.75 nm MoO_3 thicknesses in ITO/MoO_3/α-NPD structures due to growing presence of SHG electric field at MoO_3/α-NPD interface. The direction of SHG electric field at this interface is the exact opposite to the charge transfer at

ITO/MoO_3. The empty circles that represent SHG intensity from the ITO/MoO_3 is seen with a slight change as a function of MoO_3 deposition. From here, it is understood that the sign of the nonlinear susceptibility, $\chi^{(2)}$ will change with respect to the direction of the charge transfer at the interface.

The model of SHG polarization for ITO/MoO_3/α-NPD is shown in the figure on the right. This model has summarized the origin of SHG polarization as cancelling effect with the phase of SHG from the MoO_3/α-NPD is 180° away from the phase of SHG from ITO and ITO/MoO_3. It can be a correct interpretation of the SHG despite direct measurement of the phase was never made. However, it is highly attractive prospect to use SHG phase measurement on organic semiconductor system considering there can be more interpretation from the response of the charge transfer dipole. Thus, has motivates the author to pursue SHG phase measurement technique for the interface study.

1.2.2 Application of SHG phase measurement

The development of second-order nonlinear optical effects has not only yield new analytic capabilities but also improved understanding of the nonlinear process itself [31]. Initially, it was the observation by K. Chang, J. Ducuing and N. Bloembergen that demonstrated the first relative phase measurement in GaAs, InAs and ZnTe semiconductor. Their objective was to establish the imaginary part of the nonlinear susceptibility of the

semiconductor. Their phase measurement set-up employed a gas cell with air pressure served as optical phase delay [40].

It takes many years later to take the ability to extract molecular alignment from data of SHG phases. This discovery set this technique into a new milestone in the field of material science. The first report by Kemnitz at al in 1986 had showed the absolute orientation of phenol molecules at liquid/vapor interface [41]. In their measurement, the hydroxyl group of phenol solution was found to be pointed toward the bulk water. This conclusion was achieved from the calculation of the absolute phase of $\chi_{xzx}^{(2)}$ for the liquid that was 180° with respect to the quartz surface. The paper also introduced a much simpler technique of using optical dispersion in air to collect the SHG phase that works remarkably well with the sample. Another prominent work to obtain molecular orientation was also demonstrated by Sato et al. Their research provided the first example that disclosed the direction of the molecular axis of a hemicyanine sandwiched between two Langmuir-Blodgett films [42].

Another application of the phase measurement is to obtain correct interpretation of SHG when susceptibilities of different species contribute to the total SHG intensity [43]. A fine example had been shown by Buck et al in the study of SHG from hexadecane thiol on polycrystalline Au [44]. The systematic analysis was needed due to the importance of resonance contribution in the SHG. By 1996, R. Stolle and his co-workers managed to produce a complete review of the nonlinear phase techniques [43]. At this point, the interferometry technique had been established as the conventional method to obtain the

nonlinear phase.

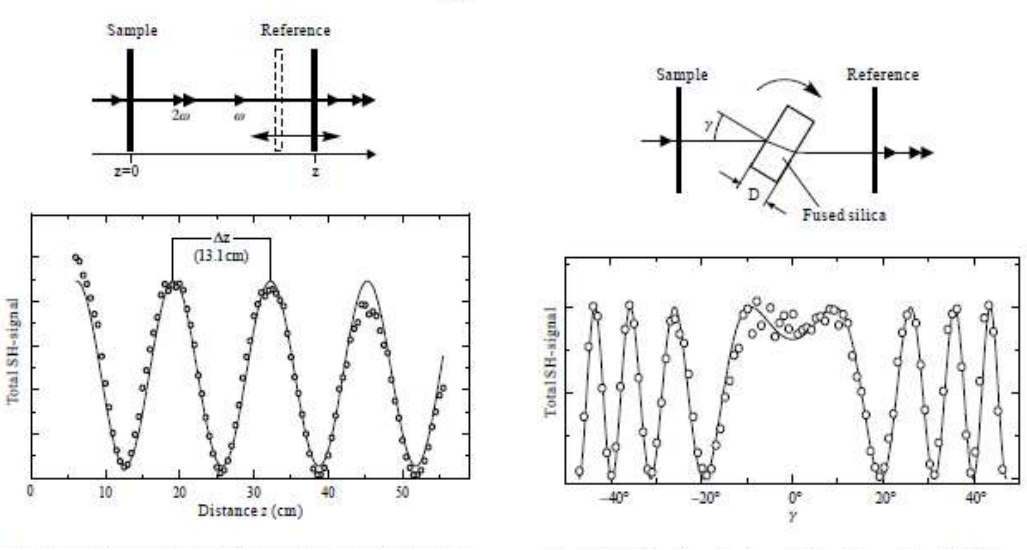

Figure 1.4 The interferometry methods of obtaining nonlinear phase. On the left is the technique of using distance variation of two SHG sources in air that implemented by Kemnitz et al. And on the right is the rotating plate technique, one of the most common SHG phase method to study molecular orientation [43].

The effect of resonance in the phase measurement was also studied. A quantitative works were produced for resonant SHG phase from Si(111) 7x7 and Si(111)-SiO_2 interface in early 2000s [45, 46]. Both works suggested the phase of resonant SHG is a frequency dependent and must be studied using oscillator model. Following the recent advancement of femtosecond lasers applications, there is also interesting development of phase measurement technique. One important reason is the researchers are trying to counter the disadvantages in the conventional interferometry method. R. Lu and his co-workers had employed the

femtosecond pulsed laser to counter the weak signal from neat air/liquid interface [47]. They have achieved an experimental set up that are well-below the detection limit of the standard set up in most laboratories, thus giving higher sensitivity for surface probe. Meanwhile, Wilson et al presented the frequency domain (FD) method for measuring SHG amplitude and phase using 60 nm bandwidth femtosecond source [48]. This method of FD-SHG offers a solution to avoid the time consuming interferometer scan at each frequency.

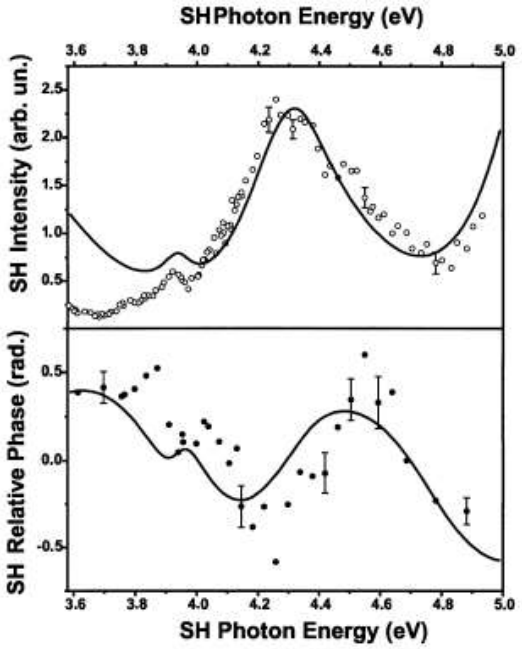

Figure 1.5 The spectral dependence of SHG intensity and SHG phase of a silicon layer in the work of Aktsipetrov et al [46]. The fits are the result calculation from the oscillator model.

Even after almost 50 years since the first observation of the SHG phase measurement, the interferometry technique is still a viable method to study material properties. There have

been more versatile applications especially for materials in cutting-edge technology. For example it is proved to be useful in determining the crystalline axis of a solid [49]. Study of SHG phase of Cr(VI) at a buried methyl ester-functionalized fused quartz/water interface was achieved by Mifflin et al with chromate concentration of 10^{-4} M [50]. And quite recently, Yamada et al investigated the absolute orientation of bacteriorhodopsin (bR) thin film using SHG interferometry [51]. The bacteriorhodopsin thin film has a light-driven proton pump function for photo-sensor device application [51].

The second harmonic phase spectroscopy is also useful for the study the refractive indices of anomalous dispersive thin film [52]. It is achieved by making a superposition of the two identical nonlinear organic dye films at transmission geometry. Unfortunately, despite the benefit in sensitivity to the nonlinear property of material, the physical meaning of the phase is not easily understood. For off-resonance SHG studies, the phase of $\chi^{(2)}$ must be real [43] thus the interpretation of the imaginary phase shift is difficult. Lu et al observed SHG phase difference of 115° for air/water interface and they could not explain the reason for this trivial number [47].

1.3 Motivation of research

General definition of the interface is the zone that the electronic structure or molecular orientation of the material is different from in the bulk [31]. The study of interface

property is typically realized by electron probe but due to the limitation in accessing significant thickness of thin film, optical probe becomes a more desirable option. The first motivation is to characterize the strength of charge transfer at the interface of organic semiconductor with ITO. The result may hopefully elucidate the hole injection barrier at ITO since the charge carrier traps at the interface could be understood from the localized property of the electron transfer [18].

Previously, the SHG at interface of ITO/MoO_3/α-NPD was analyzed with homodyne data of SHG only [30]. However, using the magnitude of SHG only, the information of the SHG phase is necessarily lost and if the $\chi^{(2)}$ is a complex valued, the information of the phase can be rather significant [43]. Thus, it is in my interest to make a direct measurement of SHG phase of organic semiconductor interface. This way, the absolute phase of $\chi^{(2)}$ can be determined as well as the direction of charge transfer at the interface. The analysis will be crucial considering the organic semiconductor is not transparent at certain visible wavelengths. On the other hand, this will be the first report of SHG phase measurement from the buried interface of organic semiconductor thin film.

1.4 Objective of the research

In order to understand dipole interaction at the interface of organic semiconductors solid, the optical second harmonic generation technique is applied. The idea to obtain

exclusive interpretation of the nonlinear effects by SHG phase measurement is also worthwhile goal of this study. The objectives of the research are given as follows:

a) To investigate the magnitude of charge transfer at the interface of hole injection contact with organic semiconductor layer.

b) To analyze the phase of SHG electric field from buried interface of indium tin oxide and organic semiconductor thin film.

1.5 Dissertation outline

This dissertation consists of 6 chapters.

The content of the first chapter of Introduction consists of brief introduction of organic device and the studies related to the device's interface. The background of the nonlinear SHG method and the application of SHG phase measurement are also elaborated.

In the second chapter of Theory of Second Harmonic Generation, the fundamental concept of the nonlinear optic is described. Relevant parameter of SHG that falls under consideration of organic molecular system is discussed. The SHG experiments are described in the chapter 3 of Nonlinear Optical Measurement of Second Harmonic Generation (SHG).

The SHG of the samples are measured in atmosphere and the linear optical measurement is the supplementary analysis to support the SHG measurement. The main feature of this investigation is the technical settings of the SHG intensity and SHG phase experiments.

The analysis of the optical signal is described in chapter 4 of The Magnitude and Phase of SHG from the Interface of ITO and Organic Semiconductor. The extensive analysis covers macroscopic Fresnel factor that is used to predict the SHG from the interface of ITO and organic thin film. In this chapter, the absolute phase of $\chi^{(2)}$ from ITO/CuPc and ITO/pentacene interfaces are obtained. Further discussion and physical interpretation of the SHG is conveyed in the chapter 5 of Origin of SHG Electric Field and SHG Phase Shift.

Finally, the overall conclusion from this study of organic semiconductor interfaces is delivered in the last chapter of Conclusion.

References:

1 E. Lim, Y. Shibata, T. Manaka, M. Iwamoto, probing the electric field in organic double layer-system by optical second harmonic generation, Thin Solid Films 518 (2009) 893-895 and the reference inside

2 Y. Nakano, Deep-level Optical Spectroscopy Investigation of Degradation Phenomena in Tris(8-hydroxyquinoline) Aluminium-Based Organic Light Emitting Diodes, Appl. Phys. Exp. 2 (2009) 092103

3 Pinato, A., Cester, A., Meneghini, M., Wrachien, N., Tazzoli, A., Xia, S., Adamovich, V., Weaver, M. S. Brown, J. J., Zanoni E., Meneghesso G., Impact of Trapped Charge and Interface Defects on the Degradation of the Optical and Electrical Characteristics in NPD/Alq_3 OLEDs, IEEE Transactions on Electron Devices 57 (2011) 178-184

4 X. Chen, D. Taguchi, K. Lee, T. Manaka, M. Iwamoto, Analyzing interfacial carrier charging in pentacene/C_{60} double layer organic solar cells by optical electric field induced second-harmonic generation measurement, Chem. Phys. Lett. 511 (2011) 491-495 and the reference inside

5 A. Sadakata, D. Taguchi, T. Yamamoto, M. Fukuzawa, T. Manaaka, M. Iwamoto, Analyzing two electroluminescence modes of indium tin oxide/α-NPD/Alq_3/Al diodes by using large alternating current square voltages, J. Appl. Phys. 110 (2011) 103707 and reference inside

6 M. T. Greiner, Z-H. Lu, Thin film metal oxides in organic semiconductor devices,

their electronic structures, work functions and interfaces, NPG Asia Materials 5 (2013) e55

7. Irfan, H. Ding, Y. Gao, D. Y. Kim, J. Subbiah, F. So, Energy level evolution of molybdenum trioxide interlayer between indium tin oxide and organic semiconductor, Appl. Phys. Lett. 96 (2010) 073304.
8. T. Matsushima, Y. Kinoshita, H. Murata, Formation of Ohmic hole injection by inserting an ultrathin layer of molybdenum trioxide between indium tin oxide and organic hole transporting layers, Appl. Phys. Lett. 91 (2007) 253504.
9. T. Matsushima, H. Murata, Observation of space-charge-limited current due to charge generation at interface of molybdenum dioxide and organic layer, Appl. Phys. Lett. 95 (2009) 203306.
10. T. Miyamae, E. Ito, Y. Noguchi, H. Ishii, Characterization of the interactions between Alq3 thin films and Al probed by two-color sum-frequency generation spectroscopy, J. Phys. Chem. C 115 (2011) 9551-9560
11. D. Taguchi, T. Shino, X. Chen, L. Zhang, J. Li, M. Weis, T. Manaaka, M. Iwamoto, Determination of lifetime of double layer CuPc/C60 organic solar cells by optical electric-field-induced second-harmonic generation measurement, Phys. Procedia 14 (2011) 167-171
12. A. Mishra, P. Bauerle, Small Molecule Organic semiconductor on the Move: Promises for Future Solar Energy Technology, Angew. Chem. Int. Ed. 51 (2012) 2020
13. H. Ishii, K. Sugiyama, E. Ito, K. Seki, Energy Level Alignment and Interfacial

Electronic Structures at Organic/Metal and Organic/Organic Interfaces, Adv. Mater. 11 (1999) 605-625.

14. H. Vasquez, Y. J. Dappe, J. Ortega, F. Flores, A unified model for metal/organic interfaces: IDIS, 'pillow' effect and molecular permanent dipole, Applied Surface Science 254 (2007) 378
15. M. G. Helander, Z. B. Wang, J. Qiu, Z. H. Lu, Band alignment at metal/organic and metal/oxide/organic interfaces, Appl. Phys. Lett. 93 (2008) 193310 and the reference inside
16. I. G. Hill, A. Rajagopal, A. Kahn, Y. Hu, Molecular level alignment at organic semiconductor-metal interfaces, Appl. Phys. Lett. 73 (1998) 5
17. S. Braun, W. R. Salaneck, M. Fahlman, Energy-level at organic/metal and organic/organic interfaces, Adv. Mater. 21 (2009) 1450-1472
18. H. Peisert, M. Knupfer, T. Schwieger, J. Fink, Strong chemical interaction between indium tin oxide and phthalocyanines, Appl. Phys. Lett. 80 (2002) 2916-2918
19. M. G. Betti, P. Gargiani, C. Mariani, S. Turchini, N. Zema, S. Fortuna, A. Calzolari, S. Fabris, Formation of hybrid electronics state in FePc chains mediated by the Au (110) surface, J. Phys. Chem. 116 (2012) 8657-8663
20. J. H. Cho, Y. D. Park, D. H. Kim, W-k. Kim, H. W. Jang, J-l. Lee, K. Cho, Reactive metal contact at indium-tin-oxide/self-assembled monolayer interfaces, Appl. Phys. Lett. 88 (2006) 102104
21. P. He, S. D. Wang, W. K. Kook, C. S. Lee, S.T. Lee, Vibrational and

photoemission study of the interface between phenyl diamine and indium tin oxide, Appl. Phys. Lett. 79 (2001) 10

22. W. Chen, H. Huang, S. Chen, Y. L. Huang, X. Y. Gao, A. T. S. Wee, Molecular orientation-dependent ionization potential of organic thin films. Chem. Mater. 20 (2008) 7017-7021
23. I. Salzmann, S. Duhm, G. Heimel, M. Oehzelt, R. L. Johnson, J. P. Rabe, N. Koch, Tuning the ionization energy of organic semiconductor via intermolecular bonds.
24. J. Ivanco, B. Winter, F. P. Netzer, M. G. Ramsey, Substrate mediated Electronic Structure and Properties of Sexiphenyl Films, Adv. Mater. 15 (2003) No 21
25. S. Duhm, G. Heimel, I. Salzmann, H. Glowatzki, R.L. Johnson, A. Vollmer, J.P. Rabe, N. Koch, Orientation-dependent ionization energies and interface dipoles in ordered molecular assemblies, Nat. Mater. 7 (2008) 326- 332.
26. H. -C. Lin, N. W. Polaske, L. E. Oquendo, M. Gliboff, K. M. Knesting, D. Nordlund, D. S. Ginger, E. L. Ratcliff, B. M. Beam, N. R. Armstrong, D. V, McGrath, S. S. Savendra, Electron-Transfer Processes in Zinc-Phthalocyanine-Phosphonic Acid Monolayers on ITO:Characterization of Orientation and Charge Transfer Kinetics by Waveguide Spectroelectrochemistry, J. Phys. Chem. Lett. 3 (2012) 1154
27. Y. Gassenbauer, A. Klein, Electronic and Chemical Properties of Tin-Doped Indium Oxide (ITO) Surfaces and ITO/ZnPc Interfaces Studies In-situ by Photoelectron Spectroscopy, J. Phys. Chem. B. 110 (2006) 4793

28. E. L. Hanson, J. Guo, N. Koch, J. Schwartz, S. L. Bersanek, Advanced surface modification of indium tin oxide for improved charge injection in organic device, J. Am. Chem. Soc. 127 (2005) 10058-10062.

29. J. Yun, J. Yang, Y. Hong, C. Lee, W. J. Song, Y. J. Song, Low-driving voltage, long-lifetime organic light emitting diode with molybdenum-oxide (MoO_3)-doped hole transport layers, J. of Korean Phys. Soc. 53 (2008) 1660-1664.

30. A.B. El Basaty, Y. Miyauchi, G. Mizutani, T. Matsushima, H. Murata, Optical second harmonic generation at heterojunction interfaces of a molybdenum trioxide layer and an organic layer, Appl. Phys. Lett. 97 (2010) 193302.

31. T. Hienz, Second-order nonlinear optical effects at surfaces and interfaces in Nonlinear surface electromagnetic phenomena, Elsevier Science Publishers (1991) and the reference inside.

32. R.M. Corn, A. Higgins, Optical Second Harmonic Generation as Probe of Surface Chemistry, Chem. Rev. 94 (1994) 107-125.

33. B. Dick, A. Gierulski, G. Marowski, G. A. Heider, Determination of the nonlinear optical susceptibility $\chi^{(2)}$ of surface layers by sum and difference frequency generation in reflection and transmission, Appl. Phys. B. 38 (1985) 107-116

34. S.J. Lalama, A.F. Garito, Origin of the nonlinear second-order optical susceptibilities of organic system, Phys. Rev. A 20 (1979) 1179-1194.

35. K. Kumagai, G. Mizutani, H. Tsukioka, T. Yamuchi, S. Ushioda, Second-harmonic generation in thin films of copper phthalocyanines, Phys. Rev.

B 48 (1993) 14488-14495.

36. J.J.H. Gielis, P.M. Gevers, I.M.P. Aarts, C.M. van de Sanden, W.M.M. Kessels, Optical second-harmonic generation in thin film systems, J. Vac. Sci. Technol. A 26 (2008) 1519-1537.

37. T. Yamada, D. Zou, H. Jeong, Y. Akaki. T. Tsutsui, Recoverable degradation and internal electric field forming process accompanied by the orientation of dipoles in organic light emitting diode, Synthetic Metals 111-112 (2000) 237-240

38. E. Ito, Y. Washizu, N. hayashi, H. Ishii, N. Matsuie, K. Tsuboi, Y. Ouchi, Y. Harima, K. Yamashita, K. Seki, Spontaneous buildup of giant surface potential y vacuum deposition of Alq_3 and its removal by visible light irradiation, J. of Appl. Phys. 92 (2002) 7306-7310

39. T. Miyamae, N. Takada, T. Tsutsui, Probing buried organic layers in organic light-emitting diodes under operation by electric-field-induced doubly resonant sum-frequency generation spectroscopy, Appl. Phys. Lett. 101 (2012) 073304.

40. R. K. Chang, J. Ducuing, N. Bloembergen, Relative phase measurement eween fundamental and second harmonic light, Phy. Rev. Lett. 15 (1965) 6-8

41. K. Kemnitz, K. Bhattacharyya, J.M. Hicks, G.R. Pinto, K.B. Eisenthal, T. Heinz, The Phase of Second-Harmonic Light Generated at an Interface and its Relation to Absolute Molecular Orientation, Chem. Phys. Lett. 131 (1986) 285-290.

42. O. Sato, R. Baba, K. Hashimoto, A, Fujishima, Second Harmonic Generation Coherent Interferometry Disclosing the Orientation of the Submerged Hemicyanine Layer in a Langmuir-Blodgett Multilayer Structure, J. Phys. Chem.

95 (1991) 9636-9638.

43. R. Stolle, G. Marowski, E. Schwarzberg, G. Berkovic, Phase measurements in nonlinear optics, Appl. Phys. B 63 (1996) 491-498.

44. M. Buck, F. Eisert, M. Grunze, F. Träger, Second-order nonlinear susceptibilities of surfaces: A systemaitic study of the wavelength and coverage dependence of thiol adsorption on polycrystalline gold, Appl. Phys. A 60 (1995) 1-12.

45. T. Suzuki, D.E. Milovzorov, S. Kogo, M. Tsukakoshi, M. Aono, Surface second-harmonic generation spectra of Si(111)-7x7 in the 1.0-1.7eV fundamental photon energy, Appl. Phys. B 68 (1998) 623-627.

46. O.A. Aktsipetrov, T.V. Dolgova, A.A. Fedyanin, D. Schuhmacher, G. Marowsky, Optical second-harmonic phase spectroscopy of the Si(111)-SiO_2 interface, Thin Solid Films 364 (2000) 91-94.

47. R. Lü, Y. Rao, W-k. Zhang, H-f. Wang, Phase measurement in nonlinear optics of molecules at air/water interface with femtosecond laser pulses, Proc. of the SPIE Conference on Nonlinear Spectroscopy 4812-15 (2002) 115-124.

48. P. T. Wilson, Y. Jiang, R. Carriles, M. C. Downer. Second-harmonic amplitude and phase spectroscopy by use of broad-bandwidth femtosecond pulses, J. Opt. Soc. Am. B 20, (2003) 12

49. Y. Jeon, H. Min, D. Kim, M. Oh-E, Determination of the Crystalline *x*-Axis of Quartz by Second-Harmonic Phase Measurement, J. Korean Phys. Soc. 46 (2005) 159-162.

50. A.L. Mifflin, M.J. Musorrafiti, C.T. Konek, F.M. Geiger, Second Harmonic

Generation Phase Measurement of Cr(VI) at a Buried Interface, J. Phys. Chem. B, 109 (2005) 24386-24390.

51. T. Yamada, Y. Haruyama, K. Kasai, T. Terui, S. Tanaka, T. Kaji, H. Kikuchi, A. Otomo, Orientation of dip-coated aceriohodopsin thin film studied by second harmonic generation interferometry, Japan J. Appl. Phys. 2 (2013) 05DB03
52. R. Macovez, M. Mariano, S. Di Finizio, J. Martorell, Measurement of dispersion or air and of refractive index anomalies by wavelength-dependent nonlinear interferometry, Optics Express 17 (2009) 13881-13888

Chapter 2

Theory of Second Harmonic Generation

Second harmonic generation (SHG) is a proficient technique for the study of molecular structure and conformations, as well as dynamics of molecular interface [1]. It is a second order nonlinear process in which two photons with the same fundamental frequency ω interact with a nonlinear medium simultaneously to generate a photon with the second harmonic frequency 2ω. In this chapter, I will present the foundation of nonlinear optics to guide a better understanding and application of SHG studies at the molecular interface in general.

2.1 Linear and nonlinear optical response

Optics is defined as the branch of physics that studies the behavior and property of light. This includes its interaction with matter, since the light is an electromagnetic radiation. The interaction of electromagnetic field can be derived from Maxwell's equations (Eq. 2.1 -2.4):

$$\vec{\nabla} \cdot \vec{D} = \rho \qquad (2.1)$$

$$\vec{\nabla} \times \vec{\mathrm{H}} = \frac{\partial \vec{\mathrm{D}}}{\partial \mathrm{t}} + \vec{\mathrm{J}} \tag{2.2}$$

$$\vec{\nabla} \times \vec{\mathrm{E}} = -\frac{\partial \vec{\mathrm{B}}}{\partial \mathrm{t}} \tag{2.3}$$

$$\vec{\nabla} \cdot \vec{\mathrm{B}} = 0 \tag{2.4}$$

The relationship of the electric field displacement, $\vec{D}$ and the electric field, $\overrightarrow{E}$ in Eq. 2.5 is purely material properties that present in both linear and nonlinearities [2].

$$\vec{D} = \epsilon_0 \overrightarrow{E} + \overrightarrow{P} \tag{2.5}$$

Here, the ϵ_0 is the permittivity of vacuum and the polarization field, $\vec{P}$ represents the bulk polarization of the dipole moment per unit volume. In a medium of condensed phase, the $\vec{P}$ is the sum of molecular electric dipoles [3]. Let us begin with the discussion of polarization in the presence of weak electric field,

$$\vec{P}(\omega) = \epsilon_0 \chi^{(1)} . \overrightarrow{E}(\omega) \tag{2.6}$$

$\chi^{(1)}$ as the first order electric susceptibility of the medium in the frequency of the incident field. In Eq. (2.6), $\chi^{(1)}$ is a linear response of the medium since the polarization field carries the same frequency. This process is related to the production of linear optical properties such as reflection and refraction in a medium.

On the other hand, the polarization is no longer linear when the incident electric field is strong. Additional higher order terms of the polarization will appear as shown in Eq. (2.7).

$$\vec{P} = \vec{P}^{(1)} + \vec{P}^{(2)} + \vec{P}^{(3)} + \cdots \tag{2.7}$$

$$\vec{P} = \epsilon_0 \overleftrightarrow{\chi}^{(1)} \vec{E} + \epsilon_0 \overleftrightarrow{\chi}^{(2)} : \vec{E}\,\vec{E} + \overleftrightarrow{\epsilon_0 \chi}^{(3)} : \vec{E}\,\vec{E}\,\vec{E} + \cdots \quad (2.8)$$

In return, additional susceptibilities are also incorporated into the term of polarization, $\vec{P}$ [3]. These nonlinearity terms are normally insignificant in the presence of weak field.

The polarization term can also be rewritten with ith component as following:

$$P_i = \sum_j \chi_{ij}^{(1)} E_j + \sum_{jk} \chi_{ijk}^{(2)} E_j E_k + \sum_{jkl} \chi_{ijkl}^{(3)} E_j E_k E_l + \cdots \quad (2.9)$$

These terms are summed over repeated indices. Here, the subscripts *i*, *j*, *k* and *l* are dummy indices. The first coefficient term $\overleftrightarrow{\chi}^{(1)}$ is the linear electric susceptibility while the higher orders of $\overleftrightarrow{\chi}^{(n)}$ are the nth order nonlinear susceptibilities. As $\chi^{(n)}$ is a (n+1)th rank tensor, the second order susceptibility that applies for second harmonic generation (SHG) is a third rank tensor.

Focusing on the second order polarization field, $\vec{P}^{(2)}(t)$, one can expand the term into Eq. (2.10) with the $\vec{E}_0$ as the static electric field in a nonlinear medium with non-zero $\overleftrightarrow{\chi}^{(2)}$. Meanwhile, the incident electric field, $\overrightarrow{E}$ is being explicitly defined as optical electric field, $\vec{E}_\omega(t) = \vec{E}_\omega(e^{i\omega t} + e^{-i\omega t})$.

$$\begin{aligned}\vec{P}^{(2)}(t) &= \overleftrightarrow{\chi}^{(2)} : \vec{E}^2(t) = \overleftrightarrow{\chi}^{(2)} : [\,\vec{E}_\omega\left(e^{i\omega t} + e^{-i\omega t}\right) + \vec{\mathrm{E}}_0]^2 \\ &= \overleftrightarrow{\chi}^{(2)} : [\vec{E}_\omega^2\left(e^{i2\omega t} + e^{-i2\omega t}\right) + 2\vec{E}_0\vec{E}_\omega\left(e^{i\omega t} + e^{-i\omega t}\right) + 2\vec{\mathrm{E}}_\omega^2 + \vec{E}_0^2]. \quad (2.10)\end{aligned}$$

The polarization contains components oscillating at both ω and 2ω frequencies. The first

term represents the light with frequency 2ω is the second harmonic generations (SHG). The second term with the fundamental frequency, ω can be referred as the linear electro-optic effect while the third term is the optical rectification that does not oscillate as a function of time. This term produce a static DC field.

Until here, the fundamental of linear and nonlinear optical response of a medium has been established. In the next section, the response of nonlinear susceptibility $\chi^{(2)}$ in the SHG of molecular system will be delivered.

2.2 Second order nonlinear susceptibilities, $\chi^{(2)}$ of nonlinear media

Using the derivation of electron oscillation motion, Eq. (2.11) can be applied as accurate definition of susceptibility of medium under study. The susceptibility $\chi(\omega)$ will be a function of angular frequency [4]. The susceptibilities are different for different angular frequencies, thus dispersion is unavoidable [4]. Dispersion as a function of frequency is shown in Fig. 2.1

$$\chi(\omega) = \frac{Ne^2}{m\epsilon_0} \frac{1}{\omega_0^2 - \omega^2 - 2i\eta\omega} \tag{2.11}$$

Equation (2.11) is based on a simple model of a number of electrons, *N* that forced to

oscillates under the force of oscillating electric field, $E(t)$. It is a sum over terms since not all electrons have the same resonance frequency, ω_0 and same damping constant, η. The static value of $\chi(0)$ is always positive and real, while the imaginary part of the susceptibility is always non-negative and can be large when close to resonance [4].

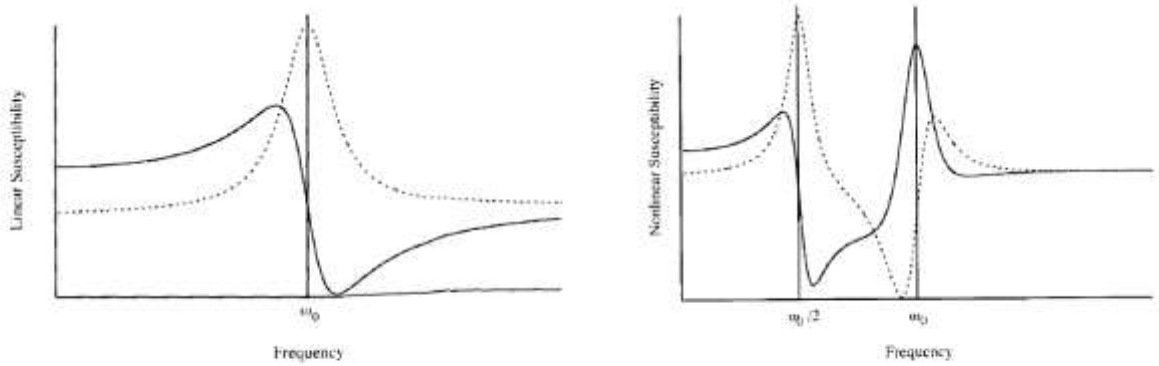

Figure 2.1 Linear (left) and nonlinear (right) susceptibility as a function of frequency, ω. In both figures, the solid lines stands for the real part and the dashed lines represent the imaginary part [5].

Because the nature of the polarization field depends on the incident electric field, the effects resulting from the nonlinear susceptibilities are given by a shorthand notation denoted by the appropriate order susceptibility and incident and resultant electric field frequencies. Thus, the second order term in Eq. (2.10) can be rewritten as:

$$P_i^{(2)}(\omega_3) = \sum_{jk} \chi_{ijk}^{(2)}(\omega_3; \omega_1, \omega_2) E_j(\omega_1) E_k(\omega_2) \qquad (2.12)$$

with ω_1 and ω_2 are the frequencies of the incident electric fields, and ω_3 is the output

frequency. SHG is emitted when the incident frequencies are the same, that is when $\omega_1 = \omega_2$. However, when the $\omega_1 \neq \omega_2$ the phenomenon is called as sum frequency generation (SFG). Among the nonlinear effects, SFG spectroscopy is a well-known nonlinear optical approach that utilizes quantitative measurement of second order nonlinear susceptibilities in material study. The SFG concepts can also be applied to SHG.

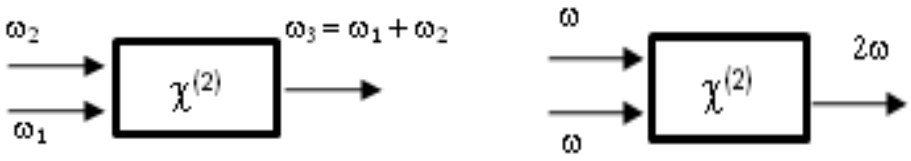

(a) SFG (b) SHG

Figure 2.2 The nonlinear susceptibilities of $\chi^{(2)}$ in (a) SFG effect, and (b) SHG effect [6]

Both SHG and SFG can serve as surface spectroscopic tools, but the SHG is mostly known to probe electronic transitions [7]. In Fig. 2.3, the SHG process is visualized using the interaction of photons with an electron. Two photons with the same photon energy $\hbar\omega$ incident on the media excite an electron, then the electron can only be temporarily excited before returning to the ground state and a new photon with energy $2\hbar\omega$ is generated simultaneously.

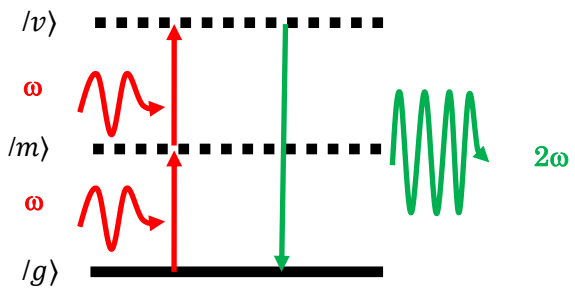

Figure 2.3 Energy-level diagram illustrating the second harmonic generation process. The |*g*>, |*m*> and |*v*> is the ground, other (virtual) and excited electronic states, respectively [6].

2.2.1 Nonlinear susceptibilities of molecular system

Nonlinear effects are only significant when the applied electric field is comparable with the field experienced by the electrons in the molecules. Field of this magnitude is normally achieved with pulsed laser [3]. Franken and co-workers had reported the first successful non-linear optical experiment in 1961 when they observed second harmonic generation from quartz crystal irradiated by ruby laser [3]. Like quartz, most solid can be considered as a second-order nonlinear material with exception of centrosymmetric material. This condition can be explained by cancellation of $\vec{P}^{(2)}(t)$ by $-\vec{P}^{(2)}(t)$ in centrosymmetric medium. The first polarization, $\vec{P}^{(2)}(t) = \overleftrightarrow{\chi}^{(2)}:\vec{E}^{2}(t)$ but because of inversion symmetry, $-\vec{P}^{(2)}(t)$ is also produced. This second polarization has the same magnitude as the first but with different sign in polarization.

$$-\vec{P}^{(2)}(t) = \overleftrightarrow{\chi}^{(2)}:[-\vec{E}(t)]^2 = \overleftrightarrow{\chi}^{(2)}:\vec{E}^2(t) \quad (2.13)$$

As a result, the net polarization and the resulting second order susceptibility, $\chi^{(2)}$ from the bulk centrosymmetric medium is zero. This effectively means that the $\chi^{(2)}$ can only originated from the surface, the only broken symmetry in the medium. This way using the SHG has become advantageous as selective probe for studying the surfaces and interfaces of a centrosymmetric media.

The nonlinear susceptibilities of common solid materials had been known for quite some time as the SHG is easily the simplest approach to measure the quantity of $\chi^{(2)}$ of nonlinear medium. Table 2.1 is a list of the second order nonlinear susceptibilities of some well-known nonlinear material cited from Ref. 8 and Ref. 9 [8, 9]. Some of the crystals served as parametric oscillators while the GaAs and α-SiO_2 are employed in typical SHG measurements as reference crystals.

Similar to the crystal solids, the symmetry requirement in molecular solid should also be fulfilled for the second order nonlinear processes to occur. Slightly challenging but one can effectively determine the $\chi^{(2)}$ of a molecular system by estimating the molecular polarizability, β of the system. The $\chi^{(2)}$ is the macroscopic average of the molecular polarizabilities, β of the molecules and each non-zero tensor component of β_{ijk} is associated with a particular molecular vibration [1, 3].

Table 2.1. Nonlinear optical susceptibilities of some well-known nonlinear materials

([a]Kumagai, [b]Shen)

Material	$\chi^{(2)}$ **(3/4π x10^{-8} esu)**
Quartz (α-SiO_2)[a,b]	$\chi^{(2)}_{XXX}$ = 0.8 ± 0.04
Potassium dihydrogen phosphate (KDP)[a,b]	$\chi^{(2)}_{XYZ}$ = 0.98 ± 0.04
Lithium niobate ($LiNBO_3$)[a,b]	$\chi^{(2)}_{ZZZ}$ = 81.4 ± 21
Gallium arsenide (GaAs)[b]	$\chi^{(2)}_{XYZ}$ = 377 ± 38
Cooper phthaocyanine (CuPc)[a]	$\chi^{(2)}_{ZYY}$ = 18.9 ± 6.3
2-methyl-4-niroaniline (MNA)[a]	$\chi^{(2)}_{XXX}$ = 500 ± 200

$$\chi_{ijk} = N_s \sum_{i'j'k'=abc} \langle R_{ii'} R_{jj'} R_{kk'} \rangle \beta_{i'j'k'} \tag{2.14}$$

The general third rank tensor, β has 27 tensor elements in total. In Eq. (2.14), the N_s is the molecular density and the operator $\langle\ \rangle$ denotes the orientational ensemble average over the Euler rotation matrix transformation element $R_{\lambda\lambda'}$ from the molecular coordinate $\lambda'(a,b,c)$ to the laboratory coordinate $\lambda(x,y,z)$, through the Euler angles [1]. The subscripts (*i*,*j*,*k*) of the χ_{ijk} correspond to the laboratory coordinate (*x*,*y*,*z*) and the subscripts (*i'*,*j'*,*k'*) of the $\beta_{i'j'k'}$ correspond to the molecular coordinate (*a*,*b*,*c*) [1]. The knowledge to perform Euler transformation analysis is a requirement in order to extract the molecular information of β_{ijk} from the measurement of second order nonlinear optical

signal.

Fortunately, the number of independent tensor elements of χ_{ijk} can be reduced to 18 in the 'permutation symmetry' in SHG. This number could be further reduced with consideration of molecular symmetry. For example in a rotationally isotropic achiral molecular system, there can be only 7 non-zero χ_{ijk} tensor elements [1]. Thus, the microscopic term of β_{ijk} of an individual molecule can be easily determined using quantitative analysis of SHG data. This demonstrates one of the useful points that can be achieved by using the SHG to study molecular interfaces and thin films.

2.3 SHG from the interface of molecular system

The restriction of SHG in a bulk centrosymmetry medium allows the contribution from surface to materialize selectively. This makes SHG a convenient tool for surface studies, and also for the study of buried interface. At the interface between two centrosymmetric media, only the first few atomic or molecular monolayers on both sides of interface participate in the symmetry breaking [1]. Equation (2.15) gives the formula of SHG intensity from the interface measured in reflection configuration [1].

$$I(2\omega) = \frac{32\pi^3\omega^2 sec^2\Omega}{c_0^3\, n_1(\omega)n_1(\omega)n_1(2\omega)} \left|\chi_{eff}\right|^2 I\,(\omega)^2 \qquad (2.15)$$

Here it is shown that the SHG intensity, $I(2\omega)$ increases quadratically with the intensity of fundamental light, $I(\omega)$. c_0 is the speed of the light in the vacuum and Ω is the incident angle from the surface normal. The effective susceptibility χ_{eff} described in this equation is macroscopic property from the medium.

$$\chi_{eff} = [L(2\omega):\hat{e}(2\omega)].\chi \ :[L(\omega):\hat{e}(\omega)].[L(\omega):\hat{e}(\omega)] \quad (2.16)$$

The 27 tensor elements of χ in total can be reduced to lower number of non-zero tensors but more importantly, by employing specific polarization combination, a particular tensor of the susceptibility can be measured. In Eq. (2.16), there is also $\hat{e}(2\omega)$ and $\hat{e}(\omega)$, both represents the unit vectors of the electric field corresponding to 2ω and ω frequencies, respectively. $L(2\omega)$ and $L(\omega)$ are the respective tensorial Fresnel factors.

In many SHG studies, all molecular information of χ_{eff} is obtained experimentally using both amplitude and phase factor [1]. However, it is also necessary to address the macroscopic effect in the SHG measurement such as the Fresnel factors in order to be accurate. Also, several researches mentioned on the importance of the refractive index of the interface/molecular layer [1]. This interface layer is constituted of several molecules with certain orientational order and its dielectric properties are different from those of the bulk materials formed with the same molecules [1]. However this macroscopic effect can become negligible for many case of molecular monolayer with thickness much smaller than the wavelength [1].

Analysis of SHG from molecular system also includes consideration of the microscopic local field factors. This analysis will be advantageous since it carries the information of the anisotropy of oriented material under the effect of molecular polarizabilities β_{ijk} of the system. The microscopic factor and also the dielectric constants in the molecular layer can be complex values, especially for closely packed chromophores with relatively large linear polarizability values at incident or second harmonic frequencies [1].

Another implication of the SHG experiment is to understand the nature of the $\chi^{(2)}$ response, in most cases is when the underlying substrate is SHG active. Thus, additional susceptibilities describing the behavior of $\chi^{(2)}$ from the substrate should be introduced [3]. The $\chi^{(2)}$ can be composed into resonant and non-resonant.as described by Eq. (2.17)

$$\chi^{(2)} = \chi_R^{(2)} + \chi_{NR}^{(2)} \tag{2.17}$$

Generally, the $\chi_{NR}^{(2)}$ of dielectric substrates is very small unless the incident ω matches the molecular transition but for metal substrates, the $\chi_{NR}^{(2)}$ can be a significant value due to the effect of surface plasmon resonance [3]. The SHG spectroscopic method is useful to investigate the complex nature of both $\chi_R^{(2)}$ and $\chi_{NR}^{(2)}$ as the output frequency can be resonantly enhanced when the input frequency is tuned over the resonance of any electronic transition [5].

The content of this chapter has introduced several ideas among wide range analysis of the interface studies using second order nonlinear effects such as SHG. The interfacial region between bulk media, although often comprising only a fraction of the material present are the site of reactions and phenomena that dominates the macroscopic properties of the entire system [3]. Since it is a considerable interest to pursue the physics originated from the interface of organic semiconductor solid, thus the SHG study is always a desirable approach.

References:

1. W-k. Zhang, H-f. Wang, D-s. Zheng, Quantitative measurement and interpretation of optical second harmonic generation from molecular interfaces, Phys. Chem. Chem. Phys. 8 (2006) 4041-4052
2. R. W. Boyd, Nonlinear Optics, third ed., Academic Press, Oxford, 2008
3. A. G. Lambert, P. B. Davies, D. J. Neivandt, Implementing the Theory of Sum Frequency Generation Vibrational Spectroscopy: A Tutorial Review, Applied Spectroscopy Reviews, 40:2 (2005) 103-145
4. P. Hertel, Lectures on Theoretical Physics: Linear Response Theory, University of Osnabrück, Germany.
5. P-F. Brevet, Surface Second Harmonic Generation, (1997) PPUR presses polytechniques.
6. A. B. El Basaty, Investigation of organic interfaces by using optical second harmonic generation (SHG) and sum frequency generation techniques. Dissertation. (2011) JAIST and the reference inside
7. X. Zhuang, P. B. Miranda, D. Kim, Y. R. Shen, Mapping molecular orientation and conformation at interfaces by surface nonlinear optics, Phys. Rev. B. 59 (1999) 19
8. K. Kumagai, G. Mizutani, H. Tsukioka, T. Yamuchi, S. Ushioda, Second-harmonic generation in thin films of copper phthalocyanines, Phys. Rev. B 48 (1993) 14488-14495.
9. Y. R. Shen, The Principles of Nonlinear Optics, (2003) Wiley-Interscience

Chapter 3

Experimental Aspects of Nonlinear Optical Measurement of Second Harmonic Generation (SHG)

Disadvantage in electron probes such as ultraviolet photoelectron spectroscopy (UPS), X-ray photoemission spectroscopy (XPS), inverse-photoelectron spectroscopy(I-PS) and low energy electron diffraction (LEED) methods is that it can not generally access interfaces with considerable front thickness [1-6]. The second-order nonlinear optics techniques, both second harmonic generation (SHG) and sum frequency generation (SFG) can be useful in probing buried interfaces [7-10]. The experimental set-up is relatively simple, particularly in the case of SHG [11].

In this study, the optical signal of SHG is measured to characterize the electric field at the interface of ITO/organic as a function of organic materials. The amplitude and the phase of SHG are measured in different experiments. And, the electronic resonance near the 2ω frequency is characterized using SHG spectroscopy. In these measurements, the bare substrate of indium tin oxide (ITO) was employed as reference. The use of ITO as reference is justified, similar to SHG measured from SAMs on a SHG active metal [12].

3.1 Sample Preparation

The samples are fabricated in collaboration with Murata Laboratory in Japan Advanced Institute of Science and Technology (JAIST). The samples consist of bare ITO and several structures of ITO/organic semiconductor thin film. The 150 nm-thick ITO-coated glass substrates are manufacturer product (Atsugi Micro). Standard cleaning of the substrates with acetone, detergent, pure water and isopropanol and UV-ozone treatment are done prior to the organic deposition. The base pressure is 10^{-4} Pa and the deposition rate is 0.1 nm/s, the organic thin films are each prepared at thickness of 100 nm. The bare ITO and ITO/organic samples are then transferred into a nitrogen filled glove box (gas concentration of O_2 and H_2O less than 2 ppm) to be encapsulated by a glass cap using UV curing epoxy resin.

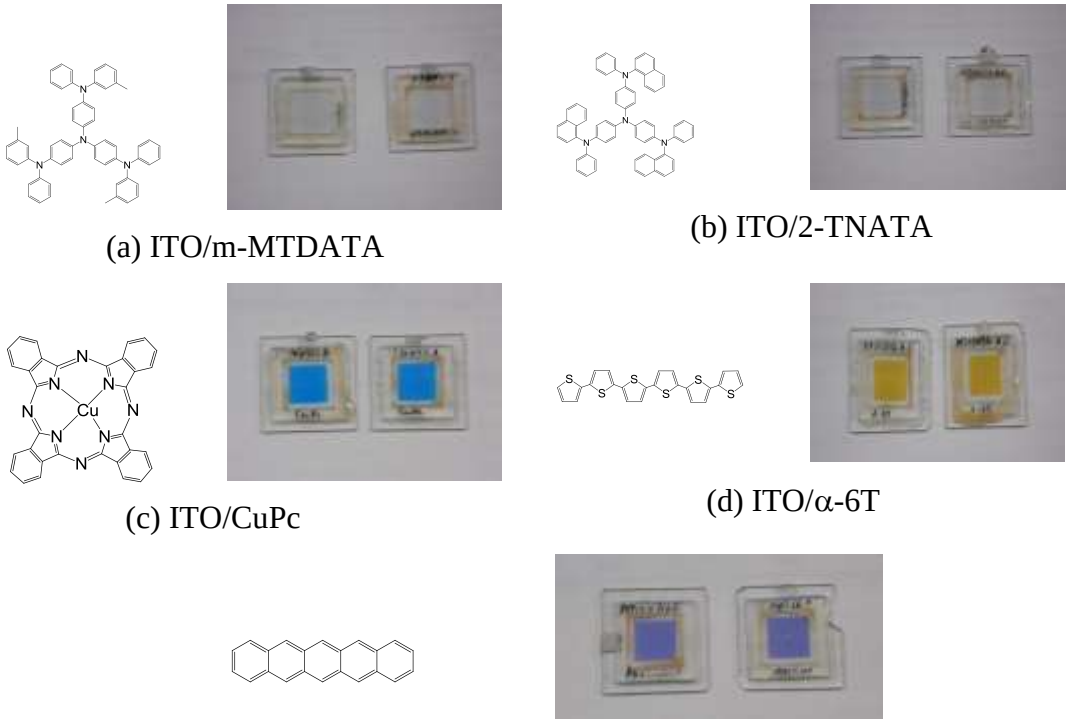

(a) ITO/m-MTDATA

(b) ITO/2-TNATA

(c) ITO/CuPc

(d) ITO/α-6T

(e) ITO/pentacene

Figure 3.1 The snapshots of the samples. ITO substrates is the pale strip at the center of the glass (4 mm x 24 mm). From the top left (a) ITO/2-TNATA (b) ITO/m-MTDATA (c)

ITO/CuPc (d) ITO/α-6T and (e) ITO/pentacene.

Figure 3.1 also shows the molecular structure of respective organic molecules. The m-MTDATA and 2-TNATA are C_3 symmetry molecules and CuPc molecule possess a C_4 symmetry structure. On the other hand, the α-6T and pentacene are C_2 and C_{2v} symmetry molecule, respectively. Prior to the SHG measurement, the ionization energies of the substrate ITO and the organic thin films are measured by AC-photoelectron spectroscopy (Riken Keiki). The ionization energy is defined as the energy difference between the highest occupied molecular orbital (HOMO) of the organic thin film with the vacuum level [13]. In this investigation, this energy is used as the bench mark to estimate the electron donating power of the molecular system. The work function of ITO is also measured in the same way.

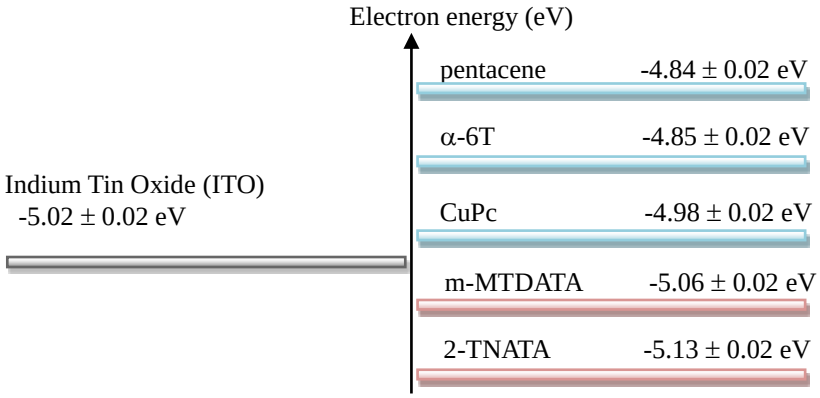

Figure 3.2 The diagram of ionization energies of organic semiconductor layer and the work function of ITO. The electron energy given by the AC-photoelectron spectroscopy (Riken Keiki) is measured with respect to the vacuum level.

The charge transfer at metal/organic and organic/organic has been discussed in many literatures by energy level alignment but still, the property of the dipole layer at the interface is not properly established among variety of organic semiconductors. Here, the general idea is to use the magnitude of the SHG signal from the sample to infer the strength of the charge transfer at the interface. However, the ITO is also an active SHG medium with SHG intensity proportional with the thickness of ITO film. The SHG from ITO is dominantly a bulk response with the surface SHG negligible in comparison. In this condition, the SHG contributed by the interface of the ITO/organic structures will be superposed to the SHG from bulk ITO, hence the main content of this dissertation will be to demonstrate the rigorous analysis to handle the SHG data so that the contribution from the interface can be determined.

3.2 SHG intensity measurement of double layered structure of indium tin oxide (ITO) and organic semiconductor

The first step is to measure the respective SHG intensity of bare ITO and ITO/organic. The optical set up for the SHG intensity measurement is illustrated in Fig. 3.3. The 1064 nm laser output from EKSPLA PL2143 Nd:YAG laser (pulse duration of 30 ps, repetition rate of 10 Hz) is used to irradiate the sample. The energy that arrived on the sample is *p*-polarized and estimated to be 45 μJ/pulse. The diameter of the laser spot on the sample surface is ~1 mm. Optical filter, F1 (Sigma Koki, R62) is used to screen out visible light in the incident output line and IR filters, F2 (Sigma Koki, SCF-50S-580) filtered the 1064 nm light going to the monochromator unit. Focusing

lens L1 (*f* = 350 mm), L2 (*f* =150 mm) and L3 (*f* =100 mm) were employed. The SHG light that arrived at the end of the optical line is 532 nm. The photomultiplier (Hamamatsu Photonics) transformed the optical signal into electrical signal and transmitted the output to the pre-amplifier (Ortec). The signal is then processed by the box car (A/D converter, Stanford Research Systems) and SHG photon counts are analyzed by the personal computer.

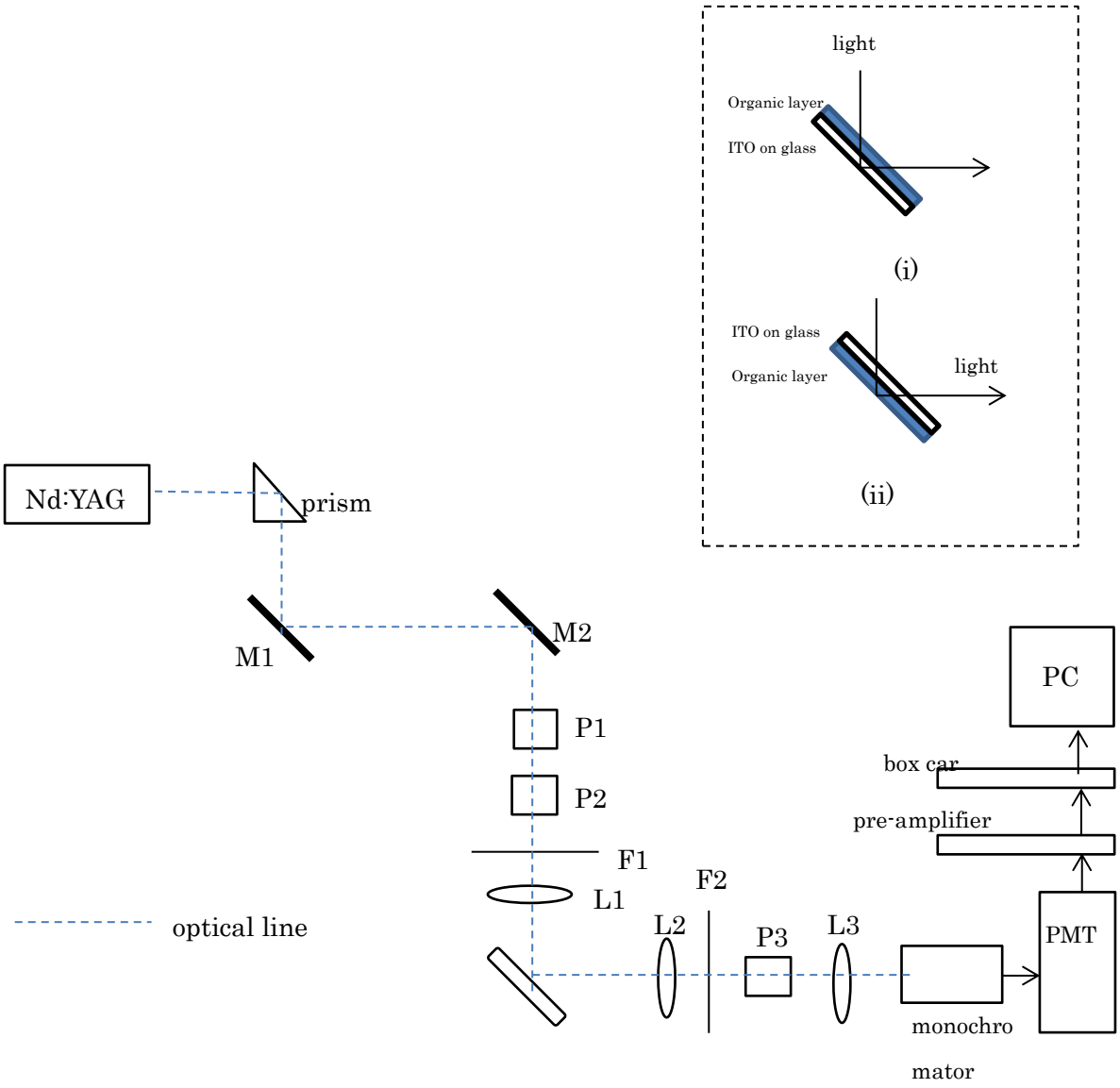

Figure. 3.3 The experimental set up of SHG measurement consists of several optics such as mirrors (M1 and M2), half-wave plate polarizer (P1), linear polarizer (P2 and

P3), optical filters (F1 and F2) and lens (L1, L2 and L3) Inset shows the sample configuration for SHG intensity measurement in (i) organic layer incident and (ii) glass incident.

The surface energy density is 3-5 mJ/cm^2. The SHG is measured from fundamental light incident on the surface of organic layer and also on surface of glass substrate of ITO for comparison purpose. Both incident configurations are shown in the top inset of Fig. 3.3. GaAs (001) is used as the reference for the measurement. In this experiment, the bulk organic films showed fundamentally negligible amount of SHG compared to the organic film deposited on the ITO.

3.2.1 Linear spectroscopy

Previously in Eq. (2.16), the macroscopic susceptibility of the material under study, χ_{eff} is shown to be comprises of L factors that relates the input macroscopic electric fields to the susceptibility, χ_{ijk} [15]. The L factors are otherwise known as Fresnel coefficients and they are also frequency dependent parameters. In thin film system, the Fresnel factor is analyzed using two or three layer model. The change of the Fresnel factor in ITO/organic system is mainly derived from the effect of absorption of incident or SHG light by organic layer coverage [14]. This is a bulk response of the material that depends on the linear refractive indices of the bulk layer. Intuitively, the linear response of the bulk organic layer must be separated from the SHG response for it can lead to misinterpretation of the data. In this example of sum frequency generation

spectra in Fig. 3.4, the Fresnel factor effects had given rise to strong spectral structures that can be confused with the presence of particular interfacial vibrational resonance [16].

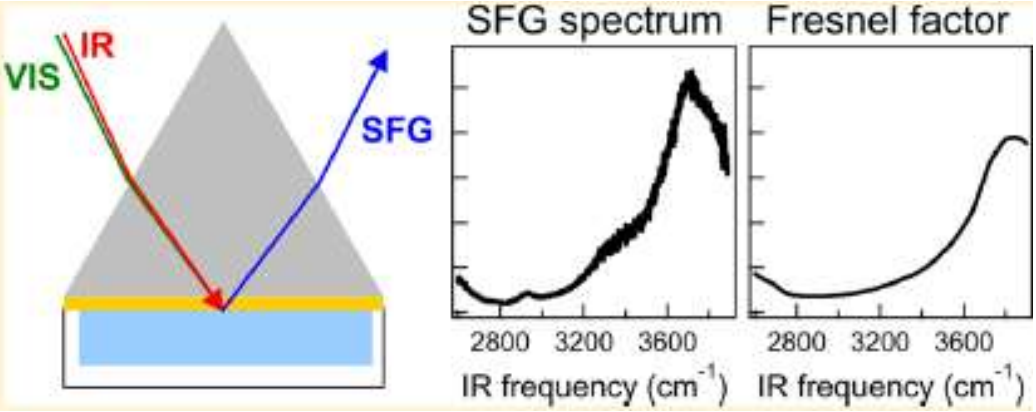

Figure 3.4 The effect of Fresnel factors to SFG spectra from metal/water and metal-oxide/water interfaces [16].

The Fresnel factor analysis is produced using the linear spectra of ITO and ITO/organic samples at both fundamental and SHG wavelengths (1064 nm and 532 nm) at reflectance and transmittance configuration. The linear spectroscopy system employed the Xenon light source and the optical set-up of linear experiment is described in Fig. 3.5. The flow chart in Fig. 3.6 shows the analysis steps taken to extract the SHG from the interface. Later in Chapter 4, the analysis of two layer model will be produced. In this model, the refractive index of the interface monolayer is set as 1 and the multireflection is not considered for the film is thick [12].

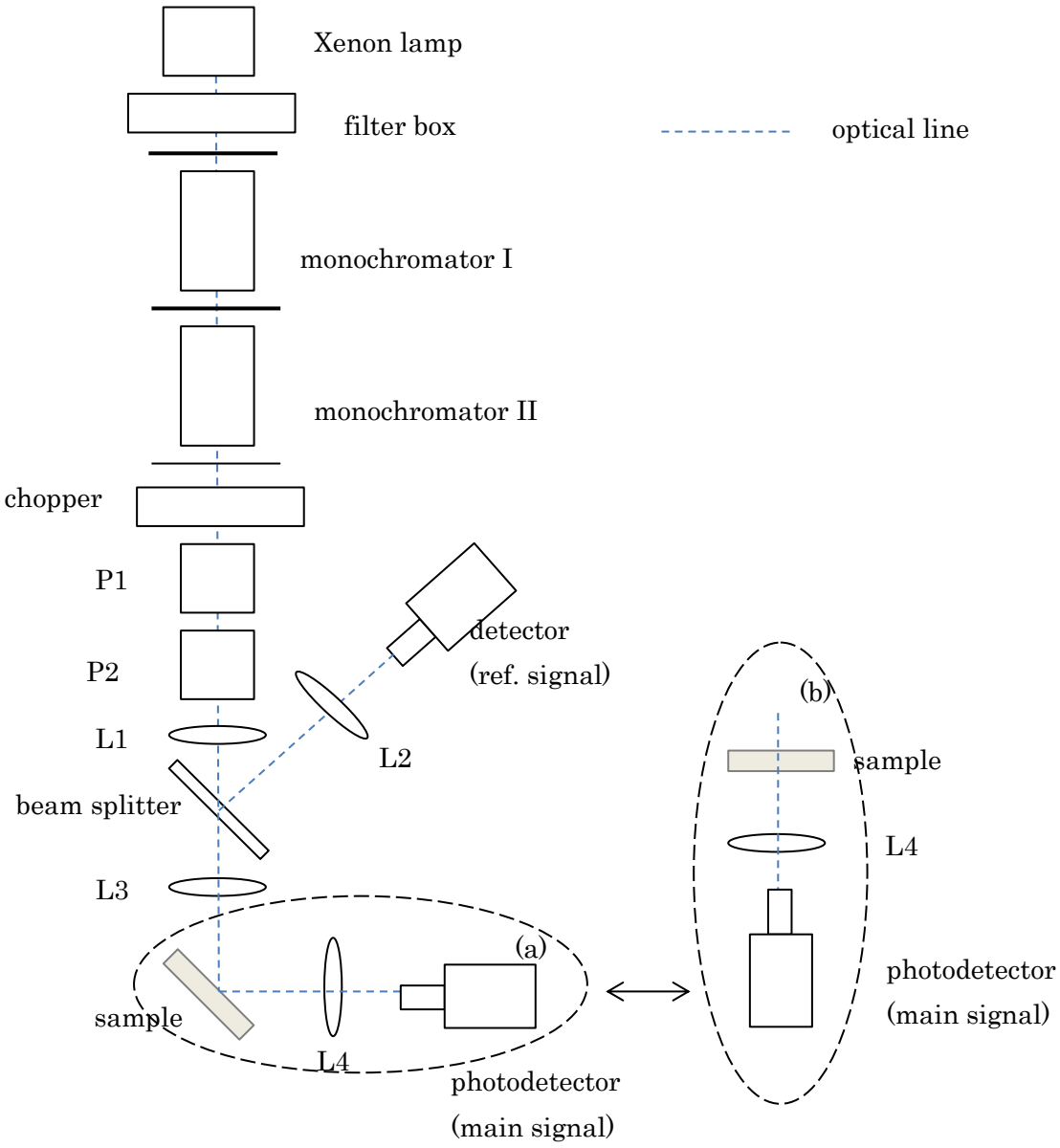

Figure 3.5. The optical set up for linear measurement. The alignments (a) for transmission configuration and (b) reflectance configuration. P1 and P2 are polarizers and L1, L2 and L3 are focusing lens.

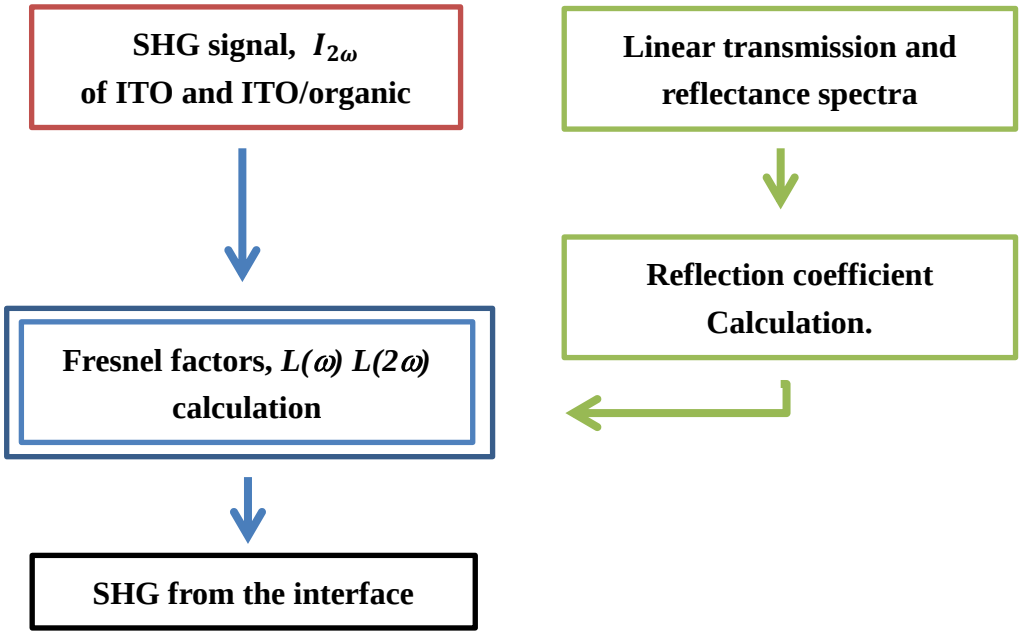

Figure 3.6 Schematic illustration of the SHG analysis on ITO/organic.

3.3 SHG spectroscopy

The purpose of the SHG spectroscopy is to study the spectral behavior of ITO and ITO/organic samples near the 2.33 eV, the SHG photon energy. The spectra can provide advantageous information as there is a need to recognize the resonant nature of $\chi^{(2)}$ contributed by electronic transition that may take place in the molecular system. As shown in Fig. 3.7, the SHG spectroscopy unit consisted of optical parametric generation (OPG) and the harmonic unit, pumped by 1064 nm output from Nd:YAG laser source. The system generated a stable and monochromatic broad range of wavelength by tuning of optical parametric crystal, lithium triborate (LBO).

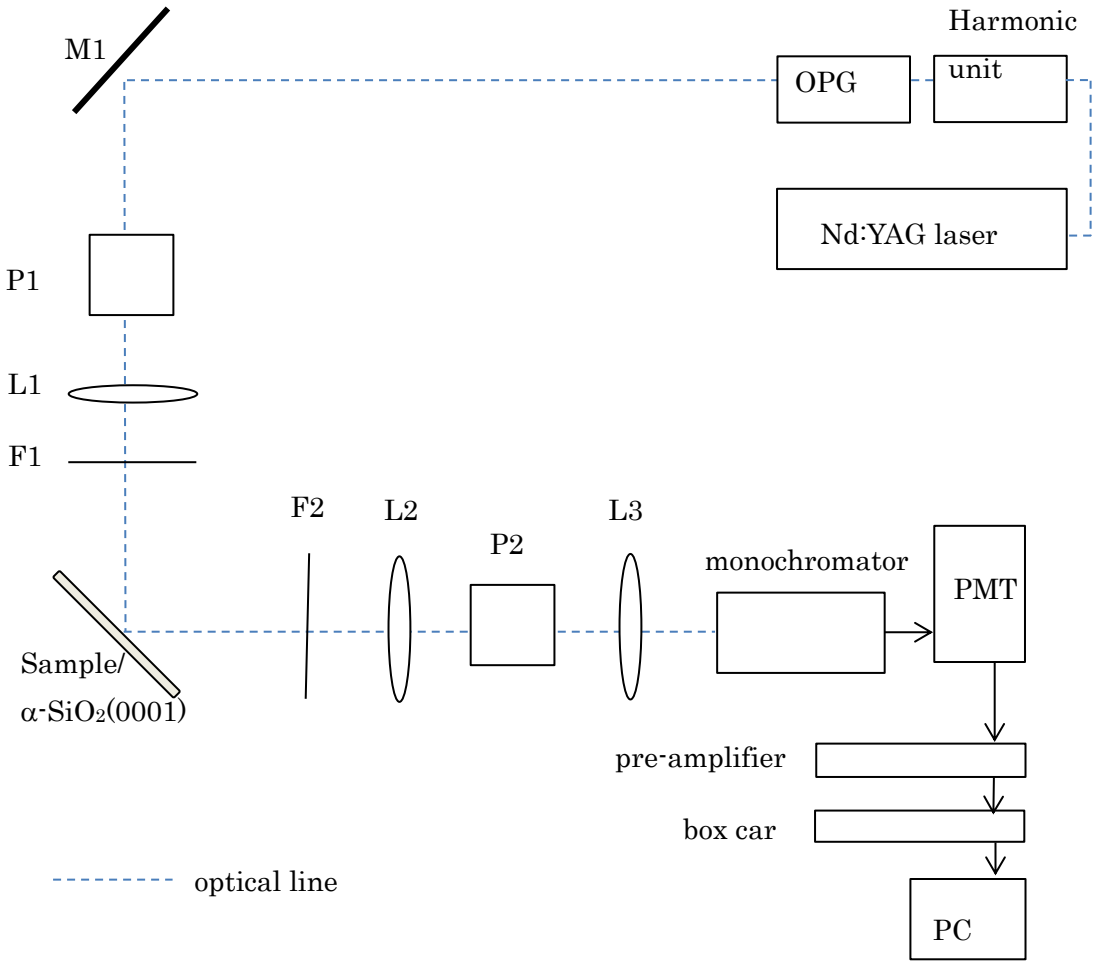

Figure 3.7 The experimental set up of SHG spectroscopy. P1 and P2 are the linear polarizer, F1 and F2 are optical filters and L1, L2 and L3 is the focusing lens.

The bandwidth of the IR output from tunable OPG (PG 401) is 0.8 meV. The SHG at the range of $2\hbar\omega$ energies, 2.04 - 2.48 eV is measured along with the SHG from α-quartz or α-SiO_2 (0001).The crystal acts as a reference to correct the signal sensitivity on the wavelength and energy dependence [14].

3.4 SHG interferometry phase measurement

In certain applications of SHG, the measurement of phase of the $\chi^{(2)}$ can be equally important [11]. The phase measurement is mandatory when the electronic resonance is responsible for generation of SHG signal [12]. The phase of SHG is conventionally measured by the interferometry technique. As implied from 'interferometry', the phase of $\chi^{(2)}$ is directly measured from superposition of the second harmonic signal of the sample, $E_{sample}^{(2\omega)}$ with another signal from of a second (reference) SHG source, $E_{reference}^{(2\omega)}$. An optical phase delay between these two sources is introduced to produce an interference pattern from which the phase of SHG can be deduced. In the experiment used by Kemnitz et al. [17], the dispersion of air has been employed as the optical phase delay. Their measurement is established with variation of distance between the two sources. The distance, l_o , taken by the second source to move in order for the interference signals to undergo one period of oscillation is given by Eq. (3.1) below.

$$l_o = \frac{\lambda}{2\,\Delta n} \tag{3.1}$$

λ is the wavelength of the fundamental light, ω and Δn is the difference of refractive indices at fundamental frequency, ω and SHG frequency, 2ω in air, $\Delta n = n_{2\omega}^{air} - n_{\omega}^{air}$.

The configuration of SHG phase measurement near the sample is shown in Fig. 3.8. The α-quartz (0001) crystal slab is employed as the second source of SHG on a moving stage in the output beam path. The crystal's thickness is ~ 2mm with surface area dimension of 8 mm x 10 mm, there is 1° wedge in the z-direction (CrysTec). The

periodicity of the SHG interference pattern, l_o as the α-quartz is translated in air is 126 mm. This can be realized with a focusing lens of 1200 mm focus length that is employed as L1 in the incident optical path. The L1 is positioned approximately 1300 mm from the sample. The SHG intensities at different positions of α-quartz crystal are collected at the distance of 30 – 170 mm from the sample's surface.

The working principle of the optical phase delay is shown in Fig. 3.9. Here, the phase difference between the fundamental and SHG lights in the distance of two SHG media will produce a phase shift. This can be understood by applying the distance-dependent term to the electric fields of $E^{(\omega)}$ and $E^{(2\omega)}$ that propagated in organic thin film and in air as shown in Eq. (3.2 - 3.3):

In organic film:

$$E^{(\omega)} = E_0^{(\omega)} \exp i \left[\left(\frac{n_\omega^{organic} \omega d}{c}\right) - \omega t \right] \quad (3.2a)$$

$$E^{(2\omega)} = E_0^{(2\omega)} \exp i \left[2\left(\frac{n_{2\omega}^{organic} \omega d}{c}\right) - 2\omega t \right] \quad (3.2b)$$

In air:

$$E^{(\omega)} = E_0^{(\omega)} \exp i \left[\left(\frac{n_\omega^{air} \omega s}{c} + \frac{n_\omega^{organic} \omega d}{c}\right) - \omega t \right] \quad (3.3a)$$

$$E^{(2\omega)} = E_0^{(2\omega)} \exp i \left[2\left(\frac{n_{2\omega}^{air} \omega s}{c} + \frac{n_{2\omega}^{organic} \omega d}{c}\right) - i2\omega t \right] \quad (3.3b)$$

The SHG signal from medium II (α-quartz) propagated at different phase from the SHG from medium I (sample ITO/organic) as the former signal will have the same phase as the fundamental electric field, $E^{(\omega)}$. Equation (3.4b) shows the SHG contribution from the α-quartz. The last term of Eq. (3.4a) is the SHG phase shift that emerged from the sample.

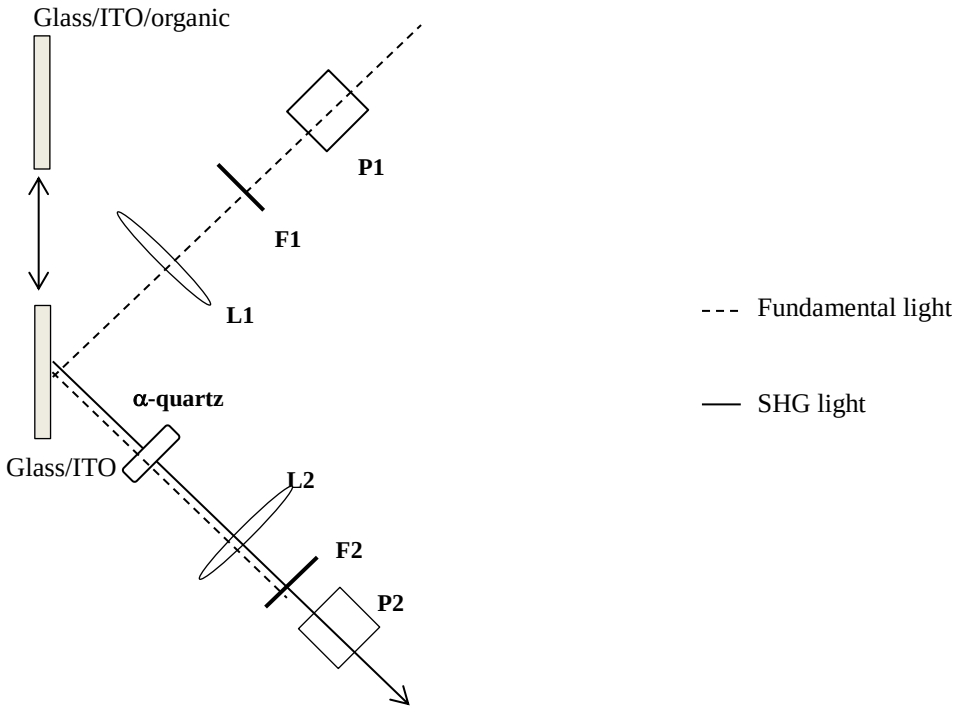

Figure 3.8 The optical line near the sample for SHG phase measurement. It is the similar set-up in Fig. 3.3 but only the L1 had been exchanged for 1200 mm focusing lens. α-quartz crystal is translated along the output beam path on a motorized moving stage. The polarization combination of this measurement is 45-in/p-out.

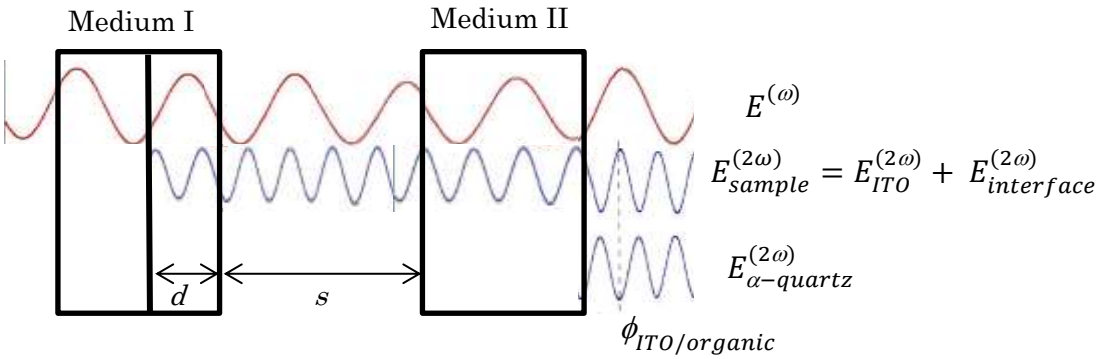

Figure 3.9 General principle of phase shifts between two SHG media separated by air. In this experiment, medium I is the ITO/organic sample and medium II is the α-quartz crystal. *d* is the thickness of organic film and *s* is the separation distance of the media.

From ITO/organic:

$$P^{(2)} \propto E_{sample}^{(2\omega)} \exp i\,[2\,(\frac{n_{2\omega}^{air}\omega s}{c} + \frac{n_{2\omega}^{organic}\omega d}{c}) - 2\omega t + \phi_{ITO/organic,0}\,] \quad (3.4a)$$

From α-quartz:

$$P^{(2)} \propto E_{\alpha-quartz}^{(2\omega)} \exp i\,[2\,(\frac{n_{\omega}^{air}\omega s}{c} + \frac{n_{\omega}^{organic}\omega d}{c}) - 2\omega t + \phi_{\alpha-quartz}] \quad (3.4b)$$

Meanwhile, the general form of SHG electric field from the interface is $E_{interface}^{(2\omega)} = \left|E_{interface}^{(2\omega)}\right| e^{i\phi_{interface}}$ with $\phi_{Interface}$ as the absolute phase shift from the interface. Same definition in Eq. (3.2-3.4) also applied to $E_{ITO}^{(2\omega)}$, the SHG from ITO. Then, the absolute sign of SHG field from interface, $\phi_{interface}$ can be deduced using $\phi_{ITO,0}$ as one of the phase components in $\phi_{ITO/organic,0}$. The phase of SHG from ITO is used to pick up the contribution from the interface as had been observed in SHG of other organic samples with substrates [8-9,11,18-20]. The phase of $\phi_{\alpha-quartz}$ remained invariant as long as the positions of translating α-quartz are constant in every measurement [19].

The phase difference between the SHG signal generated from the sample ITO/organic interface and the α-quartz - $\phi_{ITO/organic}$ can be derived from substitution of the $\frac{2\omega}{c}$ to $\frac{2\pi}{\lambda_{2\omega}}$ in previous equations.

$$\phi_{ITO/organic} = \frac{2\pi}{\lambda_{2\omega}}\left[\left(n_{2\omega}^{air} - n_{\omega}^{air}\right)s + \left(n_{2\omega}^{organic} - n_{\omega}^{organic}\right)d\right] + \phi_{ITO/organic,0}. \quad (3.5)$$

Equation (3.5) includes the phase delay by dispersion in air and in organic film.

Here the difference of the refractive indices of air, $\left(n_{2\omega}^{air} - n_{\omega}^{air}\right)$ is 4.22 x 10^{-6} [21] and the SHG wavelength, $\lambda_{2\omega}$ = 532 nm. The optical path length in the sample and the organic film thickness is d = 100 nm. Parameter s is the distance between the moving α-quartz and the sample's surface with s = 0 when α-quartz is 30 mm away from the sample's surface. $\phi_{ITO/organic,0}$ is the phase shift from the sample as well as the sum of SHG electric field of $E_{ITO}^{(2\omega)} + E_{interface}^{(2\omega)}$.

The net SHG contributions from the superposition of the SHG is simply [22],

$$I_{total} \propto \left|E_{ITO}^{(2\omega)} + E_{interface}^{(2\omega)} + E_{a-quartz}^{(2\omega)}\right|^2 \quad (3.6)$$

In this measurement, the SHG intensity of α-quartz crystal is approximately 10 times larger than the ITO and ITO/organic sample [20, 23]. It is noted that this intensity matching between the sample and the α-quartz is important in order to produce good interference pattern. The phase of SHG, $\phi_{ITO/organic}$ in Eq. 3.7 [11] can be replaced with ϕ_{ITO} for the case of bare ITO.

$$I_{total} = I_{sample} + I_{\alpha-\text{quartz}} + 2\sqrt{I_{sample}\, I_{\alpha-\text{SiO2}}}\ \cos\phi_{ITO/organic}, \quad (3.7)$$

References:

1. H. Ishii, K. Sugiyama, E. Ito, K. Seki, Energy Level Alignment and Interfacial Electronic Structures at Organic/Metal and Organic/Organic Interfaces, Adv. Mater. 11 (1999) 605-625.

2. S. Braun, W.R. Salaneck, M. Fahlman, Energy-Level Alignment at Organic/Metal and Organic/Organic Interfaces, Adv. Mater. 21 (2009) 1450-1472.

3. I.G. Hill, A. Kahn, Z.G. Soos, R.A. Pascal, Jr., Charge-separation energy in films of π-conjugated organic molecules, Chem. Phys. Lett. 327 (2000) 181-188.

4. Irfan, H. Ding, Y. Gao, D. Y. Kim, J. Subbiah, F. So, Energy level evolution of molybdenum trioxide interlayer between indium tin oxide and organic semiconductor, Appl. Phys. Lett. 96 (2010) 073304.

5. S. Braun, M.P. de Jong, W. Osikowicz, W.R. Salaneck, Influence of electrode work function on the energy level alignment at organic-organic interfaces, Appl. Phys. Lett. 91 (2007) 202108.

6. H. Peisert, M. Knupfer, T. Schwieger, J. Fink, Strong chemical interaction between indium tin oxide and phthalocyanines, Appl. Phys. Lett. 80 (2002) 2916-2918.

7. W-k. Zhang, H-f. Wang, D-s. Zheng, Quantitative measurement and

interpretation of optical second harmonic generation from molecular interfaces, Phys. Chem. Chem. Phys. 8 (2006) 4041-4052.

8. O.A. Aktsipetrov, A.A. Fedyanin, J.I. Dadap, M.C. Downer, Dc-Electric-Field-Induced Second-Harmonic Generation Studies of Surfaces and Buried Interfaces of Column IV Semiconductors, Laser Phys. 6 (1996) 1142-1151.

   O.A. Aktsipetrov, T.V. Dolgova, A.A. Fedyanin, D. Schuhmacher, G. Marowsky, Optical second-harmonic phase spectroscopy of the Si(111)-SiO_2 interface, Thin Solid Films 364 (2000) 91-94.

9. R.M. Corn, A. Higgins, Optical Second Harmonic Generation as Probe of Surface Chemistry, Chem. Rev. 94 (1994) 107-125.

10. J.J.H. Gielis, P.M. Gevers, I.M.P. Aarts, C.M. van de Sanden, W.M.M. Kessels, Optical second-harmonic generation in thin film systems, J. Vac. Sci. Technol. A 26 (2008) 1519-1537.

11. R. Stolle, G. Marowski, E. Schwarzberg, G. Berkovic, Phase measurements in nonlinear optics, Appl. Phys. B 63 (1996) 491-498.

12. M. Buck, F. Eisert, M. Grunze, F. Träger, Second-order nonlinear susceptibilities of surfaces: A systemaitic study of the wavelength and coverage dependence of

thiol adsorption on polycrystalline gold, Appl. Phys. A 60 (1995) 1-12.

13. W. Chen, H. Huang, S. Chen, Y. L. Huang, X. Y. Gao, and A. T. S. Wee, Molecular Orientation-Dependent Ionization Potential of Organic Thin Films, Chem. Mater. 20 (2008) 7017-7021

14. A.B. El Basaty, Y. Miyauchi, G. Mizutani, T. Matsushima, H. Murata, Optical second harmonic generation at heterojunction interfaces of a molybdenum trioxide layer and an organic layer, Appl. Phys. Lett. 97 (2010) 193302.

15. Y. Tong, Y. Zhao, N. Li, M. Osawa, P. B. Davies, S. Ye, Interference effects in the sum frequency generation spectra of thin organic films. I. Theoretical modeling and simulation, J. Chem. Phys. 133 (2010) 034704

16. E. H. G. Backus, N. Garcia-Araez, M. Bonn, H. J. Bakker, On the role of Fresnel factors in sum-frequency generation spectroscopy of metal-water and metal-oxide-water interfaces, J. Phys. Chem. C 116 (2012), 23351

17. K. Kemnitz, K. Bhattacharyya, J.M. Hicks, G.R. Pinto, K.B. Eisenthal, T. Heinz, The Phase of Second-Harmonic Light Generated at an Interface and its Relation to Absolute Molecular Orientation, Chem. Phys. Lett. 131 (1986) 285-290.

18. T. Suzuki, D.E. Milovzorov, S. Kogo, M. Tsukakoshi, M. Aono, Surface second-harmonic generation spectra of Si(111)-7x7 in the 1.0-1.7eV fundamental

photon energy, Appl. Phys. B 68 (1998) 623-627.

19. R. Lü, Y. Rao, W-k. Zhang, H-f. Wang, Phase measurement in nonlinear optics of molecules at air/water interface with femtosecond laser pulses, Proc. of the SPIE Conference on Nonlinear Spectroscopy 4812-15 (2002) 115-124.

20. K. Kajikawa, M. Sei, I. Yoshida, S. Okada, H. Nakanishi, K. Seki, Y. Ouchi, Ultra-thin film Local Oscillator for Determination of Complex Components of Second-Order Nonlinear Susceptibility, Jpn. J. Appl. Phys. 38 (1999) 6721-6728.

21.. D. R. Lide, Index of Refraction of Air in: CRC Handbook of Chemistry and Physics, 84th ed., Taylor & Francis, New York, 2003, pp.10-224.

22. O. Sato, R. Baba, K. Hashimoto, A, Fujishima, Second Harmonic Generation Coherent Interferometry Disclosing the Orientation of the Submerged Hemicyanine Layer in a Langmuir-Blodgett Multilayer Structure, J. Phys. Chem. 95 (1991) 9636-9638.

23. Y. Jeon, H. Min, D. Kim, M. Oh-E, Determination of the Crystalline *x*-Axis of Quartz by Second-Harmonic Phase Measurement, J. Korean Phys. Soc. 46 (2005) 159-162.

Chapter 4

The Magnitude and Phase of SHG from the Interface of ITO and Organic Semiconductor

In this chapter, the result of the SHG experiments will be shown. The goal is to extract the SHG of the interface from the raw data. The first part of the chapter will concentrate on the result of SHG intensities with Fresnel factor incorporated into the analysis. The result of the SHG phase measurement will be discussed in the second part of the chapter. Lastly, a separate study of SHG from ITO/α-NPD structures is shown.

4.1 The SHG intensity from the interface ITO/organic

Fig. 4.1 shows the *p*-polarized SHG intensities measured from the strip of ITO and ITO/organic. There is no SHG emitted from the organic thin film, but CuPc thin film emitted a number of photons that still negligible for comparison. The red bar represents the SHG intensity of bare ITO only and the blue bars are of ITO/organic structures. The blue bars on the right side of the ITO belong to ITO/CuPc, ITO/α-6T and ITO/pentacene, the organic thin films with lower ionization energy than the ITO (energy with respect to the vacuum level). The sample is measured with the organic layer as the incident surface of the fundamental light radiation. In Fig. 4.2, the sample is flipped upside down so that the surface of glass/ITO became the incident surface.

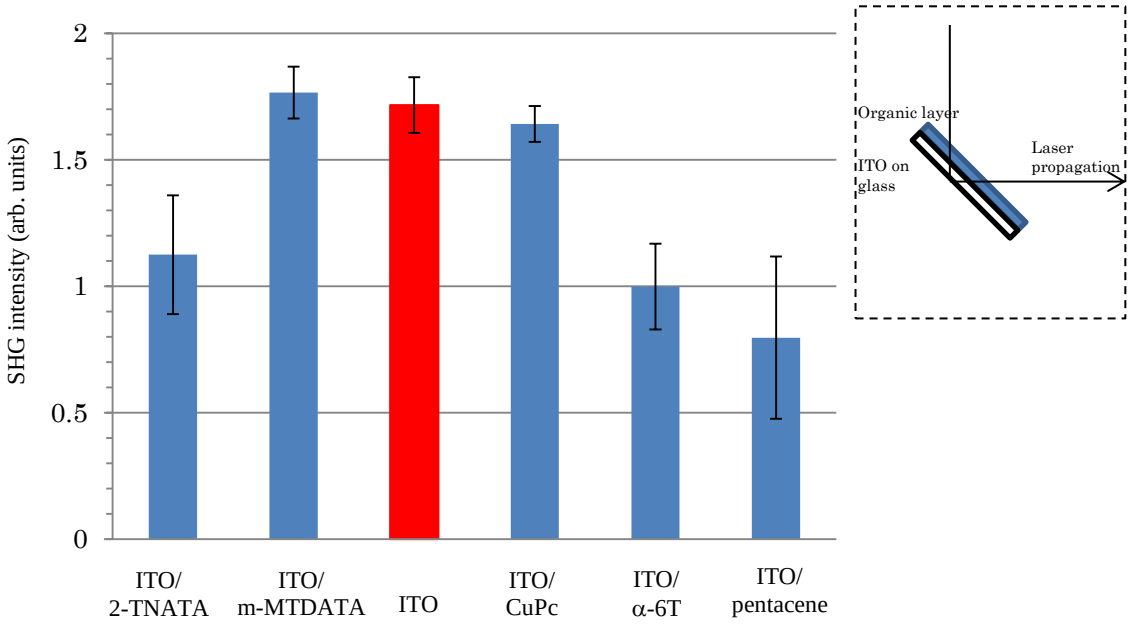

Figure 4.1 SHG intensities of ITO and ITO/organic at organic layer incidence. The red bar is the SHG intensity from bare ITO (150 nm).

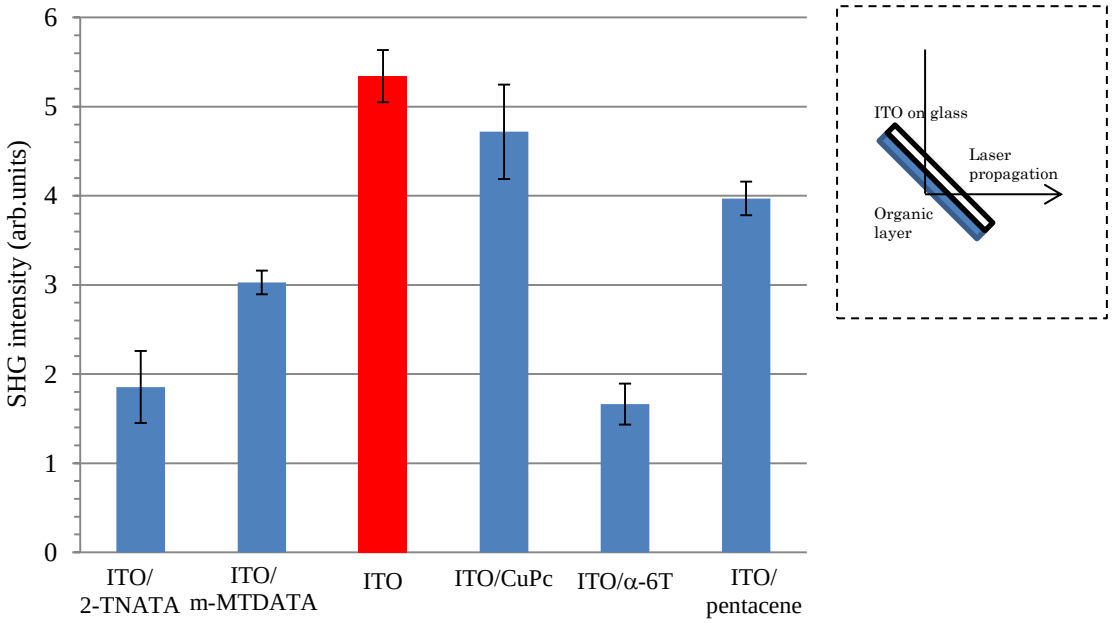

Figure 4.2 SHG intensities of ITO and ITO/organic at glass substrate incidence. The red bar is the SHG intensity from bare ITO (150 nm).

In Fig. 4.1, the SHG intensities of ITO/2-TNATA, ITO/α-6T and ITO/pentacene are shown to be weaker than that of bare ITO. Almost similar tendency between bare ITO and ITO/organic is presented in Fig. 4.2 although at different magnitude of decrease. This significant change of SHG intensity in ITO/organic may indicated interference from SHG from the interface but the same decrease can also attributed to the linear Fresnel factor of the organic layer. The Fresnel factor is different among thin films depending on the dielectric properties of organic layer hence the calculation of Fresnel factor will be utilizing the data of linear transmittance and reflectance of the samples. The spectra can be found in Appendix I of this dissertation.

4.1.1 Fresnel factor correction

This section will demonstrate a quantitative analysis of Fresnel factor for result in Fig. 4.1. The analysis is not applied to analyze the SHG data in Fig. 4.2 due to the thickness of the glass substrate. By removing the *L* factor in the thin film, the SHG induced from the electric field at the interface can be properly estimated. A two layer model is used to calculate the Fresnel factor of the system of ITO/organic samples. This model can be referred in the theoretical paper of Tong et al [1]. The refractive index of the interface layer is denoted by n_m.

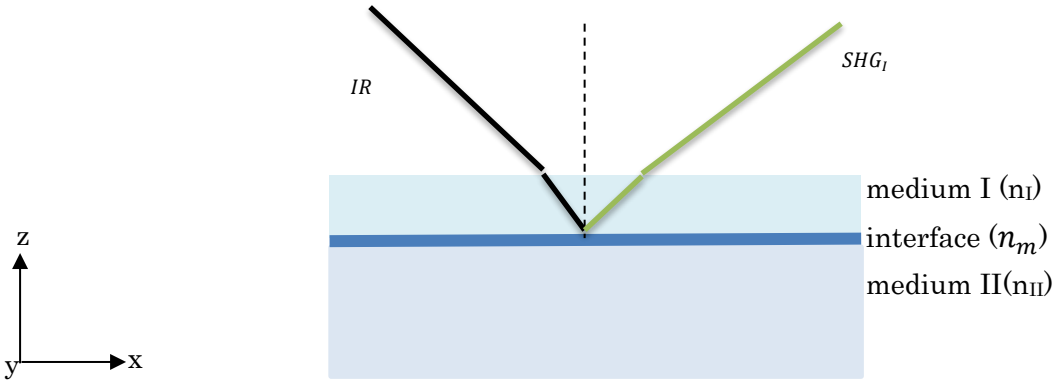

Figure 4.3 Two layer model for SHG from a thin film on a substrate (medium II). Multireflectivity in the thin film is not shown for simplicity. This illustration is a reference from discussion of Tong et al [1].

The effective susceptibilities at *p*-in/*p*-out polarization combination ($\chi_{eff,pp}$) are directly related to the susceptibilities χ_{ijk} tensor elements shown in Eq. (4.1) as below [2]. Here, the *i*, *j* and *k* notations have been replaced by the laboratory coordinates, *x*, *y* and *z*.

$$\chi_{eff,pp} = L_{zz}(2\omega)L_{xx}^2(\omega)sin\Omega\, cos^2\Omega\, \chi_{zxx} - 2L_{xx}(2\omega)L_{zz}(\omega)L_{xx}(\omega)sin\Omega\, cos^2\Omega\, \chi_{xxz} + L_{zz}(2\omega)L_{zz}^2(\omega)sin^3\Omega\, \chi_{zzz} \quad (4.1)$$

There is four non-zero tensors, χ_{zzz}, χ_{zxx}, χ_{xxz} and χ_{xzx}. The $L_{ij}(\omega)$ and $L_{ij}(2\omega)$ are the Fresnel factors at ω and 2ω frequencies and the Ω is the incidence angle in the direction normal to the surface. For both fundamental light (ω) and SHG light (2ω), their corresponding *L* factors can be calculated from the reflectance coefficient, r_p [1]:

$$L_{xx} = 1 - r_p \quad (4.2)$$

$$L_{zz} = \left(1 + r_p\right)\left(\frac{n_I}{n_m}\right)^2 \quad (4.3)$$

According to the sample structure, the n_m is the refractive index of the interface layer

and n_I is the refractive index of the organic layer. Since the thickness of the interface layer is much smaller than the wavelength of the fundamental light, the macroscopic property of the interface layer should be the same of bare interface. Thus, the $\frac{n_I}{n_m}$ is equivalent to 1. The reflection coefficient, r_p of the ITO/organic layer at corresponding wavelengths is obtained from linear spectroscopy experiments. The Fresnel factor for three effective susceptibilities χ_{ijk} in Eq. 4.1 as a function of the SHG photon energies for ITO/organic is shown in Fig. 4.4.

In data for ITO/organic, the SHG from the interface appeared as signal interference to the SHG intensity of ITO. Thus, from a rough comparison to the signal of bare ITO, the contribution from the interface can be evaluated. The change of SHG intensity and the Fresnel Factor in ITO/organic with respect to the bare ITO is shown in Fig. 4.5. The vertical axis is the energy difference of the ionization energy of the organic film and the work function of ITO. The positive energy implied strong electron donating power in organic molecules while the negative energy implied the exact opposite. Here, the SHG interference in ITO/2-TNATA, ITO/pentacene and ITO/α-6T are dominantly contributed by the SHG electric field from the interface. The percentage of SHG interference in these structures outweighed their respective Fresnel factors. On the other hand, the ITO/CuPc and ITO/m-MTDATA are shown to have a higher percentage of Fresnel factors instead. It implied that there is no effect of the SHG from the interface.

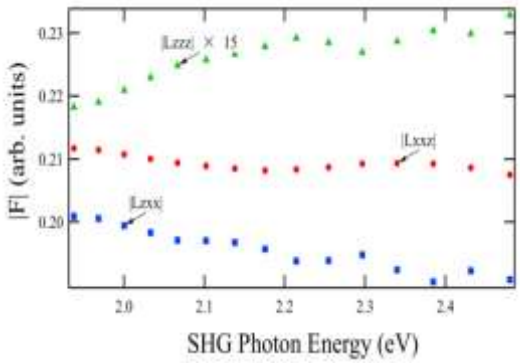

b) ITO/m-MTDATA

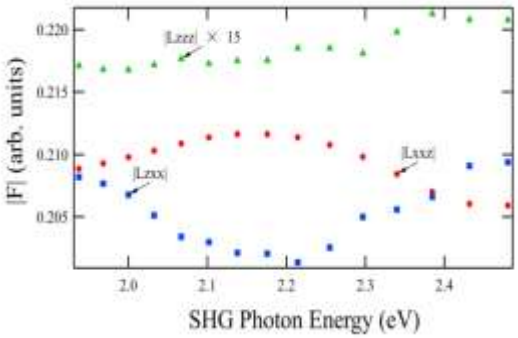

(c) ITO/2-TNATA

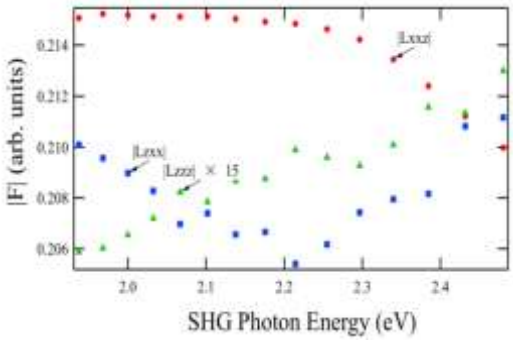

(d)ITO/CuPc

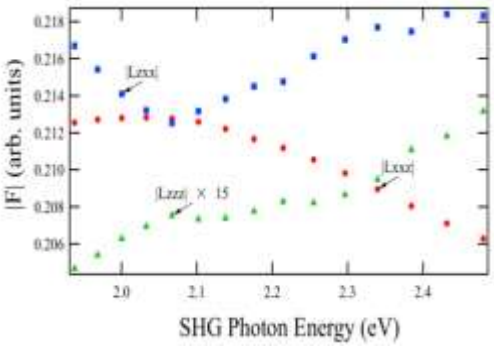

(e)ITO/pentacene

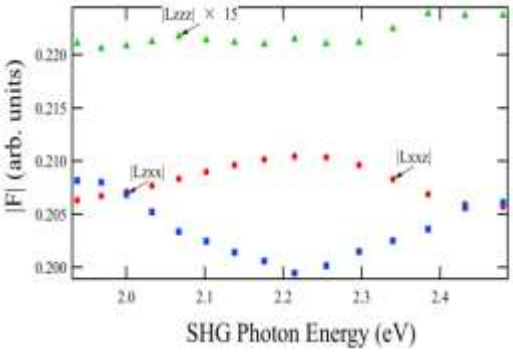

(f)ITO/α-6T

Figure 4.4 Three L factors of the χ_{zzz}, χ_{zxx} and χ_{xxz} of the p-polarized SHG from ITO/organic samples at different SHG photon energies.

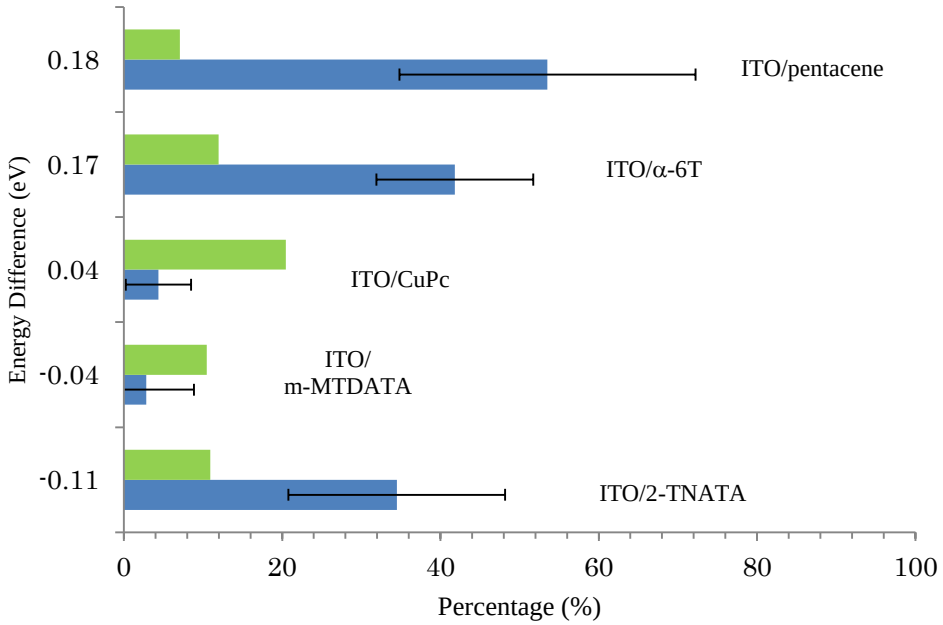

Figure 4.5 Analysis of the percentage of sample's Fresnel factor over ITO (green bar) and normalized percentage of SHG of ITO/organic, $\left|\frac{E_{ITO}^{(2\omega)}-E_{ITO/organic}^{(2\omega)}}{E_{ITO}^{(2\omega)}}\right|$(blue bar). The vertical axis is the energy difference between the ionization energy of the organic film and the work function of ITO.

4.2 The SHG's phase shift from the interface of ITO/organic

The result of interferometry SHG phase measurement is shown in Fig. 4.6 and Fig. 4.7. The oscillation patterns are the SHG intensities of (a)ITO, (b)ITO/m-MTDATA, (c)ITO/2-TNATA, (d)ITO/CuPc, (e)ITO/pentacene and (f)ITO/α-6T at different translation distance *s* of the α-quartz crystal. The interference patterns between the sample and the α-quartz are fitted by general formula of cosine function.

$$f(s) = y_o + A\,cos\,(fs + \alpha) \tag{4.4}$$

From these figures, clearly at least there is one period of oscillation measured for each pattern. The components of the function in Eq. (4.4) of ITO and ITO/organic structures are tabulated in Table 4.1 and the phase information is extracted accordingly. The theoretical frequency of SHG in air has been 49.87 x 10^{-3} mm^{-1} and the patterns are observed within the spatial frequencies of 0.04987 ± 0.006 mm^{-1}.

The phase of the SHG oscillation patterns can be determined directly using parameter α but the phase of the SHG from the interface required some rigorous analysis. The analysis is based on the knowledge of the working principle of the interferometry in Sec. 3.4. Using a simple comparison between Eq. (3.7) and Eq. (4.4), the $(fs + \alpha)$ in Eq. (4.4) can be interpreted as $\phi_{ITO/organic}$ in the former equation. The parameter of frequency f is equivalent to the term of optical dispersion in air, $\frac{2\pi}{\lambda_{2\omega}}\left(n_{2\omega}^{air} - n_{\omega}^{air}\right)$ in Eq. (3.5) and $\frac{2\pi}{\lambda_{2\omega}}\left(n_{2\omega}^{organic} - n_{\omega}^{organic}\right)d + \phi_{ITO/organic,0}$ is equal to the phase, α.

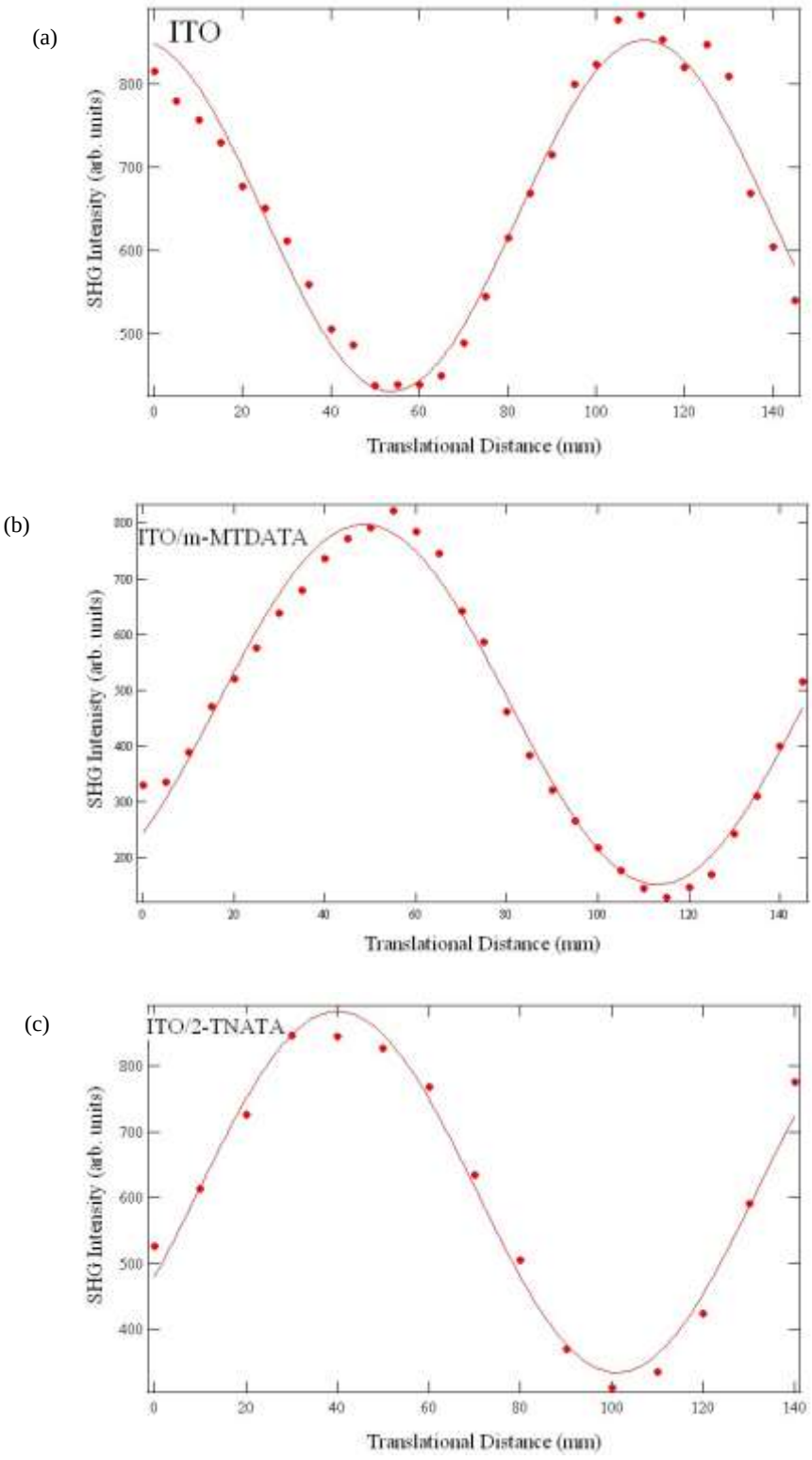

Figure 4.6 SHG interference patterns for the sets of samples (a)ITO (b)ITO/m-MTDATA and (c) ITO/2-TNATA. The horizontal axis is the translation distance of the α-quartz and the vertical axis is the total SHG intensity, I_{total}.

(d)

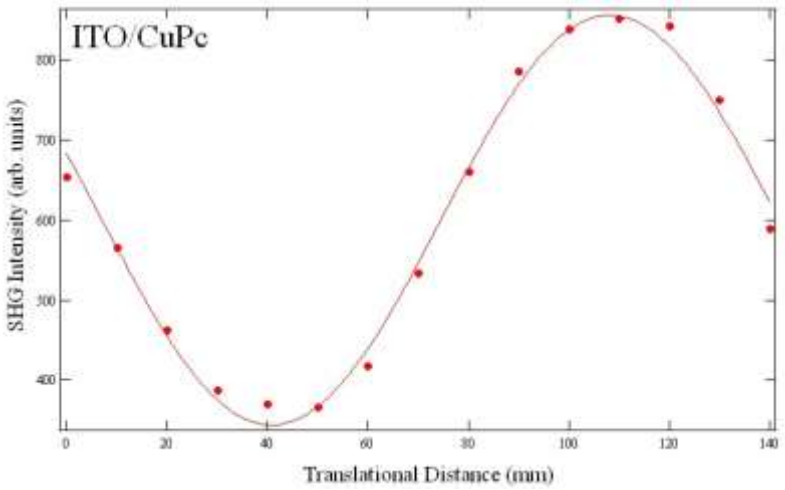

(e)

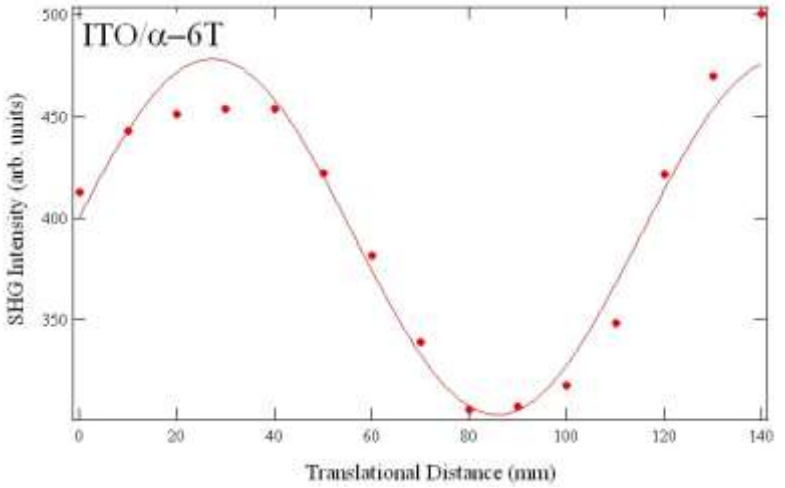

(f)

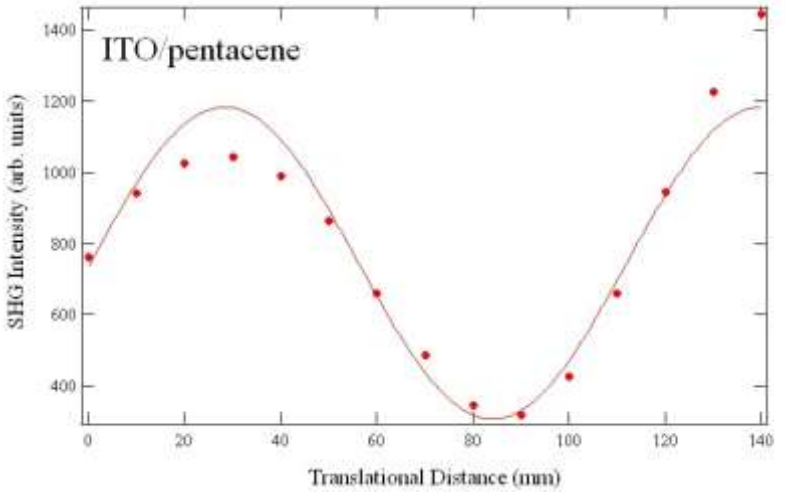

Figure 4.7 SHG oscillation patterns for the sets of samples (d)ITO/CuPc. (e)ITO/α-6T and (f) ITO/pentacene. The horizontal axis is the translation distance of the α-quartz and the vertical axis is the total SHG intensity, I_{total}.

Table 4.1 Components of cosine curve fitting on SHG interference patterns

Sample	ITO	ITO/2-TNATA	ITO/ m-MTDATA	ITO/CuPc	ITO/α-6T	ITO/pentacene
Sum of SHG interference, y_o (arb. units)	641.55 ± 5.73	608.53 ± 8.27	474.42 ± 6.04	599.69 ± 5.38	390.83 ± 4.22	745.55 ± 29.6
Amplitude of SHG interference, A (arb. units)	210.67 ± 8.08	274.9 ± 12.2	322.67 ± 8.71	255.83 ± 7.95	87.361 ± 5.82	437.72 ± 40.8
Frequency of SHG in air, f x 10^{-3} (mm^{-1})	54.793 ± 0.804	51.464 ± 0.809	48.69 ± 0.536	46.608 ± 0.597	53.658 ± 1.5	56.295 ± 2.14
Phase, α (rad)	1.7714 ± 0.0726	-0.49088 ± 0.0639	-0.79683 ± 0.0454	-3.4719 ± 0.0493	0.10748 ± 0.118	-0.025181 ± 0.163
Phase, α (degree)	101.49±4.16	-28.13±3.66	-45.65±2.6	-198.93±2.82	6.16±6.76	-1.44±9.34

The phase, α is the consequence of fundamental and SHG light dispersion in air between the sample and the α-quartz. Generally, α do not hold any meaning to the analysis but by using the phase of bare ITO as reference, the phase shift experienced by ITO/organic structure is now: $\phi_{\mathrm{ITO/organic}} - \phi_{\mathrm{ITO}}$. This term will be known as the total phase shift since the phase shift from the interface is not yet analyzed. The plot of total phase shift for all ITO/organic sample at the given energy difference is shown in Fig.4.8.

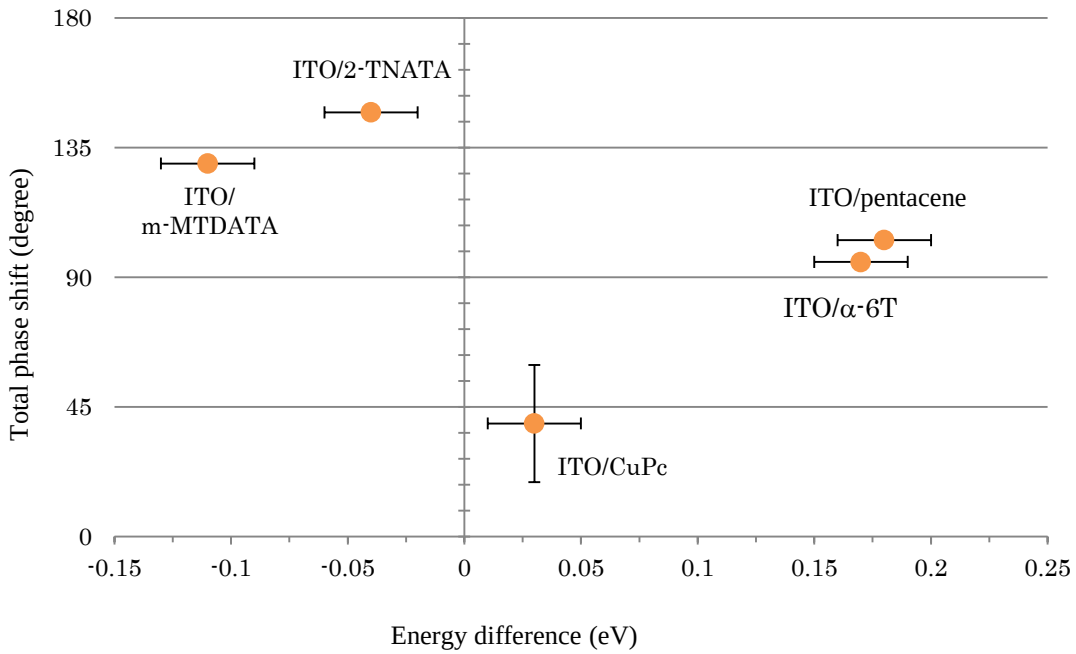

Figure 4.8 The plot of total phase shift, ($\phi_{\mathrm{ITO/organic}} - \phi_{\mathrm{ITO}}$) against energy difference given for each interface of organic semiconductor film.

Figure 4.8 above shows that the plot of total phase shift for ITO/organic samples against the energy difference calculated for each interface. The energy is suggested as the potential of the charge transfer at the interface. The phases of the ITO/organic structures are larger than 90° except for the phase of ITO/CuPc. The working principle of the phase measurement shows that the total phase shift is composed of the SHG from the interface of ITO/organic and also the phase induced by dielectric dispersion in the organic thin film. The total phase shift in Eq. (4.5) is derived mathematically from Eq. (3.2).

$$\phi_{\mathrm{ITO/organic}} - \phi_{\mathrm{ITO}} = \frac{2\pi}{\lambda_{2\omega}} \left(n_{2\omega}^{\mathrm{organic}} - n_{\omega}^{\mathrm{organic}}\right)d + \phi_{\mathrm{ITO/organic,0}} \qquad (4.5)$$

The total phase shift in Eq. (4.5) is true when the phase of bare interface of ITO, $\phi_{\mathrm{ITO},0} = 0^{\circ}$. The first term is the phase shift induced by optical dispersion in the organic film with *d* acting as the optical path length in the film. The second term, $\phi_{ITO/organic,0}$ is defined as the phase of $E_{ITO}^{(2\omega)} + E_{interface}^{(2\omega)}$ at ITO/organic interface with respect to the $\phi_{ITO,0} = 0^{\circ}$. The calculation of optical dispersion in the organic thin films used the refractive indices; $n_{2\omega}^{organic}$ and $n_{\omega}^{organic}$ obtained from other literatures. The calculation will be shown for ITO/CuPc and ITO/pentacene.

The refractive indices for copper phthalocyanine thin film reported by Kumagai et al are 2.00 and 1.43 at ω and 2ω, respectively [3]. On the other hand, the refractive indices, n_{ω} and $n_{2\omega}$ of pentacene thin film are obtained as 1.57 and 1.43, respectively [4]. The optical path length in organic layer is approximated as the 100 nm thickness of the organic layer. Hence, using this information, the components of the total phase shift can be tabulated in Table 4.2.

Table 4.2 Components of the total phase shift, $\phi_{\mathrm{ITO/organic}} - \phi_{\mathrm{ITO}}$

	Total phase shift: $\phi_{\mathrm{ITO/organic}} - \phi_{\mathrm{ITO}}$	1st: $\frac{2\pi}{\lambda_{2\omega}}\left(n_{2\omega}^{\mathrm{organic}} - n_{\omega}^{\mathrm{organic}}\right)d$	2nd: $\phi_{\mathrm{ITO/organic,0}}$
ITO/CuPc	59.5 ± 2.82˚	-38.6˚	98˚
ITO/pentacene	102.94 ± 9.34˚	-9.5˚	112˚

As a result, the phase shift $\phi_{\mathrm{ITO/organic,0}}$ is estimated as 98˚ for ITO/CuPc and the same phase shift is 112˚ for ITO/pentacene.

4.3 Absolute phase from the interface, $\phi_{interface}$

The polarization combination measured from the SHG oscillation patterns in Fig. 4.6 and Fig. 4.7 can be a possession of many non-zero $\chi^{(2)}$ components. Hence, it is difficult to evaluate the effective $\chi^{(2)}$ measured in the SHG's phase. However, the $\chi^{(2)}_{zzz}$ can be a dominant contribution since the intensities are relatively similar.to the result in the SHG intensity. This $\chi^{(2)}_{zzz}$ is strongly susceptible to the electric field at the interface. Previously, the phase $\phi_{\mathrm{ITO/organic,0}}$ is shown to be the phase shift of the sum of SHG electric fields; $E^{(2\omega)}_{ITO} + E^{(2\omega)}_{interface}$. This relationship between the SHG elecric field vectors is described in the complex plane diagram in Fig. 4.9. The SHG electric fields are drawn as two-dimensional vectors composed of both real and imaginary part of the electric field. The $\phi_{interface}$ is the absolute phase of the SHG, $E^{(2\omega)}_{interface}$ from the interface. The phase is a property of the SHG from the interface after the composition of the phase from ITO is removed from phase shift of $\phi_{\mathrm{ITO/organic,0}}$. Both $E^{(2\omega)}_{ITO}$ and $E^{(2\omega)}_{ITO} + E^{(2\omega)}_{interface}$ are obtained from the SHG intensities in Fig. 4.1 after normalization by $E^{(2\omega)}_{ITO}$. Table 4.3 shows the components used in the complex plane analysis for the case of ITO/CuPc and ITO/pentacene.

Table 4.3Vector space analysis for ITO/organic samples.

	$E^{(2\omega)}_{ITO} + E^{(2\omega)}_{interface}$	$\phi_{ITO/organic,0}$ (degree)	$E^{(2\omega)}_{interface}$	$\phi_{interface}$ (degree)
ITO	1	0	0	0
ITO/CuPc	0.96	98	1.48	140
ITO/pentacene	0.46	112	1.25	160

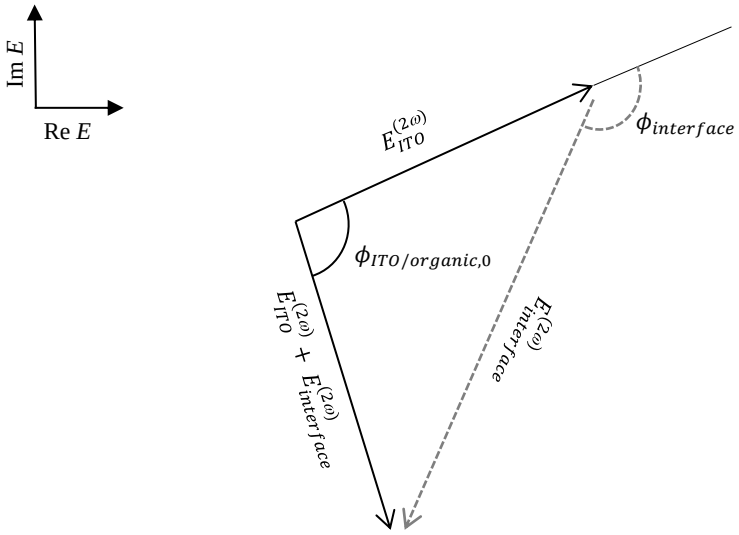

Figure 4.9 Diagram of vector components of the SHG electric fields in the relation $E_{ITO/organic}^{(2\omega)} = E_{ITo}^{(2\omega)} + E_{interface}^{(2\omega)}$ in the frame of complex plane. The dashed grey lines represent the magnitude of $E_{interface}^{(2\omega)}$ and its phase, $\phi_{interface}$. Both quantities are properties of the SHG electric field at the interface of ITO and organic layer [5].

Finally, the absolute phase, $\phi_{interface}$ of the interface SHG of ITO/CuPc is calculated as 140° with respect to the phase of the bulk ITO. It is 20° away from the absolute phase of interface SHG calculated from ITO/pentacene that is 160°. It is noted that both phases of ITO/CuPc and ITO/pentacene are not exactly 180˚ [6].

4.4 Analysis of phase shift of ITO/ α-NPD thin film

In this measurement of SHG's phase, subject of optical dispersion in the thin film is unavoidable. The dielectric dispersion can be especially large in π-conjugated

molecular films. However, the dispersion is also very sensitive to the thickness of organic layer, *d*. In thinner film, the dispersion can be reduced to negligible. In this particular experiment, the N,N'-di-[(1-napthyl)-N,N'-diphenyl]-1,1'-biphenyl)-4,4'-diamine (α-NPD) thin films are employed to investigate the effect of the thickness of organic layer to the SHG's phase shift. The α-NPD film generally possessed a high transparency at the region of visible wavelengths and the molecular density of the film is dependent of film thicknesses. First of all, the result of the SHG intensity from different thickness of α-NPD is shown to characterize the SHG signal from the interface. At the same time, the consistency between film's refractive indices and the phase of SHG obtained from SHG interference is made using the data from ellipsometry measurement of Si(001)/α-NPD films.

4.4.1 SHG from ITO/α-NPD

The energy difference at the interface of α-NPD and ITO is large with the position of the HOMO level of the organic film 0.4 eV below the work function of ITO with respect to the vacuum level [7]. It is suggested that ground state charge transfer from the α-NPD system to ITO should not occur at this interface. Fig. 4.10 shows the *p*-polarized SHG intensities of α-NPD thin films at thicknesses of 0 nm, 10 nm, 30 nm, 60 nm and 100 nm. The thickness of the ITO substrates is 150 nm. It is roughly seen that the SHG intensities from the ITO/α-NPD are not dependent on the thickness of α-NPD layer. Here, the Fresnel factor calculation is not applied but the maximum decrease of 12 % in ITO/α-NPD (100 nm) can be easily associated with the 15% optical

absorption present in the linear transmission spectra of ITO/α-NPD (100 nm) at 1064 nm in Fig. 4.11. In the reflectance spectra of ITO/α-NPD (100 nm) (spectra not shown), a ~20% optical absorption is present at 532 nm. The redshift in the transmission spectra of ITO/α-NPD (100 nm) indicated higher molecular density in the film. The small change of SHG intensity in ITO/α-NPD structures with respect to the SHG of bare ITO can be induced by the Fresnel factor, like the SHG intensity result of ITO/CuPc and ITO/m-MTDATA previously. No change of SHG intensity due to SHG from the ITO/α-NPD interface has been indicated. Nevertheless, the difference of the SHG amplitude in the complex plane should be taken into account. For that purpose, the phase of the SHG from ITO/α-NPD is to be measured as well.

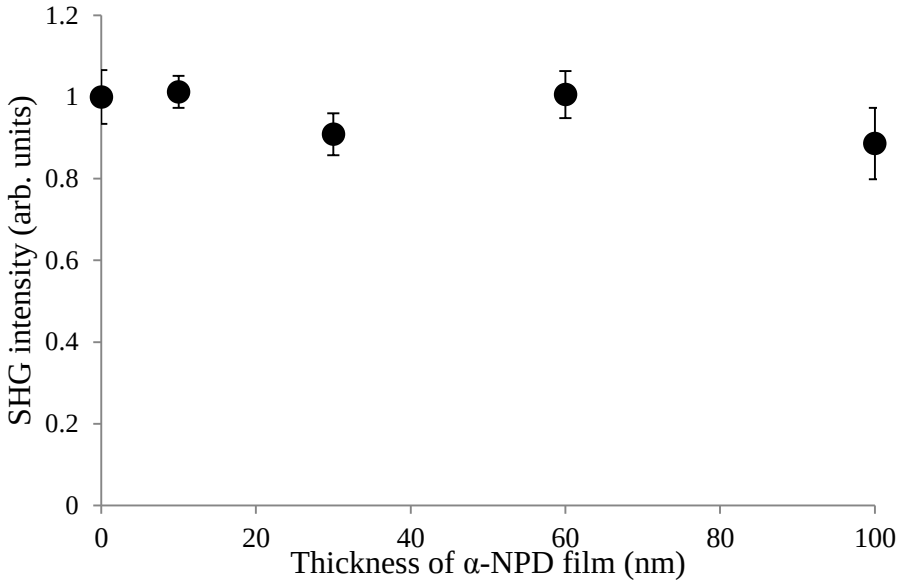

Figure 4.10 The *p*-polarized SHG intensities against different thickness of α-NPD layer in ITO/α-NPD structure. It is normalized by the SHG from bare ITO (150 nm).

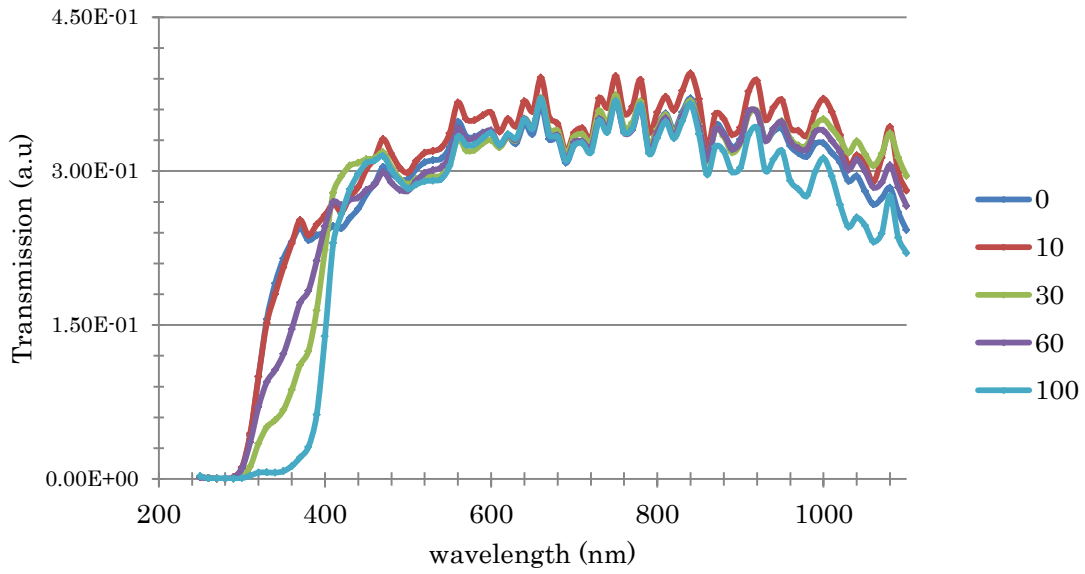

Figure 4.11Transmission spectra of ITO/α-NPD organic layer at different thickness of α-NPD layer.

Fig. 4.12 shows SHG interference patterns for ITO and ITO/α-NPD (100 nm) at the translation of α-quartz and the total phase shift, ($\phi_{ITO/\alpha-NPD} - \phi_{ITO}$) is directly obtained from the sine curve fitting. The two sine curves of the SHG intensities for ITO and ITO/α-NPD are shown to have almost the same phases as each other. This is evident from the calculation of the total phase shift of ITO/α-NPD (100 nm), ($\phi_{IT0/\alpha-NPD} - \phi_{ITO}$) to be 5.86˚ ± 7.04˚. This number is very small compared to previous results obtained with other organic layers. Furthermore, the phase shift still comprised of $(n_{2\omega}^{\alpha-NPD} - n_{\omega}^{\alpha-NPD})d$ from the organic layer. In separate experiment, the SHG's total phase shift of ITO/α-NPD (10 nm) is calculated to be 5.45˚ ± 4.08˚.

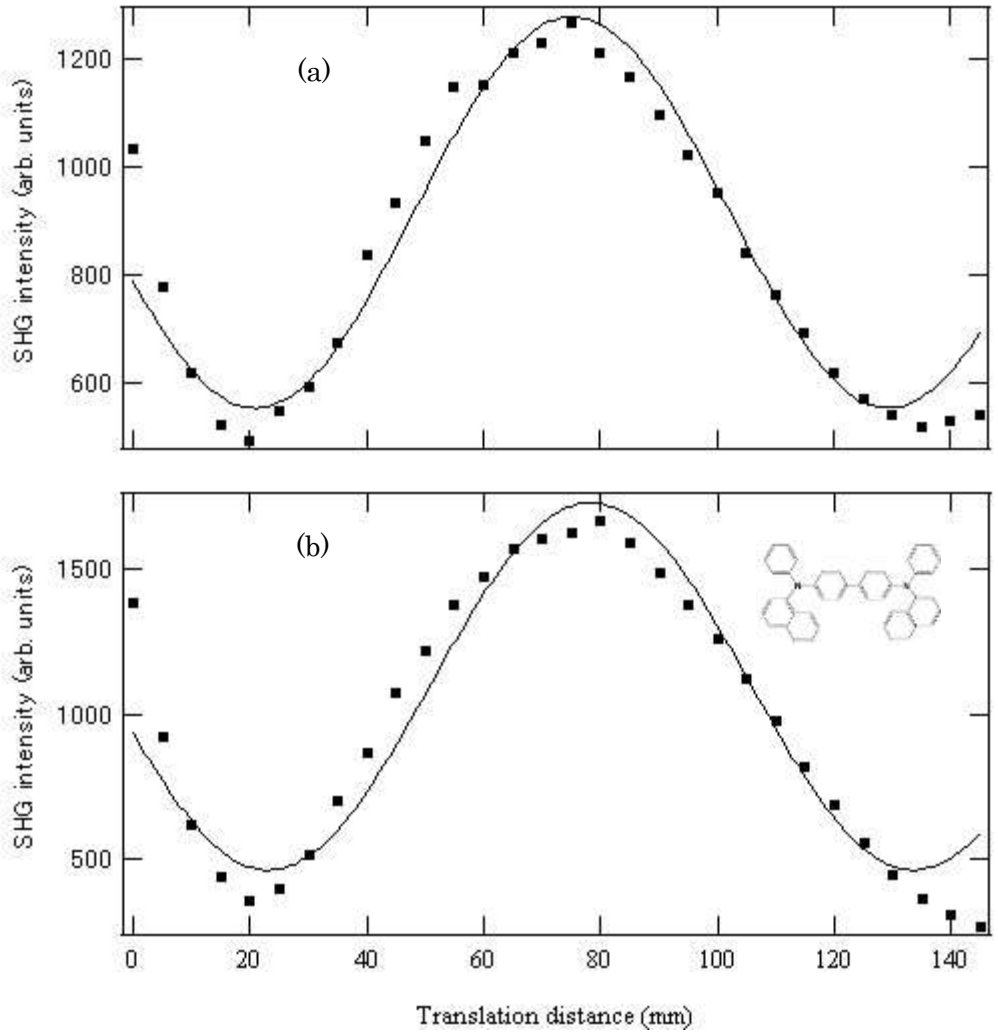

Figure 4.12 SHG interference patterns of (a) ITO and (b) ITO/α-NPD (100 nm) at every translation distance of the α-quartz crystal. The frequencies of the oscillation patterns are within 16 % of the theoretical frequency.

4.4.2 Dielectric function of α-NPD

The experiment of ellipsometry is performed to obtain dielectric function of α-NPD film. The ellipsometric spectrometer is a VASE model of J. A. Woolam. Co. For this purpose, Si(001)/α-NPD samples are prepared at thickness of α-NPD films at 10 nm,

50 nm and 100 nm. The spectra of dielectric constant of the Si(001)/α-NPD samples is included as Appendix II. The plot of refractive indices of 100 nm α-NPD film is consistent with the one obtained by Himcinschi et al [8]. The comparison of 100 nm α-NPD film is shown figuratively in Fig. 4.13, Himcinschi's result is reconstructed as black dots. Meanwhile, the arrows show the $n_{2\omega}^{\alpha-NPD}$ and $n_{\omega}^{\alpha-NPD}$ in from the spectra. Using these refractive indices, the dispersion of the 100 nm α-NPD is calculated to be 0.0933. Hence, the phase shift term, $\frac{2\pi}{\lambda_{2\omega}}(n_{2\omega}^{\alpha-NPD} - n_{\omega}^{\alpha-NPD})d$ for 100 nm α-NPD film is 6.31°. This is almost equal to the total phase shift $(\phi_{ITO/\alpha-NPD} - \phi_{ITO}) = 5.86^{\circ}$ obtained from Fig. 4.12

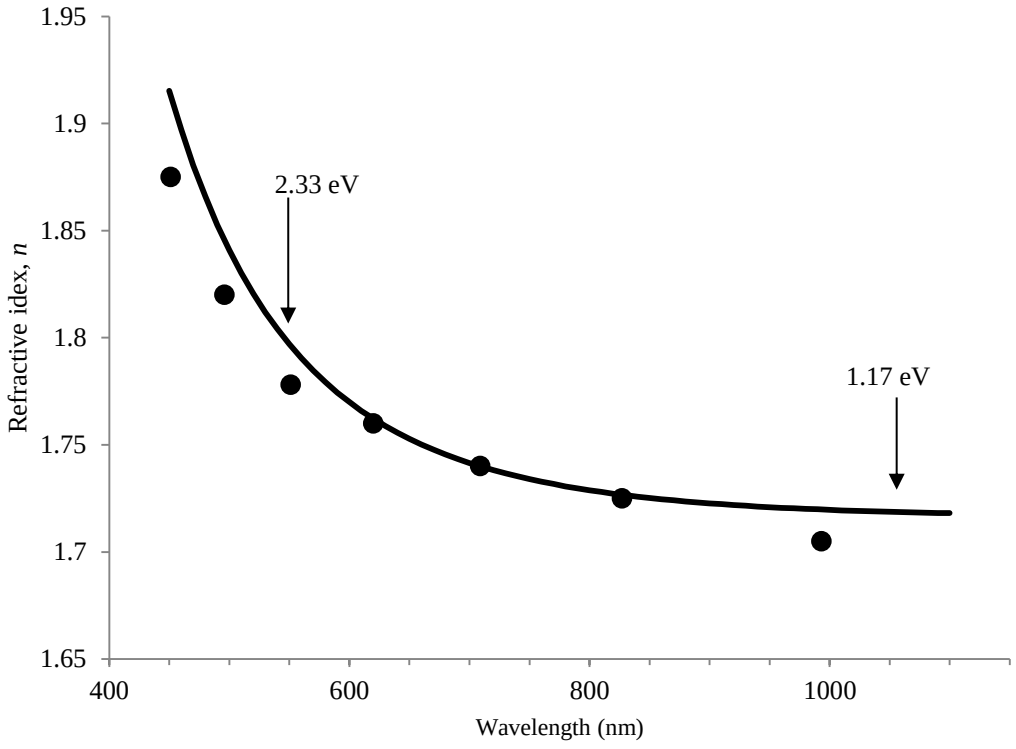

Figure 4.13 The refractive index, *n* of 100 nm α-NPD thin films obtained from the Cauchy fits of ellipsometric spectra is shown as thick line. The dots (•) are the trace of refractive indices for vapor phase deposition of α-NPD by Himcinschi et al [9].

On the other hand, the dielectric dispersion calculation is also applied to ITO/α-NPD (10 nm), using the same refractive indices. The phase shift is however, much smaller, approximately at 0.63° only. Table 4.4 has summarized the components of phase shift from the ITO/α-NPD samples. Based on the table, neither ITO/α-NPD (100 nm) nor ITO/α-NPD (10 nm) shows the emergence of phase shift from the interface SHG, $\phi_{ITO/\alpha-NPD,0}$. For ITO/α-NPD (10 nm), the effect of the dispersion is perhaps small and negligible but the error of the total phase shift is also large in comparison. It is concluded that since the SHG from ITO/α-NPD structures are in phase with SHG from bare ITO and the magnitude of SHG from the interface of ITO/α-NPD can be accurately estimated from the SHG intensity measurement.

Table 4.4 Components of phase shift of ITO/organic structures.

ITO/α-NPD (*d* nm)	10 nm	100 nm
Total phase shift, ($\phi_{ITO/\alpha-NPD} - \phi_{ITO}$)	5.45 ± 4.08deg.	5.86 ± 7. 04 deg.
Phase shift from α-NPD film: $\frac{2\pi}{\lambda_{2\omega}}\left(n_{2\omega}^{\alpha-NPD} - n_{\omega}^{\alpha-NPD}\right)d$	0.63 deg.	6.58 deg.

References:

1. Y. Tong, Y. Zhao, N. Li, M. Osawa, P. B. Davies, S. Ye, Interference effects in the sum frequency generation spectra of thin organic films. I. Theoretical modeling and simulation, J. Chem. Phys. 133 (2010) 034704
2. W-k. Zhang, H-f. Wang, D-s. Zheng, Quantitative measurement and interpretation of optical second harmonic generation from molecular interfaces, Phys. Chem. Chem. Phys. 8 (2006) 4041-4052.
3. K. Kumagai, G. Mizutani, H. Tsukioka, T. Yamuchi, S. Ushioda, Second-harmonic generation in thin films of copper phthalocyanines, Phys. Rev. B 48 (1993) 14488-14495.
4. Y. Hosoi, K. Okamura, Y. Kimura, H. Ishii, M. Niwano, Infrared spectroscopy of pentacene thin film on SiO_2 surface, Appl. Surf. Sci. 244 (2005) 607-610.
5. S. Z. N. Demon, Y. Miyauchi, G. Mizutani, T. Matsushima and H. Murata. Optical second harmonic generation at interfaces of some organic layers with indium tin oxide. Appl. Surf. Sci. 311 (2014) 715-720
6. A.B. El Basaty, Y. Miyauchi, G. Mizutani, T. Matsushima, H. Murata, Optical second harmonic generation at heterojunction interfaces of a molybdenum trioxide layer and an organic layer, Appl. Phys. Lett. 97 (2010) 193302.

7. T. Matsushima, G. -H. Jin, Y. Kanai, T. Yokota, S. Kitada, T. Kishi, H. Murata, Mater. Res. Soc. Symp. Proc. (2009) 1154

8. C. Himcinschi, N. Meyer, S. Hartmann, M. Gersdorff, M. Friedrich, H. -H. Johannes, W. Kowalsky M. Schwambera, G. Strauch, M. Heuken, D. R. T. Zahn, Appl. Phys. A 80 (2005) 551

Chapter 5

Origin of SHG Interfacial Electric Field and the SHG Phase Shift

5.1 The origin of SHG from the interface of ITO/organic

The efficiency of SHG photon conversion in this study is around 1 - 3.5 x 10^{-9}. The SHG from the substrate ITO is electronic resonance from the optical band gap of polycrystalline indium tin oxide domains structures. SHG from interface of the ITO/N_2 is negligible compared to its bulk contribution. The direction or sign of the bulk dipole is the average of the total contribution from domains with random dipole directions, however the exact sign is not established as of yet. In the first part of this work, experiment of SHG intensity measurement and Fresnel factor analysis are performed to separate contribution from the interface of ITO/organic from the bulk ITO's SHG. As a result, the change in SHG intensity of the ITO/organic samples, $|\Delta I^{(2\omega)}|$ induced by the SHG from the interface is summarized as Fig. 5.1.

In this graph, ITO/2-TNATA, ITO/pentacene and ITO/α-6T experienced change in SHG intensity due to the effect of signal interference from the interface. The magnitude of $|\Delta I^{(2\omega)}|$ are different from one another. Meanwhile, ITO/CuPc and ITO/m-MTDATA is shown without any change of $|\Delta I^{(2\omega)}|$. From the energy level relation between the organic semiconductor and the ITO, the organic semiconductor can be categorized either as a donor or an acceptor molecular system similar to n-type or p-type in inorganic semiconductor. Donor molecules are CuPc, pentacene and α-6T

while m-MTDATA and 2-TNATA are the acceptors molecules. At the interface of strong donor molecular system, the charge transfer occurs from the organic molecules to the indium tin oxide surface. The sign of the charge transfer dipole is going outside of ITO and the same sign should also be observed for the SHG polarization [1]. The SHG intensity from ITO/pentacene and ITO/α-6T shows the presence of charge transfer at the interface, but it is impossible to tell for ITO/CuPc. According to the horizontal axis, the energy difference given at both interfaces of ITO/pentacene and ITO/α-6T are larger than 0.15 eV and that of interface of ITO/CuPc. It may be acceptable that SHG from the interface ITO/CuPc appeared weaker compared to the rest. Still, there had been previous works of CuPc molecules on ITO that indicated interface states due to strong chemical interaction at interface [2]

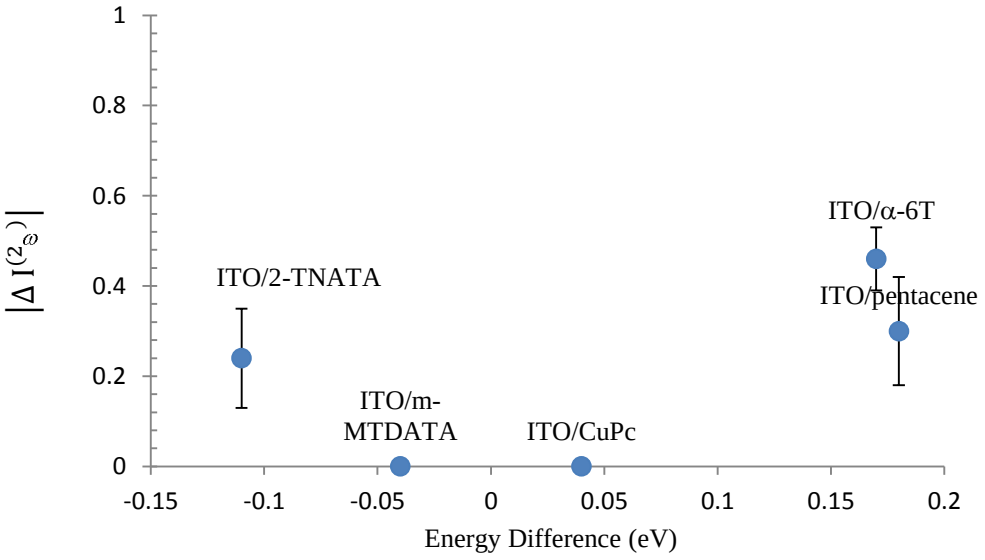

Figure 5.1 The result of $|\Delta I^{(2\omega)}|$ from the interface of ITO/organic structures against the energy difference at the interface. The $|\Delta I^{(2\omega)}|$ is normalized by the $\left|I_{ITO}^{(2\omega)}\right|$.

Also, the ITO/2-TNATA is observed with 25% change of $\left|\Delta I^{(2\omega)}\right|$. However, at the interface of ITO/m-MTDATA and ITO/2-TNATA, the position of the work function of the ITO is higher than the position of the highest occupied molecular orbitals (HOMO) levels with respect to the Fermi level. Electronic of charge transfer should be forbidden at the interface of ITO/m-MTDATA and ITO/2-TNATA since the surface of ITO does not possess electrons in the conduction band [3,4]. From this observation, however the ITO/2-TNATA has an effect from the interface by having 2-TNATA layer on ITO. Thus, this result is not consistent with the implication given by the energy difference.

Other origin of SHG should be discussed as well. The SHG can also originate from highly oriented molecules, and in this case, the molecular orientation at the interface can be different from the molecules in the bulk. The bulk molecular film is treated as an isotropic system $C_{\infty v}$ since there is no SHG emission from organic film. As quoted from Eq. (2.14), the susceptibility, χ_{ijk} is the average of orientation ensemble of microscopic susceptibility of molecules, β_{ijk} and the microscopic nonlinear optical characters induced by interface molecules is possible. SHG from two-photon absorption polarizability tensor can be dominant contribution in resonance condition for molecular symmetries such as pentacene (C_{2v}) and α-6T (C_2) [5].

The conclusion from the data of SHG intensity is rather ambiguous, but it is expected since comparison of SHG between different organic materials should be rather complicated. For one, it is difficult to suppress the effect of SHG light dispersion in the SHG intensity measurement. Secondly, the exact amount of contribution of the interface

SHG can be misleading without any information of the phase/sign of SHG. When there are two or more contributions to the SHG signal, the total SHG intensity can depend on the relative signal between them. For instance in Fig. 5.2, the behavior of total SHG signal at different relative phase (at 0°, 90° and 180°) between the χ_{sub} from the substrate and χ_{ads} of the adsorbates is shown.

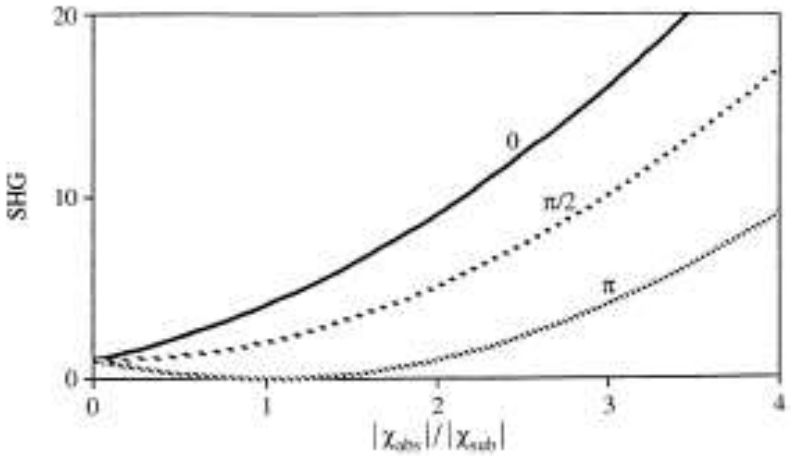

Figure 5.2 Total SHG signal as a function of the ratio of susceptibilities of adsorbed molecules and the substrate for various phase differences [6].

5.2 The origin of phase shift

Some SHG studies show that the origin of the SHG phase shift are the permanent dipole or static dipole as a result of broken symmetry in an isotropic media. The $\chi^{(2)}$ response from static dipole had been observed before with directional-sense adsorbates layer, self-assembled molecules and surface/interface of liquid crystal. These responses are related to intramolecular charge transfer from an electron-donor to

electron-acceptor [7]. It is generally a form of non-resonant SHG and the phase angle of $\chi^{(2)}$ should be either of 0˚or 180˚. However, when the SHG is measured at resonance energy, the interpretation of the phase angle is not as simple and the phase angle will lies somewhere in between the 0˚and 180˚.

5.2.1 Phase shift from the static dipole.

Earlier, El-Basaty et al reported that the static dipole at interfaces of ITO/MoO_3/α-NPD have the sign of 0° and 180° correspond to the direction of the dipoles at the interfaces [1]. Their conclusion is also supported by the SHG spectra with the absence of resonance at the measured photon energy.

Here, the SHG spectra for bare ITO and structures of ITO/organic is shown in Fig. 5.3. The dashed line indicates the 2.33 eV of SHG photon energy that is detected in both intensity and the phase measurement. Two broad SHG peaks appeared in the range of 2.1- 2.33 eV. The peaks originated from optical band gap of bulk ITO domains [1]. In the spectra of bare ITO and the ITO/organic, the SHG intensity corresponding to 2.33 eV is relatively small with no effect of resonance from ITO. The nearest peak centered at 2.23 eV was noticeably higher in intensity for ITO/CuPc and ITO/m-MTDATA compared to ITO and other ITO/organic structures. There is possibility of SHG resonance from these systems at lower energy but the resonance from the electronic state of organic molecular system at the measured photon energy is not likely.

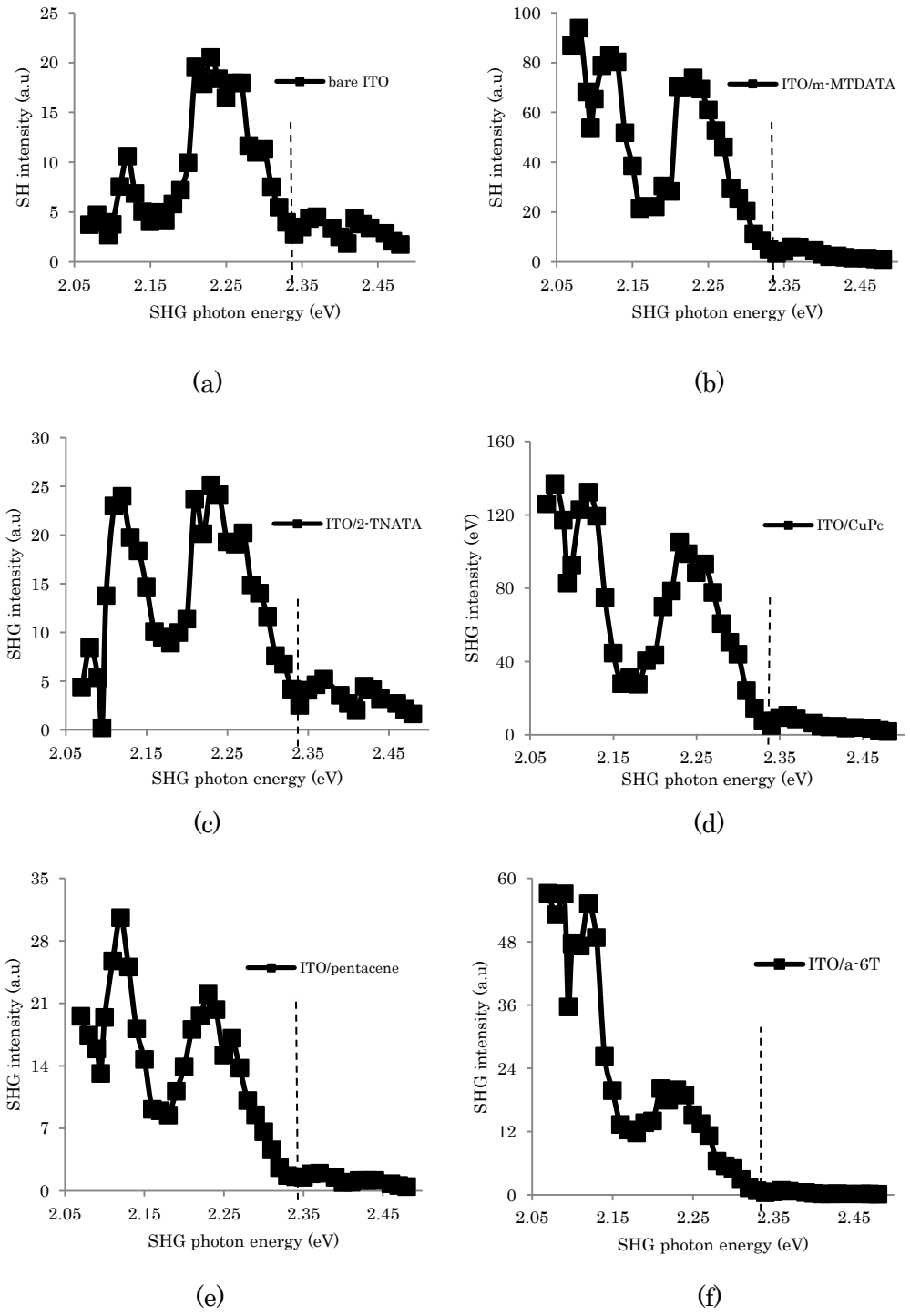

Figure 5.3 Spectra of SHG photon energy of (a) ITO and (b-f) ITO/organic samples

The SHG spectroscopic data in Fig. 5.3 revealed that the electronic contributions in ITO and ITO/organic are non-resonant at the SHG photon energy, 2.33 eV. The assumption of static dipole should also be effective to the interface of ITO/organic. This is contradicting with the absolute phase from the interface of ITO/CuPc and ITO/pentacene that shows that their relative phase with ITO is not exactly 180°. There must be additional effect to the SHG's phase shift thus, other origins of the phase shift cannot be easily dismissed.

5.2.2 Other origins of phase shift.

The complex form of susceptibility is $|\chi_{ijk}|\exp(i\kappa_{ijk})$ [7], and this also applies for the nonlinear susceptibility, $\chi_{ijk}^{(2)}$. The imaginary part contains κ_{ijk} that represents the phase shift in SHG. Naturally, this imaginary part cannot be neglected when the phase angle is not 0°/180° as observed in ITO/CuPc and ITO/pentacene interfaces. Hence, the origin of imaginary term of the susceptibility will also be discussed.

First of all, a little throwback to the complex relation between $\chi_R^{(2)}$ and $\chi_{NR}^{(2)}$ in Chapter 2 when there is multiple contributions to the total SHG. Generally, it is difficult to distinguish these two contributions from each other, just like air/water interface system [8]. But since there is $\chi_R^{(2)}$ dispersion, the phase behavior of $\chi_R^{(2)}$ and $\chi_{NR}^{(2)}$ can be characterized by measuring the phase at several photon energies. The example in Fig. 5.4 is cited from the study of Suzuki et al from Si(111) 7 x 7 [9].

However, the idea to obtain the data of SHG phase at other photon energy cannot be replicated with the present measurement system. Alternatively, an analysis in form of spectral fitting of the SHG spectroscopy data of ITO, ITO/CuPc and ITO/pentacene using a single oscillator model is obtained. The fitting is applied to the resonant peak of 2.23 eV photon energy that is 0.1 eV away from the measured SHG photon energy. The result did not show any difference of phase between $\chi_R^{(2)}$ and $\chi_{NR}^{(2)}$ on the frequency scale in spectra of bare ITO and ITO/organic. Thus, the origin of complex resonant $\chi^{(2)}$ could not be confirmed at this point of analysis.

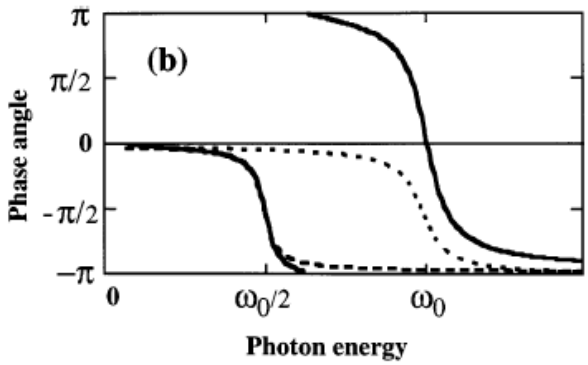

Figure 5.4 Characterization of the phase angle at resonance photon energy by Suzuki et al [9].

Another origin of phase shift is from the imaginary part of dielectric function of molecules. In Kramers-Kronig relation, this behavior is indicated by the absorption of light [10]. The absorption spectra of the organic molecules are shown in Fig. 5.5. The peaks in absorption spectra signifies resonance from the molecules and the dashed lines for wavelengths for ω (1064 nm) and 2ω (532 nm) photon energies are also shown. There is no resonance occurs at the range of fundamental photon energy but some molecules show different resonant characteristic near the 2ω wavelength. This is

particularly true for pentacene and α-6T molecules, as observed they are not totally off resonance at 2.33 eV. Thus, there is a possibility of nonlinear phase shift emerged as a result of resonance from pentacene and α-6T molecules at the interface.

In this paragraph, a more physical aspect of the phase shift origin will be proposed. A model of uniform static dipole in Fig. 5.6 (a) shows the formation of homogenous electric field across the interface. In macroscopic, the interface structure is a dielectric layer and it is treated as a sheet of nonlinear source of polarization, $P_{NLS}^{(2)}$ [11]. In this 'lossless' condition, the electric susceptibility, χ_{ijk} of the interface electric field will appear as a real number only. In the case of electric field at interface between the ITO and the organic layer, dipole model such as in Fig. 5.6 (b) is proposed. The dipole density appeared as spatial fluctuations across the surface of ITO and as a result, the susceptibility, χ_{ijk} is no longer a real number only but with the imaginary part emerging as phase shift. The association of the imaginary term with the fluctuation dielectric property of material can be followed by dissipation-fluctuation theorem [12]. Komar et al discussed the behavior of the imaginary part of complex dielectric permittivity is due to compositional fluctuations, structural defects and associated internal electric fields [13]. The electric field fluctuation will caused scattering of relaxation time within the material. Since the presence of impurities is not a concern in the organic thin film, there is possibility that the fluctuation is caused by inhomogeneous molecular orientation across the interface.

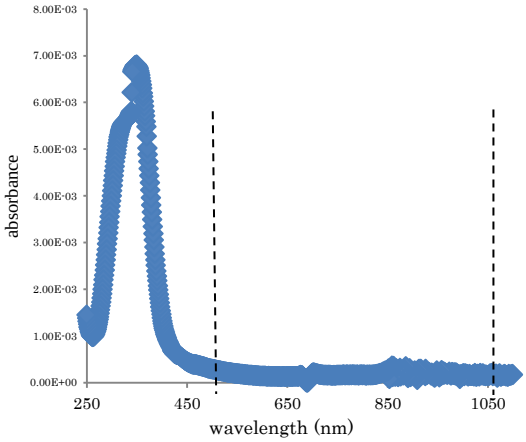

(a) m-MTDATA

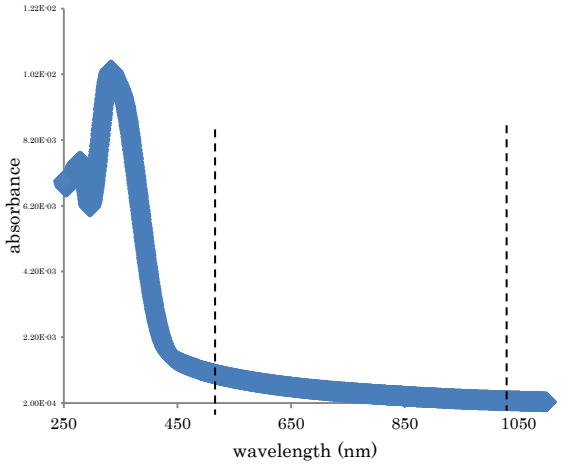

(b) 2-TNATA

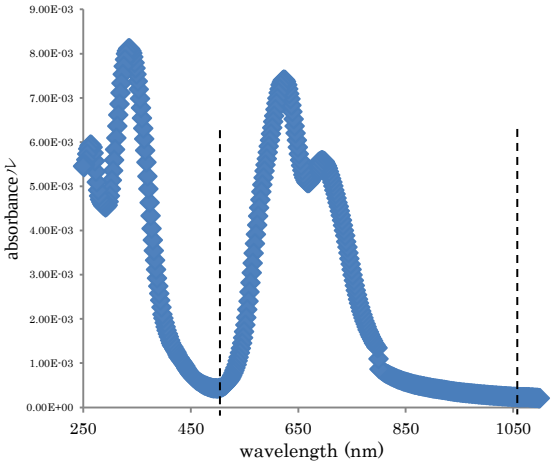

I CuPc

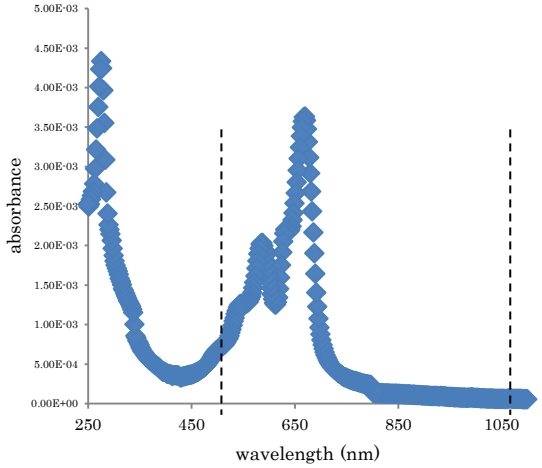

(d) pentacene

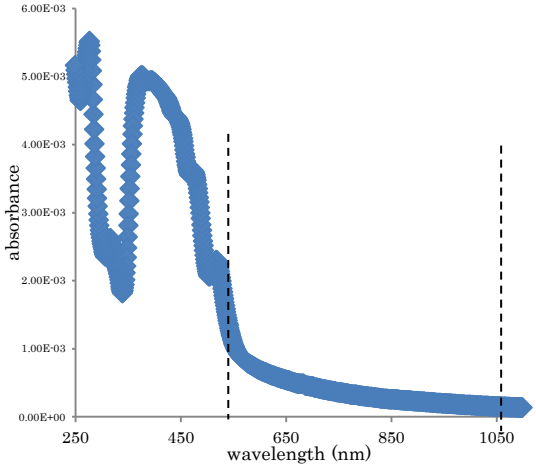

I α-6T

Figure 5.5 The absorption spectra of the organic molecules. The dashed lines represent the fundamental and SHG wavelengths.

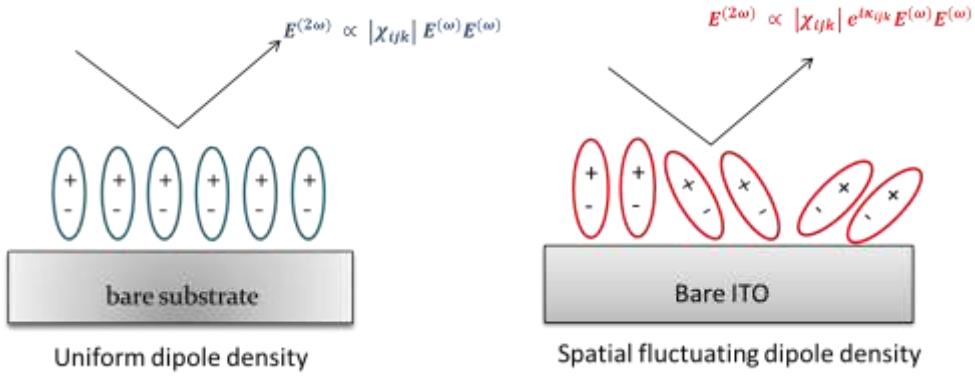

(a) (b)

Figure 5.6 The model of static dipole at interface (a) uniform dipole density at 'ideal' interface and (b) fluctuating dipoles at interface of ITO and organic layer.

The factor of inhomogeneity of molecular orientation on the surface of ITO is supported by the fact that the ITO's surface is known for its roughness [3]. The electric field fluctuation will induced an inhomogenous broadening in the optical response and as a result, the spectrum of static dipole will include imaginary part of $\chi^{(2)}$ in the SHG.

5.3 The SHG from interface of ITO/CuPc, ITO/pentacene and ITO/α-NPD

In this investigation, the complex property of the SHG from interface of ITO, ITO/CuPc, ITO/pentacene and ITO/α-NPD has been determined. For bare ITO interface, the phase is 0° or in phase with its bulk and the SHG from the ITO is normalized as 1. The result of magnitude and the phase of the SHG from interface of ITO, ITO/CuPc, ITO/pentacene and ITO/α-NPD are presented as in Fig. 5.7. The empty squares are the magnitude of the SHG and the filled squares represents the absolute phase. The SHG

from the interface of ITO/CuPc and ITO/pentacene are solved by complex plane analysis. It was found that the SHG from the interface of ITO/CuPc is approximately larger, at ratio of 1.48 of the SHG from ITO with phase shift of 140°. On the other hand, the interface of ITO/pentacene has ratio of SHG nearly1.25 of the SHG from ITO with 160° phase shift. The interface SHG is found to be negatively interfered with the SHG from the ITO, hence explained the decrease of total SHG in the sample. It is also assumed that the charge transfer dipole has the opposite sign to the electric field from the bulk ITO.

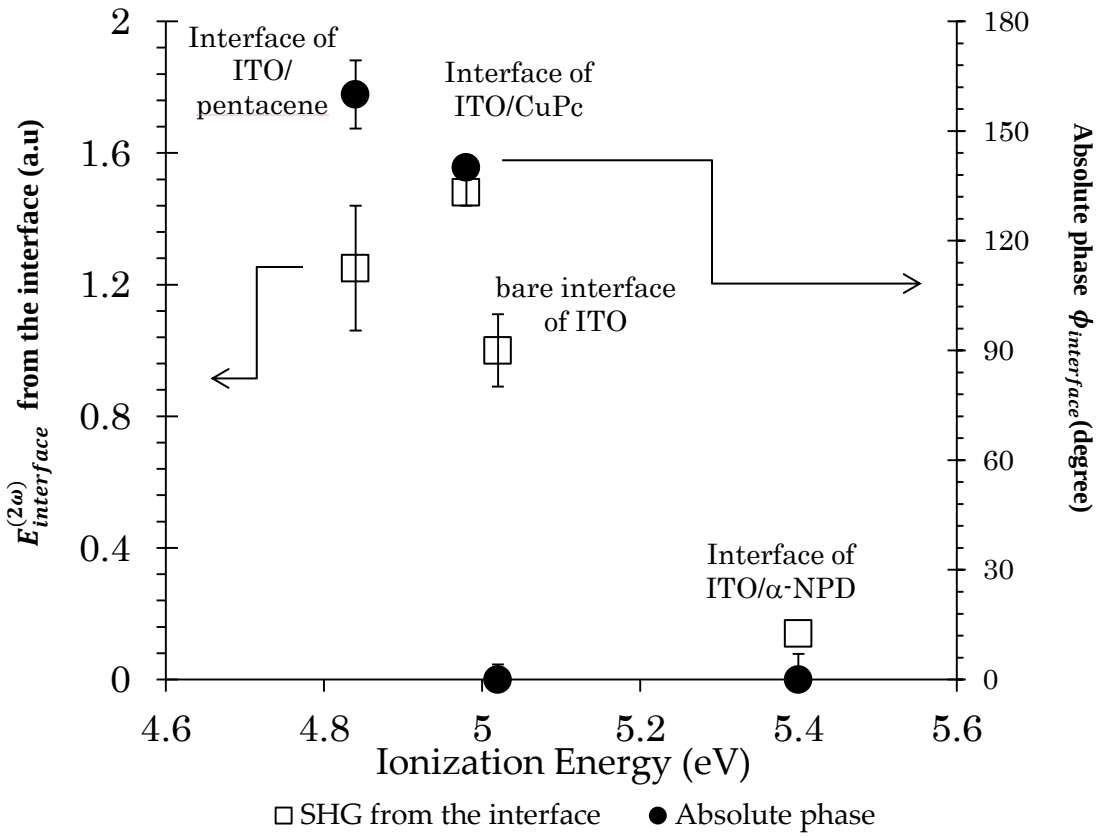

Figure 5.7 The magnitude of SHG electric field (empty squares) and its phase (filled circles). The ionization energy of the organic films is used as the horizontal axis. 5.02 eV is the work function of ITO.

The SHG from the interface of ITO/CuPc and ITO/pentacene do not change significantly despite having different ionization potential at the interface. Nevertheless, the analysis of phase shift has solved the ambiguity for the interface of ITO/CuPc made by the result of SHG intensity. In the result for ITO/α-NPD interface, the solution of complex plane is not needed since it is in phase with ITO. As shown from Fig. 5.7, the contribution of the interface SHG that is directly obtained from SHG intensity indicated barely any change of SHG intensity. The electric field at this interface is probably weak. The same observation has been implied from other study of high-resolution electron-energy-loss spectroscopy (HREELS) [14].

References

1. A.B. El Basaty, Y. Miyauchi, G. Mizutani, T. Matsushima, H. Murata, Optical second harmonic generation at heterojunction interfaces of a molybdenum trioxide layer and an organic layer, Appl. Phys. Lett. 97 (2010) 193302.

2 H. Peisert, M. Knupfer, T. Schwieger, J. Fink, Strong chemical interaction between indium tin oxide and phthalocyanines, Appl. Phys. Lett. 80 (2002) 2916-2918 and the reference inside

3. Y. Gassenbauer, A. Klein, Electronic and Chemical Properties of Tin-Doped Indium Oxide (ITO) Surfaces and ITO/ZnPc Interfaces Studies In-situ by Photoelectron Spectroscopy, J. Phys. Chem. B. 110 (2006) 4793

4. J-H. Lee, S-S, Leem, H-J, Kim and J-J, Kim, Effectiveness of p-dopants in an organic hole transporting material, Appl. Phys. Lett. 94 (2009) 123306

5. A. J. Moad, G. J. Simpson, A Unified Treatment of Selection Rules and Symmetry Relations for Sum Frequencies and Second Harmonic Spectroscopies, J. Phys. Chem. B. 108 (2004) 3548-3562

6. R. Stolle, G. Marowski, E. Schwarzberg, G. Berkovic, Phase measurements in nonlinear optics, Appl. Phys. B 63 (1996) 491-498.

7. K. Kajikawa, M. Sei, I. Yoshida, S. Okada, H. Nakanishi, K. Seki, Y. Ouchi,

Ultra-thin film Local Oscillator for Determination of Complex Components of Second-Order Nonlinear Susceptibility, Jpn. J. Appl. Phys. 38 (1999) 6721-6728.

8. W-k. Zhang, H-f. Wang, D-s. Zheng, Quantitative measurement and interpretation of optical second harmonic generation from molecular interfaces, Phys. Chem. Chem. Phys. 8 (2006) 4041-4052.

9. T. Suzuki, D.E. Milovzorov, S. Kogo, M. Tsukakoshi, M. Aono, Surface second-harmonic generation spectra of Si(111)-7x7 in the 1.0-1.7eV fundamental photon energy, Appl. Phys. B 68 (1998) 623-627.

10. P. Hertel, Lectures on Theoretical Physics: Linear Response Theory, University of Osnabrück, Germany.

11. T. Hienz, Second-order nonlinear optical effects at surfaces and interfaces in Nonlinear surface electromagnetic phenomena, Elsevier Science Publishers (1991) and the reference inside.

12. R. Kubo, The fluctuation-dissipation theorem, 1966 Rep. Prog. Phys. 29 (1966) 255-284.

13. V.K. Komar, V.P. Migal, D.P. Nalivaiko, O.N. Chugai, Dielectric Properties of Melt-Grown $Cd_{1-x}Zn_xTe$ Crystals, Inorg. Mater. 37 (2001) 449-451

14. Y. Hosoi, K. Okamura, Y. Kimura, H. Ishii, M. Niwano, Infrared spectroscopy of

pentacene thin film on SiO_2 surface, Appl. Surf. Sci. 244 (2005) 607-610

15. P. He, S. D. Wang, W. K. Kook, C. S. Lee, S.T. Lee, Vibrational and photoemission study of the interface between phenyl diamine and indium tin oxide, Appl. Phys. Lett. 79 (2001) 10

Chapter 6

Conclusion

As a powerful tool for diagnostic of electric field, the optical second harmonic generation has the capability to access the buried interface of organic thin film. In this dissertation, the electric field of charge transfer at the interface of substrate ITO and organic semiconductor thin film has been probed. Organic semiconductor molecules such as CuPc, pentacene and α-6T were inferred as potential donor of ground-state charge transfer complexes at the surface of indium tin oxide. The experiment also employed m-MTDATA, 2-TNATA and α-NPD for comparison. The presence SHG from the interface was detected at ITO/2-TNATA, ITO/α-6T and ITO/pentacene as cancellation effect on the SHG from ITO. This can be true since it was formerly implied that the SHG from charge transfer dipole at the interface can be of opposite sign to the SHG from ITO. But generally, the data of SHG intensity and Fresnel factor analysis could not be conclusive enough since the dispersion effect was not negligible for the organic layers. Because of this ambiguity of the homodyne data, the measurement of phase was also performed.

The optical set-up of SHG phase measurement is the conventional interferometry method. The SHG's phase was measured using a translating α-quartz (0001) as the second SHG source. The total phase shift of the ITO/organic structures were directly obtained from the SHG oscillation patterns using the phase from bare

interface of ITO as reference, $\phi_{ITO,0}$ = 0. From this phase only, the phase shifts of ITO/organics showed significant change possibly related to the electronic of the organic thin film. Since the dispersion of the ω and 2ω waves had a big effect on the phase shifts itself, the absolute phase were obtained after the dielectric function of organic thin film analysis and the complex plane solution. The phase from the interface of ITO/CuPc and ITO/pentacene were shown with relative to the ITO's phase. It is noted that the complexity of analyzing the SHG's phase can be avoided by using small thickness of organic layer as had been observed for ITO/α-NPD (10 nm). In this dissertation, the interface of ITO/CuPc and ITO/pentacene had the absolute phase of 140° and 160°, respectively. This number, however, were slightly deviated from 180° that correspond to the direction of charge transfer (static) dipole at the interface.

To explain the effect of dipoles on the SHG's phase shift, most of candidate origins were discussed. There is origin of resonance and also the effect of imaginary part of the susceptibility induced by the interface molecules. The spectroscopy data showed that both electronic state of ITO and the static dipole at interface are not resonant to both ω and 2ω frequencies. However, the fact that some of the molecules were not totally off resonance at 532 nm implied that the nonlinear phase shift can emerged from interface molecules. Last but not least, the model of spatial fluctuation was suggested as a feasible model for the case of dipole density at the interface of ITO and organic semiconductor molecules.

Regarding the charge transfer dipole at the interface, the present result did not indicated whether or not the property the dipole is being governed by the vacuum level

alignment rule. It may have due to difficulty of obtaining enough information on the SHG as the present measurement system is only capable of doing a measurement at one photon energy. The same solution can also be suggested for the case of ITO/2-TNATA, ITO/m-MTDATA and ITO/α-NPD since the sensitivity of the optical probe may vary from each interface.

Nevertheless, the SHG experiment of SHG's phase was proved to be useful for the analysis of SHG from the interface, here, the separation of the interface contribution from the bulk contribution had been demonstrated. Furthermore, more information of the $\chi^{(2)}$ of the electric field can be understood using the phase data. Since there is a crucial need to construct the SHG phase experiments, several concerns in the experiment are in a need of improvement. This had been highlighted in this dissertation. There is a reason to believe that the result of SHG phase measurement may imply the orientation of CuPc and pentacene molecules at the interface. More accurate data interpretation pertaining to the molecular orientation can be established if substrate like quartz is to be employed. The quartz has a single crystal orientation however it will be interesting to explore this possibility with ITO substrate in the future. It is noted that the phthalocyanine molecules are likely to orient themselves ~30° to 40° from the surface normal while the pentacene had been observed to be standing molecules on many amorphous substrates.

List of Appendices

Appendix I

Linear spectra of ITO and ITO/organic

A-Transmission

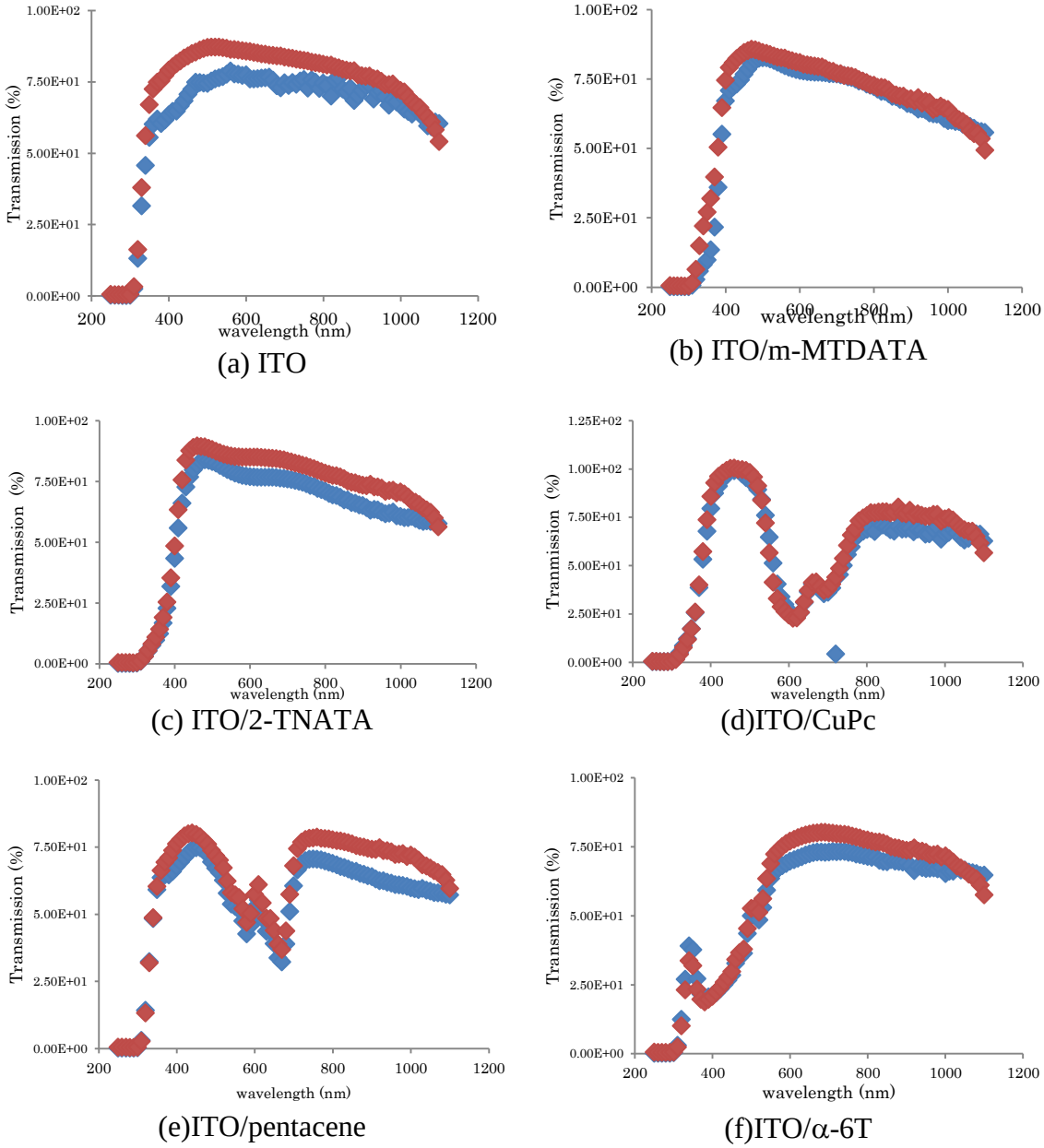

Figure 1 The transmission spectra of (a)ITO and (b-f) structures of ITO/organic. The blue and red symbols are transmission angle at 0 and 45 degree, respectively.

B-Reflectance

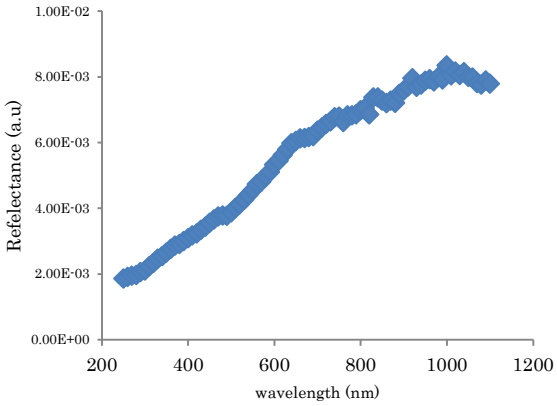

(a) ITO

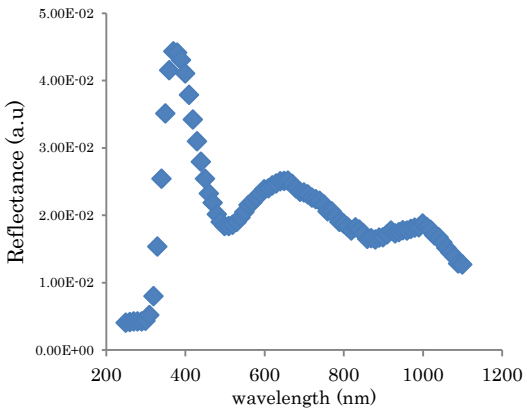

b) ITO/m-MTDATA

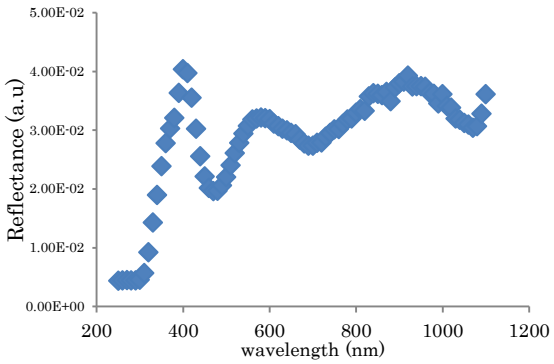

(c) ITO/2-TNATA

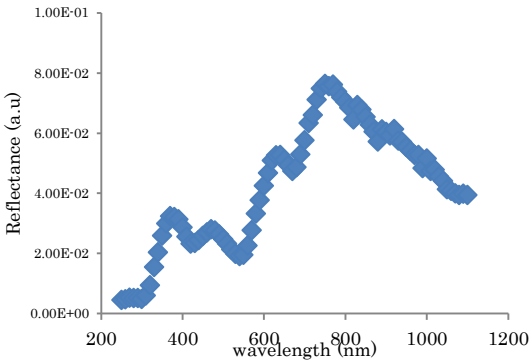

(d)ITO/CuPc

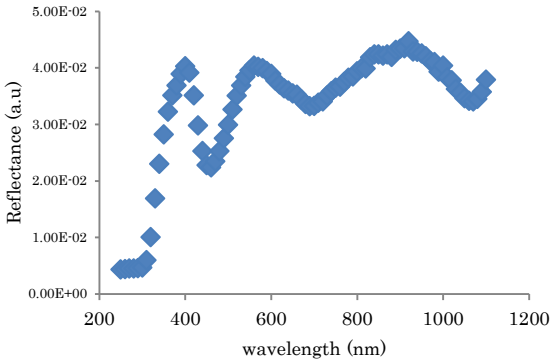

(e)ITO/pentacene

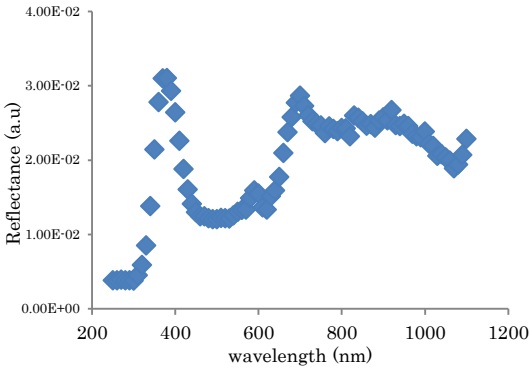

(f)ITO/α-6T

Figure 2 The reflectance spectra of (a)ITO and (b-f) structures of ITO/organic. The surface of incidence radiation is the organic layer.

C-Reflectance

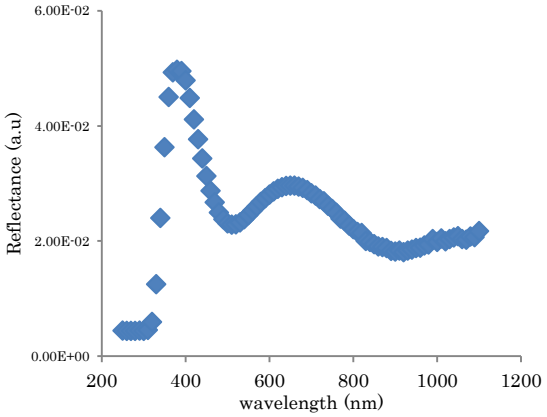

(a) ITO

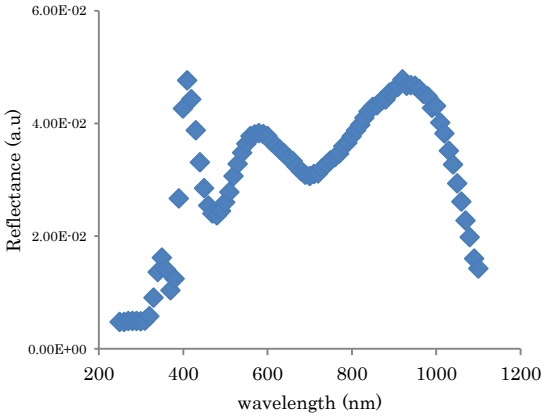

b) ITO/m-MTDATA

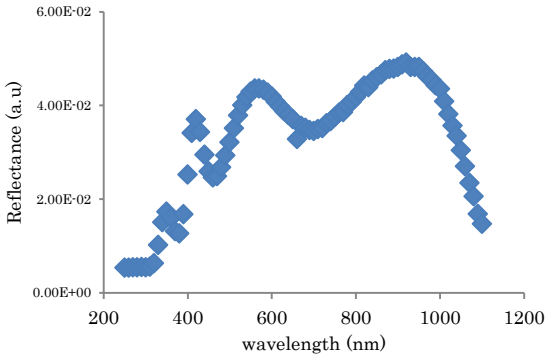

(c) ITO/2-TNATA

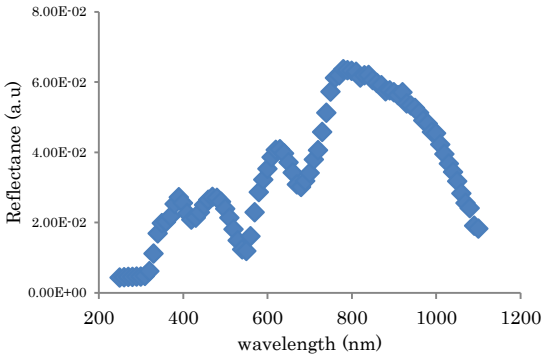

(d)ITO/CuPc

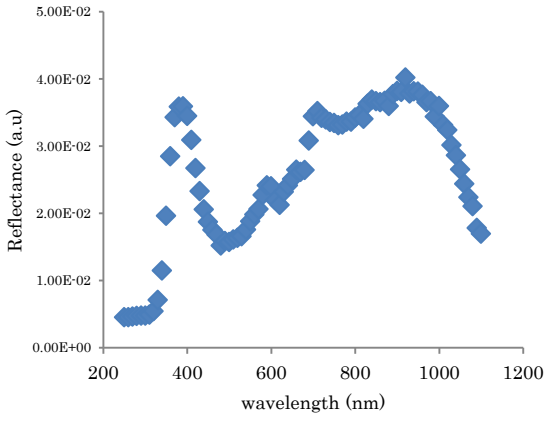

(e)ITO/pentacene

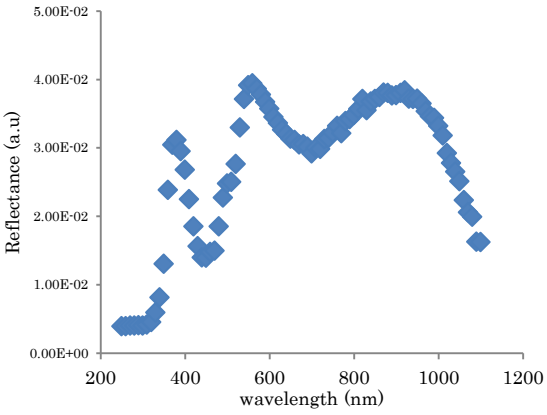

(f)ITO/α-6T

Figure 3 The reflectance spectra of (a)ITO and (b-f) structures of ITO/organic. The surface of incidence radiation is the glass substrate of ITO.

D-Reflection Coefficient

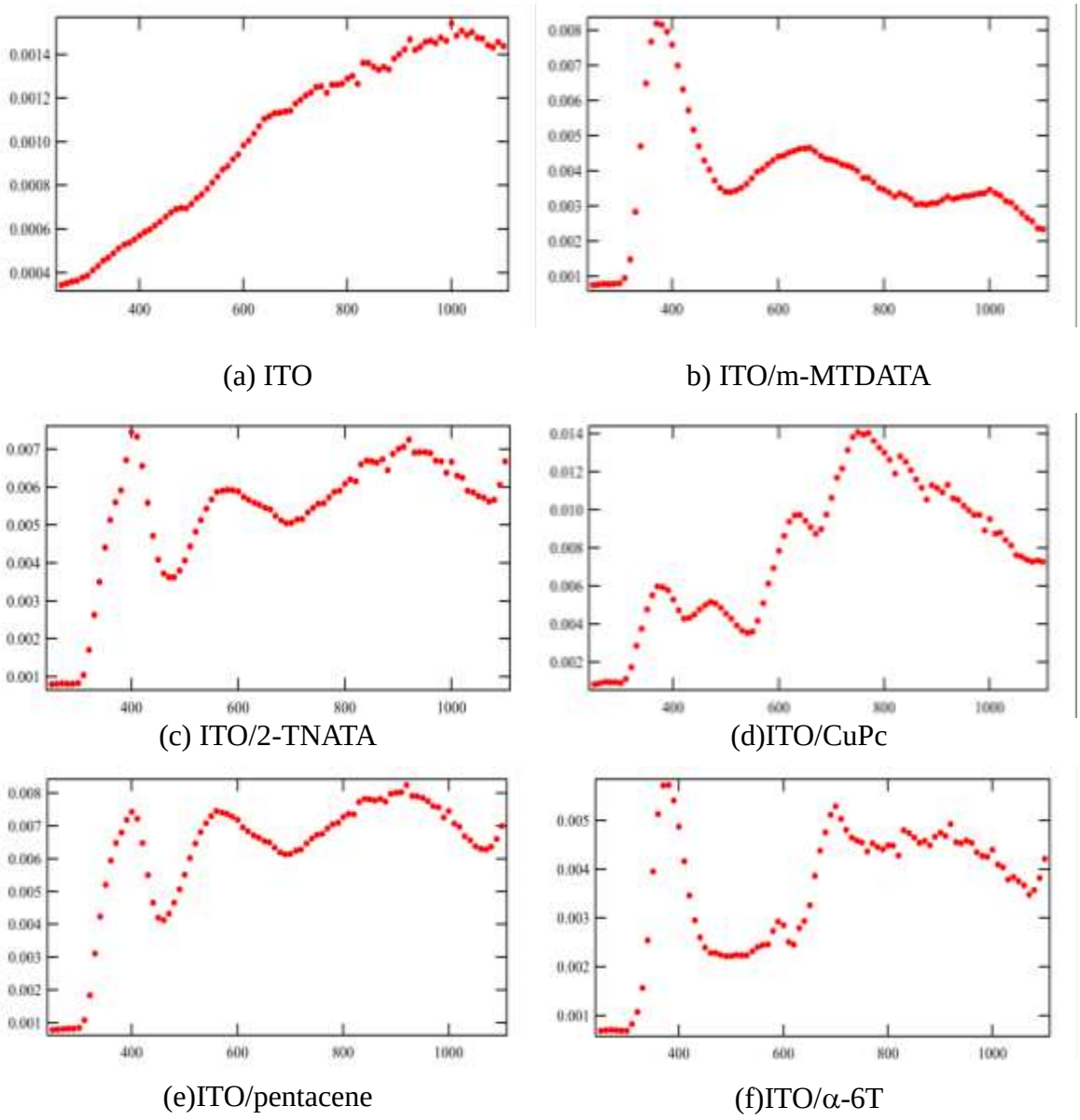

Figure 4 The horizontal axis represents the reflectance coefficient, r_p for (a) ITO and (b-f) ITO/organic samples as a function of wavelength (unit in nm). They are calculated from the ratio of the amplitude of optical reflectance over the transmission.

E-Reflection Coefficient.

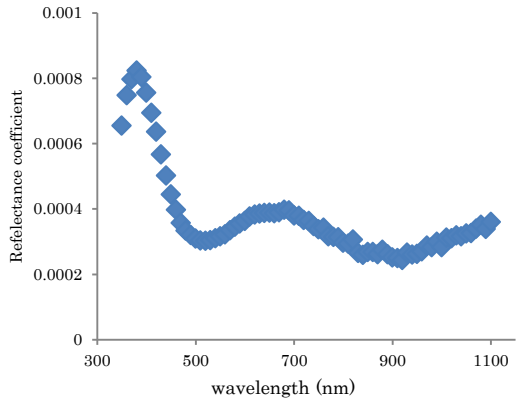

(a) ITO

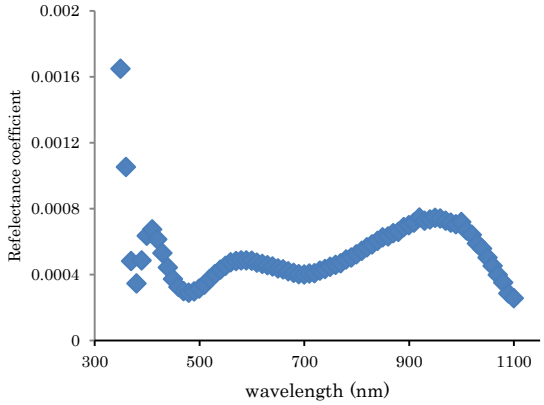

b) ITO/m-MTDATA

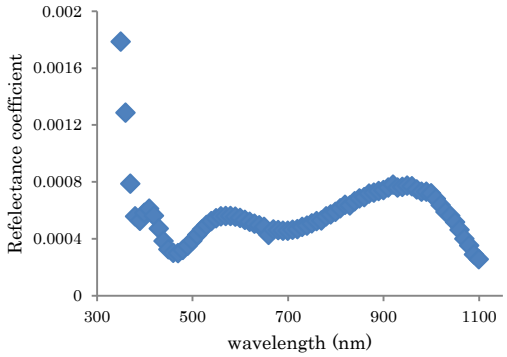

(c) ITO/2-TNATA

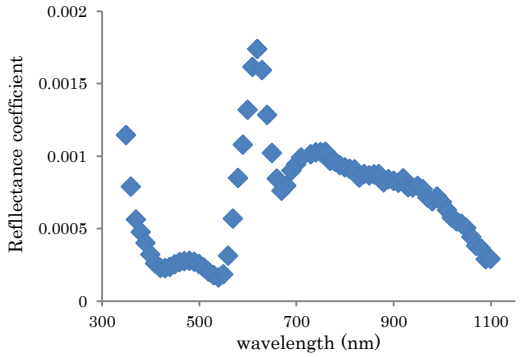

(d)ITO/CuPc

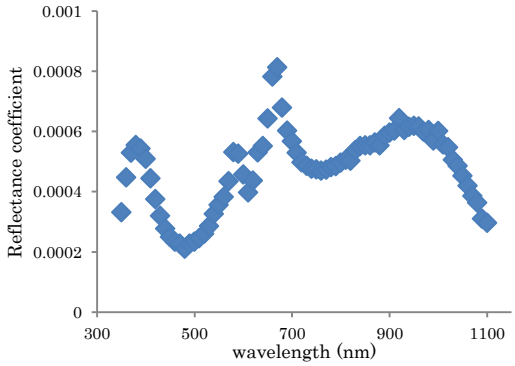

(e)ITO/pentacene

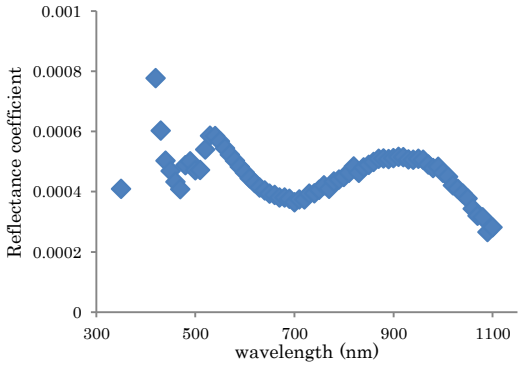

(f)ITO/α-6T

Figure 5 Reflectance coefficient, r_p for (a) ITO and (b-f) ITO/organic samples in configuration (ii) of Fig, 3.3. They are calculated from the ratio of the amplitude of optical reflectance over the transmission

Appendix II

Ellipsometry spectra of Si(001)/α-NPD thin film

Si(001) substrates were cut and prepared in the Centre for Nano Materials and Technology, JAIST with the help of Mr. T. Murakami, the α-NPD thin film at different thicknesses were prepared by Murata Lab. The ellipsometry observation was performed in Ohdaira Laboratory of School of Materials Science, JAIST. I acknowledged the guidance from Miss T. C. Trinh in this measurement. The ellipsometry spectrometer was VASE model of J. A. Woollam Co. Inc. The dielectric function of the Si(001)/α-NPD thin film was measured at wavelength range from 250 nm to 1100 nm.

Figure 1 (a) shows the spectra of refractive indices, *n* of the samples obtained by the ellipsometry spectrometer. The complex form of refractive index, $\hat{n} = n - i\kappa$, constructed of the real part and the imaginary part. The spectra of real and imaginary parts of the dielectric constant, ε_1 and ε_2 are given as (b) and (c), respectively. The dielectric coefficient, $\hat{\varepsilon} = \varepsilon_1 + \varepsilon_2$, is the square of the $\hat{n}$.

In Fig. 2, the optical constant of α-NPD films were obtained by fitting of normal dispersion simulated by the software. The optical thickness of the 100 nm α-NPD film determined from Cauchy fit is 72.17 ± 0.37 nm. The refractive indices of the thin film at 100 nm are the Cauchy model fits in the region of transparency (λ > 450 nm). In this fitting, the extinction coefficient, κ(λ) = 0. The index of refraction of a respective wavelength $n(\lambda)$ was obtained using the Cauchy model fitting equation.

$$n(\lambda) = A + \frac{B}{\lambda^2} + \frac{C}{\lambda^4} \qquad (1)$$

Constant A sets the index range while constant B and C give the dispersion shape.

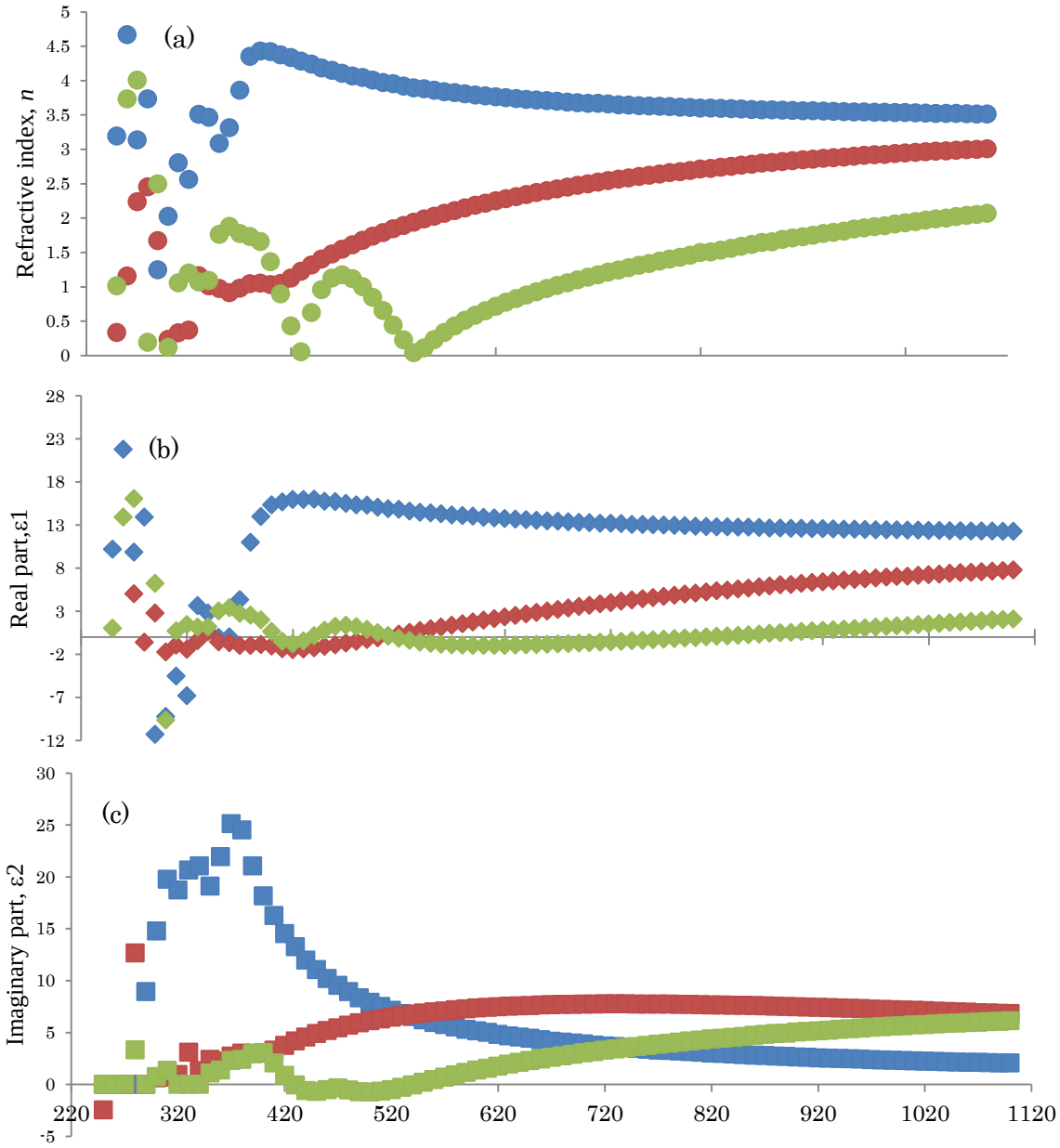

Figure 1 (a) Spectra of refractive indices for Si(001)/α-NPD of different thickness of organic layer. (b) real part, and (c) imaginary part of dielectric constant at respective wavelengths. The blue, red and green markers represent the 10 nm, 50 nm and 100 nm of α-NPD film thickness, respectively.

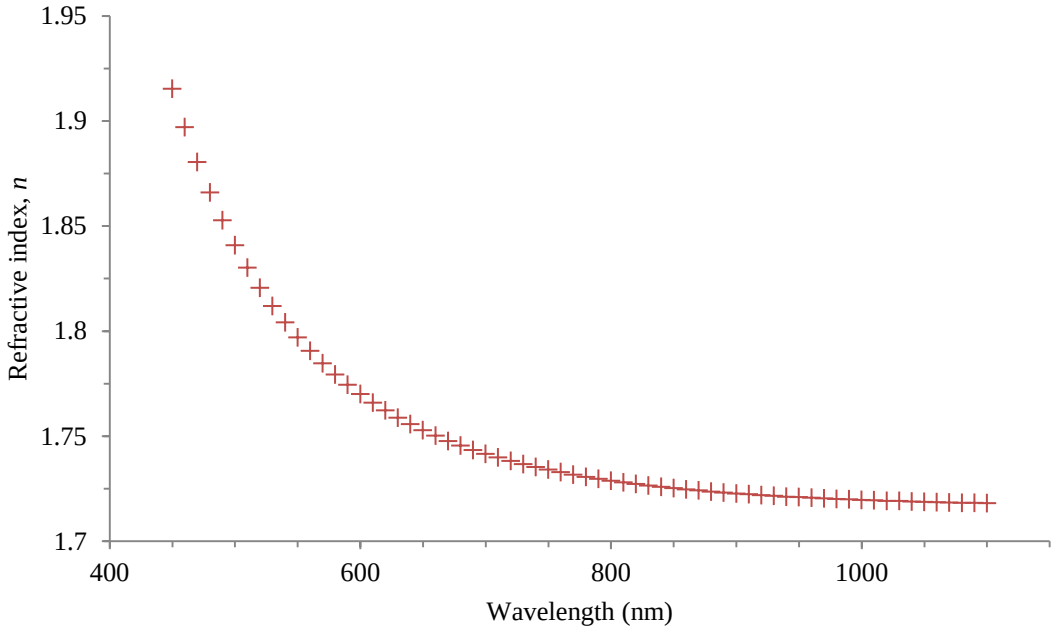

Figure 2 The refractive index, *n* of 100 nm α-NPD thin film obtained from the Cauchy fits of ellipsometric spectra.

Appendix III

SHG measurement on organic light emitting diode (OLED) degradation

1.0 Introduction and Background Review: Luminescence degradation in OLED

While the development of organic light emitting diode (OLED) in the industries has matured over the years, the problem on lifetime of the device via luminescence degradation remains as disadvantage. One can generally relate this problem to the recombination centers at the interface between the hole transport layer (HTL) and the electron transport layer (ETL) of OLED, also the sole origin of luminescence emission hence the origin of the device degradation. Here, a sample of green light OLED structure is used to study the origin of the degradation at the interface. The OLED device is made of several layers of thin film and different interfaces structures but the possible origin of charge and optical traps and luminescence degradation is the interface between the α-NPD layer and the AlQ_3 layer [1,2]. Due to the construction of the device, access to this interface can be very challenging to achieve via electron probe. However, recently the electric-field-induced doubly resonant SFG had been successfully demonstrated as a selective probe in the OLED structure [3]. Under illumination of coherent IR light, it is proposed that the carbonyl molecules at the degraded interface will respond in the change of the SHG electric field from the interface.

2.0 Experiment : Cross-section SHG on degraded organic light emitting diodes (OLEDs)

The material construction of the OLED devices is Al(100 nm)/LiF(0.5 nm)/Alq_3(70 nm)/NPD(10 nm)/MoO_3(0.75 nm)/ITO(150 nm) layers. The OLED construction is provided in Fig. 1.1 in Chapter 1. Four devices were prepared for the SHG measurement. Two of the devices were electrically degraded at 55% and 75% from its initial luminescence and another two were pristine devices at 100% initial luminescence.

The SHG measurement was performed by radiating the fundamental 1064 nm laser light on the surface of the glass covered ITO. The thickness of the glass was ~1 mm. SHG intensities of device area were measured by 'scanning' the beam horizontally across the device using a manual sample positioning. This is a simple alternative to the SHG microscopy. The dimension of each device is approximately 2 mm x 2 mm and the diameter of the beam was approximately 1 mm^2. In all devices, significant SHG increment near the area of the device had been observed. Figure 1 shows the result of scanning the fundamental beam horizontally on pristine/degraded OLED.

As shown in Fig. 1, dramatic increase in SHG intensities was seen near all the devices (a-d). The scanning distance of the increase was ~2 mm matched the exact device's size. The SHG intensity of the device was almost twice of SHG at other scanning distances. Along 3 mm from the device area, SHG intensities were detected as pointed by the red arrows and the intensity deteriorated over longer scanning distance. It is suggested that this optical configuration was highly effected by the geometrical Fresnel factor of the glass. As the 1064 nm fundamental light propagated inside the glass with high total internal reflectivity at the glass/ITO boundary, the contact of the IR light with ITO became very strong. Thus, the reason for SHG emission was observed at other distance away from the devices.

The increase of SHG intensities in the area of device indicated an origin of SHG from degraded interfaces. The average SHG intensities at every scanning position among the OLED devices showed that they are indistinguishable from each other. However, the SHG induced by the degraded devices (c-d) were observed to be narrower than in the pristine devices (a-b). As far as it is concerned, Pinato et al also reported the current crowding at the center of the degraded OLED device as the device's edge emitted lower emission profile [1].

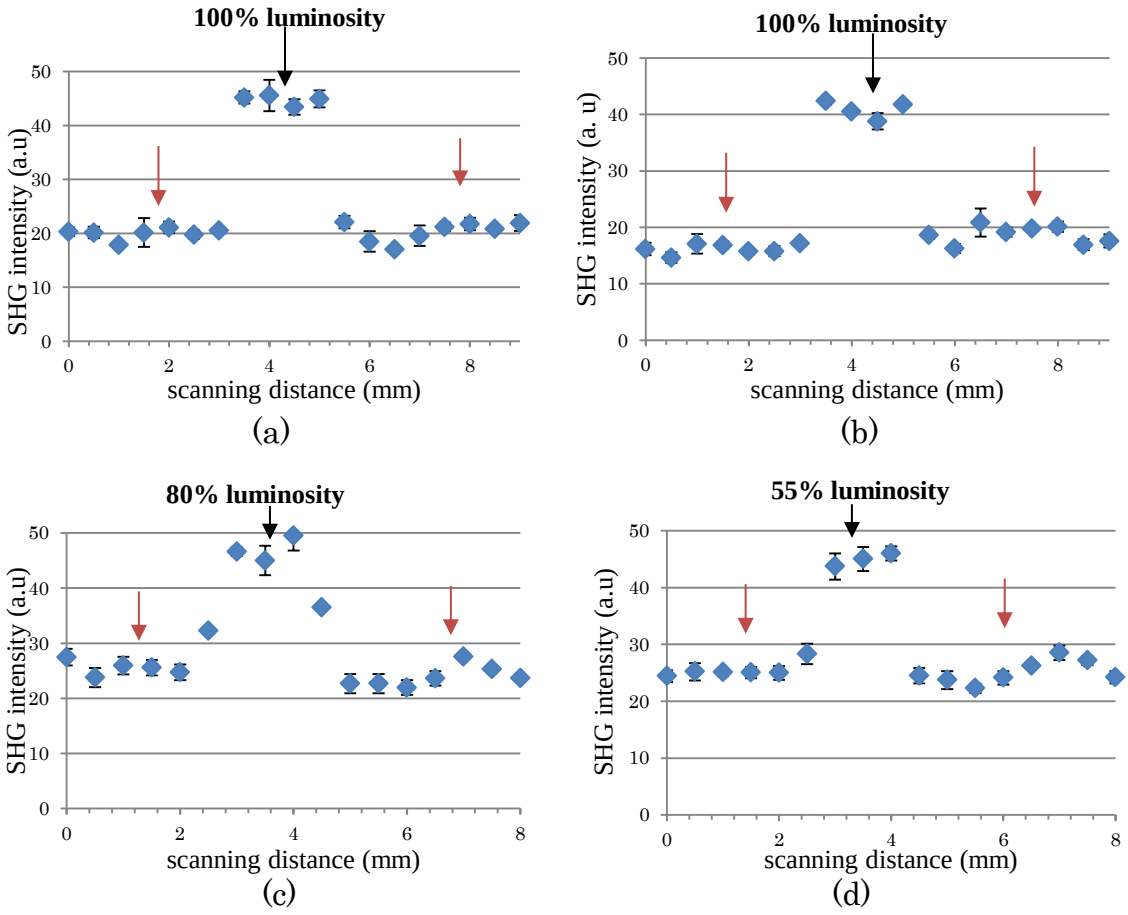

Figure 1 The SHG intensities at cross section area of (a-b) pristine OLEDs and (c-d) degraded OLEDs. The red arrows show the area affected by the multireflectivity in the glass.

3.0 Experiment 2: SHG's phase from the OLED

The SHG interference patterns in Fig. 2 were obtained with superposition of the SHG from the OLED with the translating α-quartz. The phase ϕ of the SHG interference was calculated from sine curve fitting. The phase from other areas of the sample occupied by ITO and organic layers only is 229.76°, it is the same area shown by red arrows scanned

in Fig. 1. As can be seen, there was no significant change of phase between the patterns. The phases of the degraded devices (c-d) had shifted by ~15° with respect to the phase in pristine device (b). In short, the phases of the SHG from the devices were relatively in phase with each other. To sum it all up, the SHG electric field from the interface of degraded OLED was found to induce a small change in overall SHG intensities from the devices. Following the small change in phase shift, the electric field from degraded α-NPD/AlQ_3 interface possibly possessed the same sign as the interface that is not degraded.

References

1. A. Pinato, A. Cester, M. Meneghini, N. Wrachien, A. Tazzoli, S. Xia, V. Adamovich, M. S. Weaver, J. J. Brown, E. Zanoni G. Meneghesso, (2011) *IEEE Transactions on Electron Devices* **57**, 178-184
2. Y. Nakano, (2009) *Appl. Phys. Exp.* **2**, 092103
3. T. Miyamae, N. Takada, T. Tsutsui, (2012) *Appl. Phys. Lett*, **101**, 073304

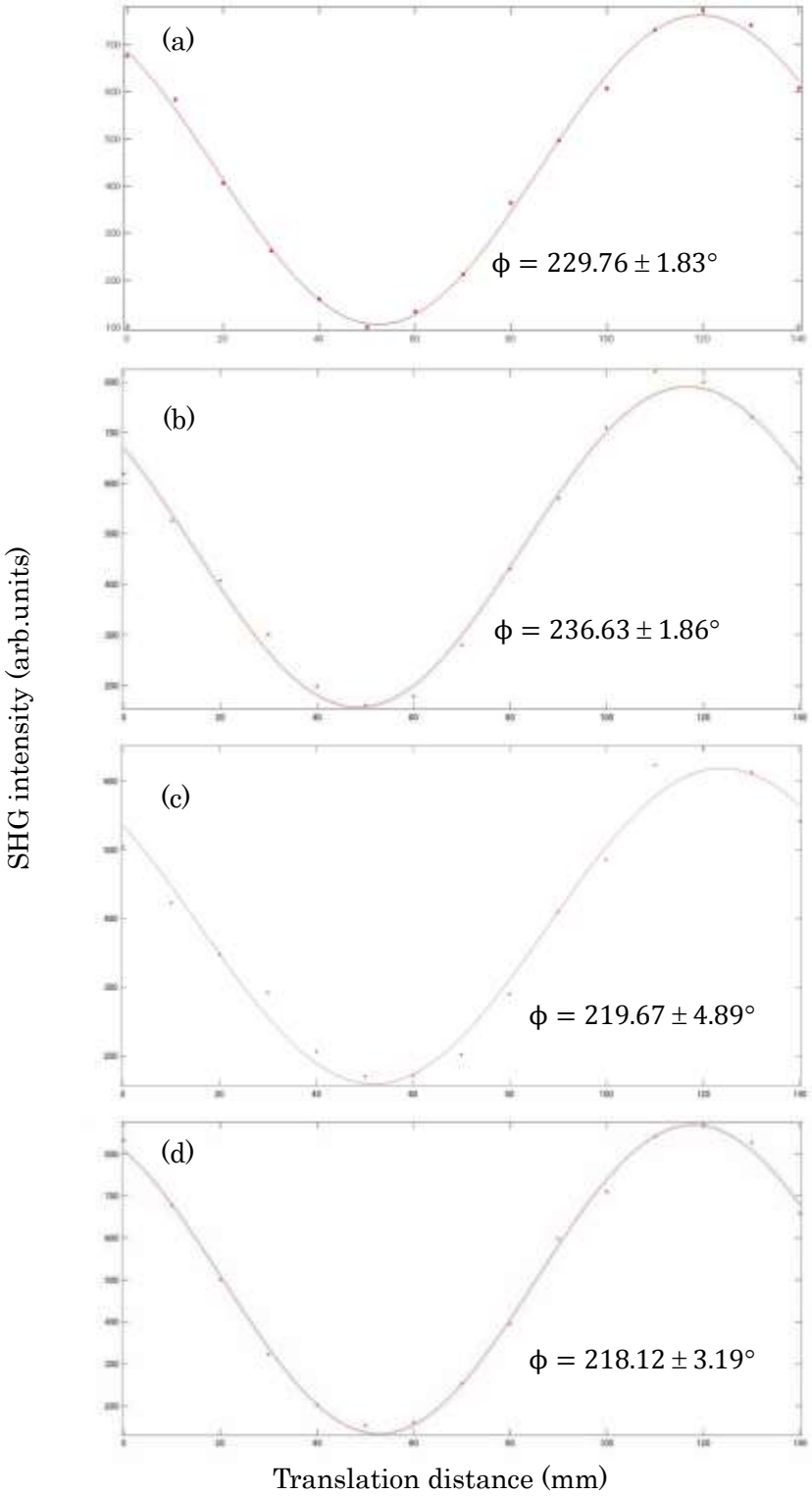

Figure 2 The SHG interference patterns of the area of (a) red arrows and the devices; (b) pristine, (c)80% degraded and (d)55% degraded from initial luminosity.

List of Publications and Academic Conferences

Publication:

1 **S. Z. N. Demon**, Y. Miyauchi, G. Mizutani, T. Matsushima and H. Murata. Optical second harmonic generation at interfaces of some organic layers with indium tin oxide. Appl. Surf. Sci. 311 (2014) 715-720

International Conference:

1 **S. Z. N. Demon**, Y. Miyauchi, G. Mizutani, T. Matsushima and H. Murata. Study of ITO/organic interfaces by optical second harmonic generation phase measurement. Poster presentation. International Symposium on Advanced Materials 2013. 17th-18th October 2013. JAIST, Ishikawa.

2 **S. Z. N. Demon**, Y. Miyauchi, G. Mizutani, T. Matsushima and H. Murata. Study of ITO/organic interfaces by optical second harmonic generation (SHG). Poster presentation. The 4th International Symposium on Organic and Inorganic Electronic Materials and Related Nanotechnologies (EM-NANO '13). 17th-20th June 2013. Kanazawa, Ishikawa.

3 **S. Z. N. Demon**, Y. Miyauchi, G. Mizutani, T. Matsushima and H. Murata. Study of ITO/organic interfaces by optical second harmonic generation phase measurement. Proceeding (not refereed) and Poster Presentation. 9th International Symposium on Atomic Level Characterizations for New Materials and Devices (ALC '13). 2nd-6th December 2013. Big Island, Hawaii, USA

Local Conference:

1 **Demon, S. Z. N.**, Miyauchi, Y., Mizutani, G., Matsushima, T. and Murata, H. Interface of indium tin oxide (ITO)/organic media probed by second harmonic generation (SHG). 2012 Autumn Meeting of the Physical Society of Japan (JPS) Vol. 67. September 2012 Yokohama National University, Yokohama.

2 **S. Z. N. Demon**, Y. Miyauchi, G. Mizutani, T. Matsushima and H. Murata. Interfaces of indium tin oxide and organic semiconductor by optical second harmonic generation phase measurement. 2013 Japan Society of Applied Physics (JASP) Hokuriku Branch Meeting. November 2013. Kanazawa Institute of Technology, Ishikawa.

Award:

1. Recipient of **Student Award**. Study of ITO/organic interfaces by optical second harmonic generation phase measurement. 9th International Symposium on Atomic Level Characterizations for New Materials and Devices (ALC '13). 2nd-6th December 2013. Big Island, Hawaii, USA

Title:

ELECTRONIC STRUCTURE OF SELF-ASSEMBLED NUCLEOSIDES INVESTIGATED BY ULTRAVIOLET PHOTOELECTRON SPECTROSCOPY

Supervisor:

Assoc. Prof. FRIEDLEIN, Rainer

Summary:

Inspired by life itself, the supramolecular assembly of RNA and DNA base unit is of high scientific and practical interest. Following the previous successful preparation of well-ordered multilayer films of guanine and adenine assemblies [1,2], here, are reported the result of our study of assemblies of the nucleosides adenosine and guanosine as well as of the nucleotide guanosine 5'-triphosphate. The preparation of thin multilayer films by spray deposition of adenosine, guanosine and guanosine 5'-triphosphate has been performed in the controlled environment of a ultra-high vacuum (UHV) set-up. The electronic structure of the thin films has been probed by ultraviolet photoelectron spectroscopy (UPS). Photoelectrons emitted along the stacking direction of molecules have been analyzed for films with increasing thickness. From the spectra, the binding energy of the features related to highest occupied molecular orbital (HOMO) as well as the work function and the ionization potentials have been derived. Following the preparation of dry films at elevated temperature, changes of the electronic structure upon hydration have been verified. Electronic band dispersion in the spectra of adenosine, guanosine and guanosine 5'-triphosphate indicated extended electronic states along the quasi-one-dimensional assemblies.

References:

[1]Y. Wang, A. Fleurence, Y. Yamada-Takamura, R. Friedlein, *Chem. Commun.* **47** (2011) 12349-12351

[2]R. Friedlein, Y. Wang, A. Fleurence, F. Bussolotti, Y. Ogata, Y. Yamada-Takamura, *J. Am. Chem. Soc.* **132** (2010) 12808-12810